Titre: Title:	Metering film hydrodynamics in film coating
Auteur: Author:	Sergio Alonso-Romero
Date:	2000
Type:	Mémoire ou thèse / Dissertation or Thesis
Référence: Citation:	Alonso-Romero, S. (2000). Metering film hydrodynamics in film coating [Thèse de doctorat, École Polytechnique de Montréal]. PolyPublie. https://publications.polymtl.ca/8850/

UNIVERSITÉ DE MONTRÉAL

METERING FILM HYDRODYNAMICS IN FILM COATING

SERGIO ALONSO-ROMERO
DÉPARTMENT DE GÉNIE CHIMIQUE
ÉCOLE POLYTECHNIQUE DE MONTRÉAL

THÈSE PRÉSENTÉE EN VUE DE L'OBTENTION
DU DIPLOME DE PHILOSOPHIAE DOCTOR (PhD)
(GÉNIE CHIMIQUE)
NOVEMBRE 2000

UNIVERSITÉ DE MONTRÉAL

ÉCOLE POLYTECHNIQUE DE MONTRÉAL

Cette thèse intitulée :

METERING FILM HYDRODYNAMICS IN FILM COATING

présentée par : ALONSO-ROMERO Sergio
en vue de l'obtention du diplôme de : Philosophiae Doctor
a été dûment acceptée par le jury d'examen constitué de :

M. CHAOUKI Jamal, Ph.D., président
M. TANGUY Philippe A., Ph.D., membre et directeur de recherche
M. CARREAU Pierre J., Ph.D., membre
M. ESMAIL Nabil, Ph.D., membre

To God

To my family

ACKNOWLEDMENTS

First and foremost, thanks God for allowing me to fulfill this goal.

It also gives me great pleasure to acknowledge Prof. Philippe A. Tanguy, director of the chair CRSNG/PAPRICAN, for having given me the opportunity to do my doctoral studies under his supervision. It has been a wonderful experience. His financial support, sincere advice, great confidence, and our multiple scientific discussions have been the key to the success of this project.

Words are not enough to thank my family, especially my mother, for her love, encouragement and blesses, and my father, although not being here now with us, he also spirited me to achieve my goals. Furthermore, I thank my brothers Jose Lucio, Juan Gerardo, Ignacio, Luis Ernesto, Victor Manuel, Hector Aniceto, Alma Rosa, Javier, Mario y Gabriel, and all my sisters-in-law, nieces and nephews for their stimulating moral support.

I am thankful to the members of the URPEI for their friendship and contribution to this work. I specially thank of Olivier Réglat for his priceless scientific advice, and his wife Alfa Arzate for her immense moral support and valuable discussions about this thesis. François Bertrand for his support to the numerical simulations, Francis Thibault for his help and availability during the numerical stage of this work, Olivier Furling for the French language and his special friendship, and Richard Labrie for his aid on the computers. At last but not least, Nathalie Tourangeau for her efficient services.

Special thanks to Professor Pierre Carreau, director of CRASP, and Professor Lionel Choplin, director of GEMICO, for allowing me each to use the rheometers of CRASP and GEMICO, respectively, for the rheological characterization of the fluids. Moreover, thanks to Philippe Marchal and Frédéric Cotton for their valuable help in the use of the rheometers. Carol Painchaud, technician of the Chemical Engineering Department, for the technical support in the laboratory, and Michel Drainville, from PAPRICAN, concerning the instrumentation of the laboratory coater.

I will also remember in a special manner my friends Francisco Rodriguez and his wife Stella Maris for the great time we had together. Mr. Fernando Rodriguez and Ms. Clara Rodriguez, as well as Tomas Lozano and Gabriel Ascanio, for their valuable friendship and moral support. And finally, all my friends in Montreal and Mexico, you all have also been always in my mind.

I would like to thank CONACYT (from Mexico) and the NSREC (Canada) for the financial support provided to carry out my doctoral studies.

Finally, I would like to thank Martha for her patience, moral support and affection during this four years away. Sweetheart, you have been always in my mind.

ABSTRACT

The Film Coating technique is used for the surface treatment of fragile webs, as very little stress is applied on the paper. Film coating is also known to produce a contour-like coating with superior fiber coverage. These advantages are achieved due to the use of a pre-metering step, in which the film is first formed, before being applied to the paper. Since the metered film is an essential part of the final product, a thorough understanding of the metering nip flow is central to the better design of film coating equipment.

Thus, this thesis deals with the understanding of the hydrodynamics of the metering nip flow, the hydrodynamic instabilities generated and the rheological behavior of coating colors in the nip. To carry out this investigation, a laboratory coater featuring industrial operating conditions and the CFD commercial software POLY2D™ were used. Industrial paper coating colors were tested, as well as Newtonian reference fluids. The instabilities that appear in the metering nip were evaluated in terms of operating conditions and coating color rheology. Moreover, three models of process viscosity were proposed, which were functions of either the maximum pressure, the torque, or the combination of the pressure gradient and the torque. Each process viscosity model was assessed by means of Computer Fluid Dynamic simulations of the metering nip flow.

Among the main findings, we observed that the instabilities are related to the process speed, coating color rheology, and mixing makedown procedure. The ribbing pattern is practically insensible to the metering and transfer speeds (at very high transfer speeds), whereas increasing the metering speed can eliminate the spitting phenomenon. Very viscous fluids generate wide ribs and the spitting appears at higher transfer speeds. In terms of the nip gap, three hydrodynamic configurations were observed, depending on the capillary, inertia, or air entrapment effects. The spitting phenomenon was found to be independent of the hydrodynamic configuration. Moreover, metering nip pressure measurements were found useful in assessing the

stability of the coating flow in the nip in terms of ribbing and spitting. And finally, from temperature measurements, viscous dissipation in the nip was found to be negligible.

From a rheological viewpoint, the viscosity of the coating colors in the metering nip, the process viscosity, was found different from that measured in the rheometer. This is due to the different conditions that prevail between the rheometer and the metering nip, and because under such different conditions the fluid responds differently. That difference is due to the different conditions encountered between the rheometer and the metering nip. The results are independent of the three process viscosity models proposed in this investigation: either based on the maximum pressure, on the torque, or a combination of the pressure gradient and torque. Furthermore, structure breakdown of the coating colors was found such that steady state may not be reached in the nip, so that the process viscosity becomes relevant. From the numerical simulations, it was found that the pressure-driven contribution to the flow (due to the nip contraction) in the center of the nip is independent of inertia, constant for Newtonian fluids, and dependent of the shear-thinning index of the coating colors.

From the assessment of the process viscosity models, the process viscosity from maximum pressure measurements should preferably be used when the extensional behavior of the coating colors is known. The process viscosity from torque measurements, on the other hand, should be applied at low speeds, range in which the coating colors behave as power law fluids. The process viscosity from the pressure gradient and the torque (lubrication theory) was found to be the more reliable one to describe the hydrodynamics of the metering nip. A combination of a transient Cross model with the process viscosity from the lubrication theory is suggested as first attempt at describing the coating color rheological behavior in the metering nip.

In summary, this investigation have shown new insights about the metering nip flow in terms of behavior, control and elimination of the instabilities generated, flow stability assessment, and the manner coating colors behave, from a rheological viewpoint, when flowing through the metering nip.

RÉSUMÉ

Le procédé de couchage permet d'améliorer les propriétés de la surface du papier et donc la qualité d'impression. Parmi les méthodes de couchage disponibles, la technique de Couchage à Film présente des avantages multiples, par exemple, celui de pouvoir coucher avec un faible taux de contrainte sur le papier. Ces avantages sont dus à la présence d'une section de dosage où un film mince est d'abord formé, avant d'être appliqué sur le papier. Le fait que ce film devienne partie intégrante du papier couché fait de la section de dosage une partie très importante du procédé de couchage à film.

Cette thèse traite de la compréhension des instabilités hydrodynamiques produites dans la section de dosage. Le comportement rhéologique des sauces de couchage est aussi étudié. Afin de reproduire les conditions d'opération dans une coucheuse industrielle, une coucheuse de laboratoire a été employée. De plus, des simulations numériques ont été effectuées à l'aide du logiciel commercial POLY2D™.

Nous sommes intéressés aux relations entre la machinabilité des sauces de couchage et l'apparition de défaut comme les rides ou les projections. La machinabilité peut être relié à la mesure du profil de pression dans l'entrefer de dosage, tandis que les principaux facteurs conditionnant les instabilités de la couche son la vitesse de transfert, la rhéologie des sauces de couchage ainsi que leur préparation. Il apparaît que le comportement des rides est indépendant de la vitesse de dosage dans la gamme des hautes vitesses de transfert. De plus, trois configurations hydrodynamiques ont été observées, chacune caractérisée par des effets de capillarité, d'inertie ou d'entraînement d'air. Il faut souligner l'importance du mélange particulier de sauces pour leur machinabilité. De plus, il est établi grâce à des mesures de température, que la dissipation visqueuse est négligeable dans l'entrefer de dosage.

Dans l'entrefer, trois méthodes son utilisés pour évaluer la viscosité des sauces de couchage. Elles font appel soit à la mesure de la pression maximale dans l'entrefer, soit à la mesure du couple sur la barre de dosage, soit à la mesure du gradient de pression

et du couple. Dans tous les cas la viscosité de procédé a été trouvée différente de la viscosité mesurée dans un rhéomètre classique, soit en régime permanent ou transitoire. Il faut souligner qu'il a été observé que le passage de la sauce dans l'entrefer provoque une modification de la structure de la sauce sans qu'un régime stable ne soit atteint. Il est alors toujours nécessaire de définir et d'évaluer correctement la viscosité de procédé. En autre, à partir de simulations numériques, nous avons constaté que la contribution de Poiseuille à l'écoulement dans le centre de l'entrefer est indépendante des effets d'inertie, constante pour des fluides newtoniens mais dépendantes de la rhéofluidifiance des sauces de couchage.

Finalement, la comparaison des résultats numériques et expérimentaux nous a permis de conclure que la pression maximale peut être utilisée pour déterminer la viscosité de procédé seulement lorsque le comportement extensionnel des sauces est connu. Le couple est plus utile pour évaluer la viscosité de procédé à bas taux de cisaillement, lorsque le modèle de la loi de la puissance décrit bien le comportement rhéologique des sauces de couchage. La théorie de lubrification peut être utilisée pour déterminer la viscosité de procédé au centre de l'entrefer, mais des travaux supplémentaires sont nécessaires afin de clarifier l'influence du comportement extensionnel, du préconditionnement, et du temps sur la rhéologie des sauces de couchage.

En résumé, ces travaux ont permis d'éclaircir l'état de connaissance concernant l'écoulement dans l'entrefer de dosage en termes du comportement, du contrôle et de l'élimination des instabilités. La stabilité de l'écoulement et la manière dont les sauces de couchage se comportent dans l'entrefer ont aussi été éclaircies.

CONDENSÉ EN FRANÇAIS

L'importance du papier et du carton dans la vie moderne de tous les jours est évidente. Le papier fournit les moyens d'enregistrement, de stockage et de propagation de l'information. Actuellement, le dernier cri de la technologie d'impression et d'emballage demande une meilleure qualité de la surface du papier. Ainsi, pour améliorer la qualité d'impression et l'apparence du papier, une sauce de couchage est appliquée sur sa surface. La sauce de couchage du papier, dans sa forme la plus simple, consiste en des pigments plus un adhésif. Les pigments augmentent la qualité de la surface et l'adhésif lie simplement les particules de pigment entre elles et au papier.

Dans l'industrie de couchage du papier, la demande croissante de papier couché a emmené le procédé à des vitesses de couchage de plus en plus hautes, mais en même temps le procédé de couchage a généré un certain nombre de contraintes. À haute vitesse, une série de défauts se présente réduisant la qualité du produit. Des rides, des projections et un phénomène de brouillard apparaissent dans la technique de couchage à film, tandis que des rayures se forment dans le couchage à lame.

La technique de couchage à transfert de film est basée sur la presse à film. Aujourd'hui, cette technique est surtout employée pour recouvrir le papier de liquides pigmentés. Les avantages principaux de ce procédé sur celui de couchage à lame sont la manipulation de suspensions à haut contenu de solides et la réduction du nombre de déchirements, entre autres. Une presse à film est composée d'un rouleau de support et d'un rouleau de transfert (aussi appelé rouleau applicateur) qui tournent à contre sens, et d'une petite barre de dosage. La sauce de couchage parvient au système de couchage par une chambre d'alimentation avant l'entrefer de dosage. La barre de dosage, tournant dans le même sens que le rouleau de transfert mais à une vitesse beaucoup plus basse, contrôle la quantité de sauce de couchage qui reste sur la surface du rouleau de transfert. Le papier, soutenu par le rouleau de support, arrive à l'entrefer d'application et prend la couche qui a été déposé sur le rouleau de transfert.

Une fois que la couche a été appliquée, le papier passe à travers d'une série de tambours de séchage et de rouleaux de calandrage avant l'entreposage.

Afin remplir son objectif, la sauce de couchage doit pénétrer dans le réseau des fibres du papier. Ce procédé de pénétration dépend des propriétés physiques du papier –la perméabilité et la porosité, par exemple– et de la rhéologie de la sauce de couchage. Les propriétés rhéologiques les plus communes sont la rhéofluidifiance et la viscoélasticité. Aux grandes vitesses de cisaillement cependant, le comportement rhéologique peut changer selon la formulation. Le comportement rhéologique est aussi responsable de l'apparition de défauts sur la couche. Les propriétés rhéologiques des sauces de couchage sont donc contrôlées afin de diminuer les problèmes liés à la qualité du film lors du dépôt de la couche sur le papier.

Le but principal du procédé de couchage est de créer un film uniforme sur le papier. Les mécanismes qui génèrent les défauts doivent être mieux compris afin que les défauts soient réduits ou, si possible, éliminés. La connaissance du comportement rhéologique des fluides est aussi importante afin d'améliorer la performance du procédé. L'objectif général de cette thèse est donc d'étudier de façon intensive l'hydrodynamique et le rôle de la rhéologie des sauces de couchage dans l'écoulement dans l'entrefer de dosage. Nous considérerons des conditions opératoires et des formulations de sauces de couchage rencontrées dans l'industrie.

Dans le procédé, un des problèmes liés à la qualité du film est la formation de rides. En fait, c'est l'imperfection la plus commune sur le film. Ce défaut résulte de l'équilibre entre la tension superficielle et les forces visqueuses dans le ménisque en aval de l'entrefer de dosage. Le nombre capillaire, qui détermine le rapport des forces de tension superficielle et des forces visqueuses, a été employé pour déterminer les conditions opératoires pour lesquelles ce phénomène de ride apparaît. De la littérature, on apprend que dans chaque ride il y a deux petits vortex dont l'élimination entraîne la disparition des rides. En pratique, une corde placée sur le ménisque en aval de l'entrefer peut retarder la formation des vortex et donc l'apparition des rides à des

nombres capillaires élevés. De plus, les rides peuvent aussi être réduites lors des changements appropriés des conditions opératoires. Ainsi, en diminuant la vitesse de la barre de dosage, le ménisque se déplace vers le centre, ce qui diminue la taille de rides.

Un autre défaut commun dans l'entrefer de dosage est l'apparition des projections. Du point de vue pratique, il semble facile de les éliminer, par exemple en augmentant la vitesse de la barre de dosage. On peut aussi faire de petits changements dans la formulation des sauces de couchage afin de retarder leur apparition à plus hautes vitesses de transfert. Cependant, on connaît mal les phénomènes hydrodynamiques et les conditions de fonctionnement responsables de leur apparition.

Par ailleurs, la plupart des rouleaux employés dans l'industrie ont un revêtement déformable. Il a pour objectif de retarder ou de diminuer l'apparition des rides. Le revêtement diminue aussi la sensibilité de la qualité de la couche aux conditions opératoires. La déformation du revêtement a comme conséquence une interface liquide-solide dont la forme est à priori inconnue. Une meilleure compréhension du phénomène exige l'utilisation de modèles numériques en complément des travaux expérimentaux d'abord menés. La déformation du revêtement peut être représentée avec des modèles unidimensionnels. Des études à deux ou trois dimensions exigent l'utilisation des équations de Navier-Stokes, mais la complexité liée à la modélisation du procédé de couchage, et plus particulièrement en ce qui concerne la surface libre, a donné lieu à un nombre minimum de travaux à ce sujet.

La rhéologie des sauces de couchage joue un rôle très important dans le procédé de couchage. Pour étudier le comportement rhéologique des sauces de couchage, des tests de cisaillement à l'état stable et oscillatoire sont réalisés. Toutes les sauces sont rhéofluidifiantes à des vitesses de cisaillement moyennes. À des vitesses de cisaillement plus élevées, le comportement rhéologique peut être soit rhéoépaississant, soit avec un plateau de viscosité ou soit rhéofluidifiant. Les sauces de couchage sont

aussi viscoélastiques à très basses déformations, une propriété qui peut affecter dans une certaine mesure la machinabilité du procédé de couchage.

Les effets des propriétés rhéologiques des sauces de couchage sur la machinabilité du procédé sont très importants. Un fluide rhéofluidifiant présente des rides plus minces qu'un fluide newtonien. D'autre part, lorsqu'un fluide est viscoélastique, les problèmes de machinabilité apparaissent à des vitesses plus basses. Les rides deviennent très irrégulières et dépendantes du temps. L'épaisseur de la couche change aussi en fonction du degré d'élasticité du fluide. Finalement, lorsque la viscosité élongationnelle est trop élevée, elle génère des rides plus grandes et plus difficiles à niveler.

La thixotropie est une autre propriété rhéologique qu'on peut rencontrer avec les sauces de couchage. L'étude de la thixotropie a besoin des tests rhéologiques à l'état transitoire. Le test rhéologique transitoire le mieux adapté au procédé de couchage est celui de la croissance de la vitesse de cisaillement. Lorsque ce test est exécuté sur les sauces de couchage, on observe un dépassement du signal de viscosité, suivi d'une chute. L'amplitude du dépassement dépend de la vitesse de cisaillement imposé initialement et de la formulation. Les essais de croissance de vitesse de cisaillement suggèrent que les structures dans le fluide se cassent en traversant l'entrefer de dosage. En outre, des tests rhéologiques de fluage peuvent être réalisés et liés à la machinabilité du procédé. La contrainte maximale mesurée pour des fiables vitesses de déformation est proportionnelle à la vitesse de couchage. Ce résultat, établi dans une coucheuse à lame, n'a pas encore été confirmé dans une coucheuse à film.

Le concept rhéologique appelé «viscosité de procédé » a été utilisé à partir de l'analyse des champs de déformation identifiés dans le procédé de couchage. Ces champs de déformation sont différents de ceux mesurés en rhéomètrie classique. La viscosité de procédé du fluide est déterminée et comparée à celle mesurée dans un rhéomètre. Pour le couchage à lame, la viscosité de procédé des sauces de couchage est similaire à celle donnée par le rhéomètre. Cependant, dans le couchage à rouleau, la viscosité de procédé de suspensions de $CaCO_3$ est différente de celle donnée par le rhéomètre.

Il faut alors établir si la viscosité de procédé des sauces de couchage, qui sont de suspensions plus complexes que les simples suspensions de $CaCO_3$, est similaire a celle mesurée dans rhéomètre classique.

Avec l'information disponible jusqu'à maintenant, nous sommes en mesure de présenter le premier objectif de cette thèse. D'abord, on se propose de déterminer si les sauces de couchage se comportent dans l'entrefer de dosage comme dans celui d'un rhéomètre classique. Une nouvelle méthode pour évaluer la viscosité de procédé est proposée. Elle est comparée à une méthode présentée antérieurement dans la littérature, ainsi qu'aux méthodes de rhéologique classique. Le deuxième objectif de cette thèse consiste à étudier l'hydrodynamique de l'écoulement dans l'entrefer de dosage et les instabilités qui y sont produites. Les défauts sont reliés aux conditions opératoires et au comportement rhéologique. Comme troisième objectif, nous nous proposons de reprendre de manière approfondie la problématique de la viscosité de procédé, en mettant l'accent sur le comportement rhéologique des sauces de couchage. Une troisième méthode pour évaluer la viscosité de procédé est introduite et ses résultats sont comparés à des essais rhéologiques réalistes. Finalement, le quatrième objectif comprend l'évaluation des trois méthodes proposées pour la détermination de la viscosité du procédé à l'aide des outils numériques.

Afin d'accomplir les objectifs spécifiques, on a réalisé des essais expérimentaux avec une coucheuse à film de laboratoire. La coucheuse représente fidèlement les conditions de couchage industrielles (1900 m/min, par exemple). Divers appareils de mesure sont installés sur la barre de dosage : un capteur de pression pour permettre de mesurer le profil de pression dans l'entrefer de dosage, deux capteurs de déplacement pour déterminer à tout moment la position de la barre de dosage, et un couplemètre. La température peut aussi être mesurée dans le réservoir, à la tête d'alimentation, sur la barre de dosage, et dans le film sur le rouleau de transfert.

Les fluides utilisés dans les expériences sont des fluides newtoniens et des sauces de couchage modèles et industrielles. Les fluides newtoniens ont été élaborés à partir de

solutions de polyéthylène glycol de 45, 84 et 104 mPa.s de viscosité. Les sauces de couchage modèles ont été préparées sur une base sèche de 100 parties d'argile, 10 de latex, 0,04 de dispersant, avec différents contenus de solides et de concentrations de carboxymethylcellulose. Deux sauces de couchage industrielles ont été aussi testées. Ces sauces ont été préparées avec deux mélangeurs différents mais à partir de la même formulation.

Les tests rhéologiques montrent que toutes les sauces de couchage présentent un comportement rhéofluidifiant avec un plateau de viscosité à haut taux de cisaillement. Le modèle de loi de puissance à viscosité plateau s'est bien ajusté aux données expérimentales. Les sauces de couchage ont aussi présenté un comportement viscoélastique à de fiables déformations caractérisé par un module élastique variant entre 100 et 300 Pa, selon la formulation.

Pour accomplir le premier objectif de cette thèse, l'évaluation de la viscosité de procédé des sauces de couchage a été faite à partir de deux méthodes. La première, à partir de données sur la pression maximale, telle qu'introduite dans l'article de Réglat et Tanguy (1998), et la deuxième à partir des mesures de couple sur la barre de dosage. Pour cette dernière méthode, une analyse dimensionnelle sur l'entrefer de dosage a été effectuée. Le concept de Metzner et Otto a aussi été utilisé en considérant que les sauces de couchage obéissent au modèle de loi de puissance. Des liquides newtoniens ont été utilisés comme fluides de référence pour les deux procédures.

La viscosité de procédé calculée à partir de la pression maximale a été environ six fois plus grande que celle mesurée dans le rhéomètre. On en conclut que les formulations testées ont présenté un comportement rhéoépaississant dans l'entrefer de dosage. Cependant, la viscosité de procédé calculée à partir du couple a été relativement près de la valeur de la viscosité dans le rhéomètre. Des formulations testées, certaines ont une viscosité de procédé plus grande que celle du rhéomètre, et d'autres plus petite. En comparant les viscosités de procédé calculées à partir de la pression maximale, du couple et la viscosité mesurée dans le rhéomètre, on a trouvé que les trois viscosités

différaient les unes des autres. On a pu imputer ces disparités aux différences existantes entre les deux équipements employés : la géométrie particulière de l'entrefer de dosage et celle du rhéomètre (cisaillement pur), l'histoire de cisaillement qui n'est pas reproduite dans les essais de rhéologie classique, et le temps caractéristique de procédé, qui est très petit dans l'entrefer comparé à la déformation infini dans le rhéomètre.

En ce qui concerne le deuxième objectif, les instabilités hydrodynamiques dans l'entrefer de dosage ont été étudiées. À partir des expériences en laboratoire, on a trouvé que, à haute vitesse, les rides des sauces de couchage ont été plus petites que celles observées avec des fluides newtoniens et des suspensions de $CaCO_3$. Lorsque la largeur de l'entrefer a été diminuée, la transformation des rides larges en de petites rides a été plus significative dans le cas des sauces de couchage que dans les cas des suspensions de $CaCO_3$. Ce phénomène peut être attribué à la rhéofluidifiance accrue des sauces de couchage, à l'utilisation d'un petit diamètre de barre de dosage, et probablement, aux propriétés élastiques des fluides.

L'effet de la vitesse de transfert a été non significatif, particulièrement à de hautes vitesses de procédé, où la largeur des rides s'est trouvée dans la gamme attendue pour des très grandes valeurs de nombre capillaire. Dans les mêmes conditions, la vitesse de dosage a aussi eu peu d'influence. Par contre, aux basses vitesses de procédé la vitesse de la barre de dosage a significativement diminué la largeur des rides, en stabilisant l'écoulement et en augmentant le taux de nivelage des rides. Du point de vu rhéologique, les sauces les plus visqueuses ont présenté les rides les plus larges. D'autre part, les deux sauces de couchage industrielles, plus visqueuses que les sauces modèles, ont déclenché des rides plus petites. Pour les deux formulations industrielles, le comportement des instabilités a été significativement différent. La sauce de couchage industrielle préparée à de très haut taux de cisaillement a présenté moins de défauts sur la couche.

Un autre défaut, les projections, a été aussi étudié. On a observé que les projections dépendent de la concentration de CMC et du contenu de solides. Plus la concentration de CMC et de solides sont élevées, plus la vitesse de couchage peut être augmentée sans projections. D'autre part, le comportement des projections a été tout à fait différent pour les deux sauces de couchage industrielles, ce qui a montré à nouveau l'importance du mélange. De l'information complémentaire a été obtenue à partir des mesures rhéologiques pour des écoulements rampants. La vitesse à laquelle le début des projections a été observée ne semble pas être fonction de la contrainte seuil maximale à l'état transitoire mesurée dans le rhéomètre.

En ce qui concerne le profil de pression, un profil plus stable a été obtenu lorsqu'il y a absence de projections. La pression minimale en aval de l'entrefer a diminué avec l'augmentation de la vitesse de transfert, mais elle s'est accru avec l'augmentation de la vitesse de dosage. A haute vitesse de dosage, l'écoulement a été plus stable et sans projections.

Après avoir étudié le comportement rhéologique et l'hydrodynamique des sauces de couchage dans l'entrefer, on a considéré à nouveau la notion de viscosité de procédé afin de mieux comprendre le procédé de couchage. Dans ce troisième objectif, la viscosité de procédé a été essentiellement évaluée à partir des prédictions obtenues à l'aide de la théorie de la lubrification. Cette théorie a été appliquée dans le centre de l'entrefer, où les lignes de courant sont presque linéaires. Au centre, l'écoulement est une combinaison d'écoulements de Couette et de Poiseuille. La contribution de Couette vient de la rotation des rouleaux, mais celle de Poiseuille, qui vient de la contraction de l'entrefer, a été déterminée à partir des simulations numériques, puisque cette information n'est pas accessible expérimentalement.

Afin de comparer la viscosité de procédé avec l'information qu'on peut obtenir du rhéomètre, des essais de croissance de vitesse de cisaillement ont été menés. Un petit dépassement de la contrainte a été observé pour toutes les formulations. Ce dépassement est proportionnel à la concentration en CMC et au taux de solides.

Lorsqu'on augmente la vitesse de cisaillement, la viscosité transitoire diminue toujours, même pour des déformations plus grandes que celles du procédé. Ces résultats suggèrent qu'un cassement partiel des structures dans les sauces de couchage a lieu lors du passage par l'entrefer, et que l'état stable n'y est pas atteint.

De plus, des simulations numériques ont été réalisées pour évaluer la contribution du type Poiseuille à l'écoulement au centre de l'entrefer. Une contribution constante et égale à 1.95 a toujours été obtenue, indépendamment des conditions opératoires et des effets d'inertie, pour des fluides newtoniens. Cependant, cette valeur varie lorsque on considère des fluides rhéofluidifiants. Les résultats numériques ont aussi été employés pour calculer la valeur de la contrainte au centre de l'entrefer, valeur nécessaire pour l'interprétation des résultats expérimentaux.

Pour les sauces de couchage testées, la viscosité de procédé a été trouvée inférieure à la viscosité transitoire. Il semble que les sauces de couchage ont un comportement plus rhéofluidifiant que celui prédit par le rhéomètre. Les structures sont cassées plus rapidement dans l'entrefer parce que la vitesse de déformation est aussi beaucoup plus grande que dans le rhéomètre.

Le quatrième objectif a été l'étude de la rhéologie de procédé des sauces de couchage à l'aide des outils numériques, afin d'évaluer les procédures utilisées pour déterminer la viscosité de procédé. Les résultats numériques présentés dans cette thèse dépeignent une application de la méthode numérique décrite en Fourcade et al., (1999). Le modèle numérique rend compte de la déformation du revêtement déformable du rouleau de transfert, mais ne permet pas d'inclure une surface libre. Les sauces de couchage sont modélisées comme des fluides dont la rhéologie est représentée par le modèle de Cross. La méthode des éléments finis de Galerkin a été utilisée dans le code commercial POLY2D™.

La méthode basée sur les mesures de pression maximale donne une viscosité de procédé de cinq à sept fois plus grande que celle du rhéomètre. La comparaison des

résultats numériques pour la pression maximale avec les résultats expérimentaux a montré que les paramètres rhéologiques utilisés dans le modèle de Cross surestiment la viscosité des sauces de couchage. D'autre part, la viscosité de procédé surestime encore plus les résultats expérimentaux. En tenant en compte de la viscosité élongationnelle les résultats analytiques auraient pu être meilleurs. De fait, cette méthode doit être préférablement utilisée lorsque le comportement élongationnelle des sauces de couchage est connu, comportement rhéologique qui n'a pas été vérifié pour les sauces de couchage utilisées dans le cours de cette investigation.

La méthode basée sur les mesures de couple donne une viscosité de procédé plus proche de celle mesurée dans le rhéomètre. Les résultats numériques du couple ont montré à nouveau que les paramètres rhéologiques utilisés surestiment la viscosité des sauces de couchage. L'applicabilité du concept de Metzner and Otto (1957) et la rhéologie des sauces de couchage apparaissent comme les raisons des différences. Dans les conditions opératoires étudiés, l'écoulement dans l'entrefer n'est plus laminaire, contrairement a ce qu'exige le concept de Metzner et Otto. De plus, les sauces de couchage sont considérés comme des fluides de loi de la puissance. Aux taux de cisaillement normalement trouvés dans l'entrefer, il est plus probable que les sauces soit plutôt à la viscosité de plateau. En résume (régime laminaire, loi de la puissance valide), la méthode de couple est plutôt applicable pour des vitesses de procédé basses.

La méthode basée sur le gradient de pression et sur le couple semble être la mieux adaptée. En effet, l'évaluation de la viscosité de procédé a été faite dans une région de cisaillement dominant. De plus, dans ce cas, la viscosité de procédé a été comparée à avec des mesures de viscosité transitoire, tests plus représentatifs de ce qui se passe dans l'entrefer de dosage. La viscosité de procédé trouvée par cette méthode est plus petite que la viscosité transitoire.

Comme les paramètres du model de Cross ont surestimé la viscosité des sauces de couchage, une nouvelle façon de représenter sa rhéologie a été suggérée afin de

mieux représenter les donnés expérimentales à l'aide des outils numériques. On a suggéré l'utilisation des paramètres de Cross pour les sauces de couchage, mais en état transitoire, en combinaison avec la viscosité de procédé comme viscosité plateau. Des nouvelles simulations numériques ont montré que le modèle rhéologique semi-analytique, représente mieux la rhéologie des sauces de couchage. Cependant, une meilleure caractérisation rhéologique du comportement élongationnelle de la sauce, de l'influence du temps de cisaillement et du préconditionnement de la sauce avant d'arriver à l'entrefer de dosage sont nécessaires afin de mieux modéliser le comportement des sauces de couchage dans l'entrefer de dosage.

En résumé, ce projet a amené plus de connaissance sur l'hydrodynamique de l'écoulement dans l'entrefer de dosage, sur les instabilités qui y sont générés, et sur le comportement rhéologique des sauces de couchage du papier. Avec les essais expérimentaux, nous avons permis de constater que les sauces de couchage se comportent d'une façon similaire aux fluides plus simples, mais avec des rides plus petites; la génération des instabilités dépend de la formulation des sauces de couchage, c'est à dire, de leur comportement rhéologique; la pression et le couple peuvent être utilisés pour évaluer la stabilité de l'écoulement; le mélange des sauces de couchage affecte directement la machinabilité des sauces de couchage. Des simulations numériques, nous savons que, au centre de l'entrefer, la contribution Poiseuille est indépendante des effets d'inertiels, constante pour des fluides newtoniens, et dépendante de la rhéofluidifiance du fluide. Du point de vu rhéologique, nous avons vu que la viscosité des sauces de couchage dans l'entrefer de dosage est différente de celle mesurée dans un rhéomètre. Des tests d'écoulement rampant ont montré que la machinabilité des sauces de couchage n'est pas directement reliée à la contrainte transitoire maximale. Finalement, l'état stationnaire n'est probablement pas atteint dans l'entrefer de dosage. On sait maintenant également que les trois procédures pour déterminer la viscosité de procédé fonctionnent si on prend toutefois en compte les effets extensionnelles dans le cas de la méthode basée sur la pressure maximale, et si on fait le calcul aux taux de cisaillement bas pour le cas du couple. La combinaison du couple et du gradient de pression donne une meilleure approximation

de la rhéologie du procédé des sauces de couchage. Un nouvel modèle rhéologique semi-analytique est proposé comme première approche lors de la modélisation de la rhéologie des sauces de couchage dans l'entrefer de dosage. Cependant, des tests rhéologiques sont encore nécessaires pour mieux comprendre le rôle de la rhéologie des sauces de couchage dans le procédé.

Ces résultats ouvrent de nouvelles perspectives de recherche. Il reste encore beaucoup des détails qu'il faut clarifier, par exemple, l'étude numérique tridimensionnelle du procédé de dosage en incluant la surface libre, données qui peuvent être validées avec des mesures tridimensionnelles (en utilisant, par exemple, deux ou trois capteurs de pression sur la barre de dosage). Un autre axe de recherche important serait l'étude des effets de migration de particules sur les mesures de couple. Il serait aussi intéressant d'étudier le comportement rhéologique du recouvrement du rouleau en faisant de visualisations dynamiques de sa déformation pour valider les résultats numériques.

IMPORTANT

The results of this PhD thesis are presented in four articles. Each paper is published in a conveniently chosen journal. Consequently, some redundancy will be found, especially with the literature survey and with materials and methods section. For clarity reasons, the second chapter contains only the literature survey, the third one contains the experimental setup, but all the bibliographic references are compiled at the end of the document. Some of the four articles is followed of additional results and remarks which are not part of the submitted manuscript.

INDEX

LIST OF TABLES

LIST OF FIGURES

Chapter 1

Chapter 2

Chapter 3

Chapter 4

Chapter 5

Chapter 6

Chapter 7

NOMENCLATURE

SI Units

b = distance between parallel plates

F_N = fluid normal stress

g = gravity

G = shear modulus of the deformable cover

h = nip gap in the lubrication region

h^* = metering rod relative position (apparent nip gap)

h^*_0 = reference metering rod relative position (reference apparent nip gap)

h^*_{cc} = metering rod relative position for coating colors

H = calculated nip gap

k = Trouton ratio (μ_{sh}/μ_{ex})

K = thermal conductivity

K_s = Metzner and Otto constant

K_2 = shear-thickening index (Eq. 2.2)

K_3 = critical shear rate at which shear-thickening behavior is observed (2.2)

l = metering nip length

L = capillary length

m = consistency index in the power law model

n = normal vector to the transfer roll surface

n = power index in the power law model

n_s = number of samples

$\mathbf{n}_F$ = vector normal to the boundary of the fluid domain

$\mathbf{n}_S$ = vector normal to the boundary of the solid domain

p = shear-thinning index in the Cross model

P = pressure within the nip

P_i = variable measured (statistic analysis)

P^* = average variable measured (statistic analysis)

P_{max} = maximum pressure within the nip

P_{max0} = reference maximum pressure within the nip (Newtonian fluids)

$P_{max\,cc}$ = coating color maximum pressure measured within the nip

P_{maxi} = maximum pressure within the nip at V_{ti}, μ_i and h_i

q = Lagrange multiplier

Q = flow rate

r_m = metering rod radius

r_t = transfer roll radius

R = capillary radius

S = wetted surface of the metering rod

S_d = standard deviation

S_N = solid normal stress

S_R = speed ratio

S_v = rate of viscous heat production by viscous dissipation by unit volume

t = tangent vector to the metering rod surface

t = consistency index in the Cross model

t_e = elastomer thickness

t_δ = probability coefficient

t_F = tangent vector for the fluid domaine

T = effective torque measured on the metering rod

T_n = numerical torque calculated on the metering rod

u = displacement vector for the deformable cover

v = velocity vector for the fluid

v_s = slip velocity

v_x = velocity in the main flow direction

v_y = velocity in the transverse flow direction

V = speed of the upper or lower plate

V_t = transfer roll speed

V_m = metering rod speed

V_{t0} = reference transfer roll speed

dP/dx = pressure gradient in the lubrication region

x = main flow direction

y = transverse flow direction

Greek symbols

α = Poiseuille contribution to the flow in the center of the nip

α_e = extensional flow contribution to the maximum pressure

α_s = shear flow contribution to the maximum pressure

δ = delta de Kroneker

ε = linearized stress tensor for the deformable cover

$\dot{\gamma}$ = shear rate

$\dot{\gamma}_a$ = apparent shear rate

$\dot{\gamma}_{proc}$ = effective process shear rate

μ = viscosity

μ_{exp} = steady state shear viscosity from the rheometer

μ_{Cross} = steady state shear viscosity from the Cross rheological model

μ_{pl} = steady state shear viscosity from the power law rheological model

μ_{sh} = shear viscosity (Eq. 4.15)

μ_{ex} = extensional viscosity (Eq. 4.15)

μ_0 = reference Newtonian viscosity

μ_{proc}^{P} = process viscosity calculated from pressure measurements

μ_{proc}^{T} = process viscosity calculated from torque measurements

μ_{proc} = process viscosity from the lubrication approximation

η^+ = transient viscosity

η_0 = viscosity plateau at low shear rates (Cross model)

η_∞ = viscosity plateau at high shear rates

ρ = density

τ = shear stress between parallel plates

τ_w = wall shear stress

σ = shear stress in the center of the metering nip

σ^+ = transient shear stress

σ_F = stress tensor for the fluid

σ_S = stress tensor for the solid

σ_T = surface tension

ω = relaxation parameter

Ω_F = fluid domain

Ω_S = solid domain

Γ = solid-fluid interface

Γ_{Fm} = solid-fluid interface along the metering rod

Γ_{Ft} = solid-fluid interface along the transfer roll

CHAPTER 1

INTRODUCTION

The significance of paper and paperboard products in modern life is obvious to everyone: no manufactured product plays a more meaningful role in every area of human activity. Paper provides the means of recording, storage and dissemination of information; "Paper is a vehicle: it transmits not only written language, but the deepest thoughts, the most vivid illustrations" (ECC Int. Tappi J. 82(1999):6, p32). Virtually, all writing and printing is done on paper; it is the most widely wrapping and packaging material and is also important to structural applications (Smook, 1997).

Paper has traditionally been defined as a felted sheet formed on a screen from a water suspension of fibers (Smook, 1997). Paper derives its name from the reedy plant Papyrus. The ancient Egyptians produced the world first writing material by heating and pressing together thin layers of the plant stem. The first authentic papermaking originated in China as early as 100 AD utilizing a suspension of bamboo and mulberry. The Chinese subsequently developed papermaking into a highly skilled art (Smook, 1997).

The advanced technology of printing and packaging has placed great demands on the surface quality of the paper sheet. The principal reasons for applying a pigment coating to paper and paperboard are to improve both printability and appearance. In its simplest form, the paper coating fluid –the coating color, as it is called in the paper industry– consists of a pigment plus an adhesive. Pigment coating provides a surface that is more uniform in appearance and more receptive to printing ink than natural paper fibers, and the adhesive binds the pigment particles to one another and to the base paper. The coating film, in turn, facilitates the paper printing process and enhances the graphic reproduction by providing enhanced gloss, smoothness, and

color printing detail and brilliance. The improvements in print quality are readily apparent, particularly in image areas or when multiple colors are involved.

The origin of coated paper is obscure. Historical references indicate that efforts to coat paper with pigments were made as long as several hundred years ago. In the beginning of the 19th century, coating was a manual task. In the latter half of the 19th century, the situation changed markedly when substantial technical effort resulted in the development of mechanical methods for coating paper at commercial scale (Hagemeyer, 1997).

The growth in demand for coated paper has moderated considerably from that experienced during 1935 to 1970 (Hagemeyer, 1997). In Canada, the demands for coated paper rose in sales by 5.8% from 1997 to 1998 (Desbiens, 1999). The current outlook remains quite favorable, with demand expected to be dominated by the influence of economy development, higher level of education, increasing in leisure time and literature readers in the growing population (Hagemeyer, 1997). The pronounced growth in the less developed part of the world will also demand higher quality paper that will particularly influence the necessity for coated paper (Gerstenberger, 1999).

The increasing concern for a higher productivity in the paper coating industry has resulted in higher process speeds, but at the same time the application process has met a certain number of constraints. When the application speed is increased, the film applied on the paper is not uniform anymore. A series of defects appear; thus, not only is the quality of the coated paper reduced, but also the printing quality and profits. The kind of defects in the coating film depends on the process speed and the coating technique. For example, in blade coating, typical defects are streaks, bands and weeps; misting, ribbing, spitting and orange peel correspond to film coating, technique that is delineated in this introductory chapter by using the metering size press as a representative example.

1.1 Film coating

One of the key components in the successful manufacturing of a coated product is the choice of the process to be used. About a dozen major coating applications techniques can potentially apply a coating color to a web: blade coating, slot coating, curtain coating, slide coating, spray coating, *film coating*, etc (Coyle, 1992). Many specific configurations exist within each one of these techniques. As a result, a wide variety of coating methods is available to choose from. Good examples of final coated products are magnetic and adhesive tapes, photographic films, and magazine and photographic paper.

In the paper industry, the film coating transfer technique is based on the use of the *metering size press*, which was originally created to apply sizing solutions of starch to the paper as means to add value to the product by enhancing the paper quality. Today, this equipment is also used for pigmented fluids and for other specialized surface applications with the descriptive term maintained. The simplest example of that same technique, familiar to every homeowner, is the painting of walls and ceilings with a paint roller.

Metered size presses were introduced on the European paper market in 1992 (Ahlroos et al. 1999). Since then, the process has developed rapidly and is commonly used as a cost efficient way of upgrading newsprint and supercalendered paper grades:

- It produces fewer breaks than the blade coating technique (3-5% more efficient).
- It allows the application of coatings with high solids content.
- It yields a coating surface following the web contour with superior fiber coverage.
- It permits to use weaker and less expensive furnish with higher filler content.
- It also allows coating both sides of the paper simultaneously.

These advantages are mostly obtained due to a metering process, where a thin film is first formed, before being applied to the paper. A typical metering size press is composed of a contra-rotating backing roll, a transfer roll (also called applicator roll), and a metering rod (Fig. 1.1a). The coating color -continuously homogenized in a delivery tank- is introduced to the coating system by a coating feeder chamber before the metering nip. A rigid, smooth, and small-diameter metering rod, co-rotating with the transfer roll but at much lower speed, controls the amount of coating color that remains on the transfer roll surface. The metered film quality is of primary importance since it becomes part of the final product (Fig. 1.1b). The paper web, supported by the backing roll, is introduced in the application nip and picks up the metered film that has been applied on the transfer roll beforehand (Fig. 1.1c). In the application step, the paper is subjected to almost no stress, an important advantage over the blade coating technique. Both equal-diameter backing and transfer rolls have an elastic cover to avoid

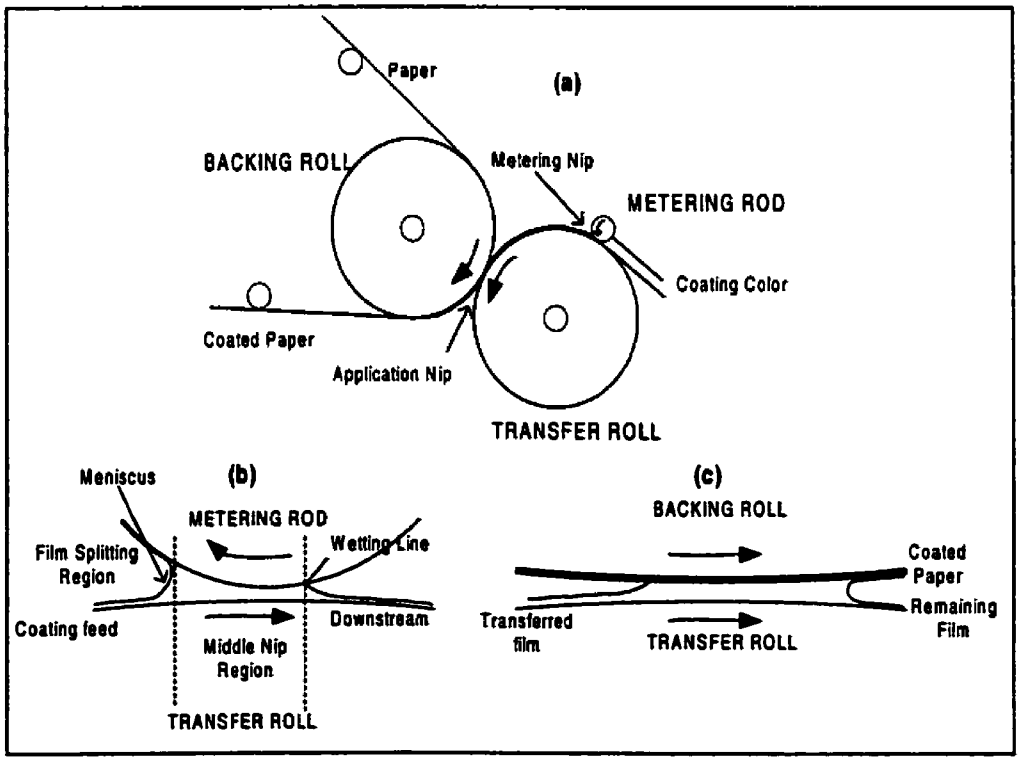

Figure 1.1 The metering size press (a), the metering nip (b), and the application nip (c).

them from clashing and to improve the final coating film quality on the paper. Once the film coating layer has been applied, the paper goes to a series of dryer drums and calendering rolls before being wrapped.

1.2 Paper Structure and Paper Coating

The basis of paper manufacture has been the same for many years. The fiber suspension can be produced either mechanically or chemically. In the first process, mechanical energy is used to separate the fiber from the wood matrix. In the second procedure, the bonding material, i.e., lignin, is separated chemically. Still, a combination of both methods may be employed to produce the pulp; the pulp ratio must be chosen according to the need of the final paper properties. Once the pulp is made, it is deposited onto a rotating cylinder, where the paper web is formed on the outside because of water removal. The wet web is removed at the top of the cylinder, passes through press rolls for dewatering, and then into steam-heated, cylindrical drier drums.

The final paper web is composed of a series of fibers of different sizes and lengths packed in a random way creating a porous structure. Most of the fibers are long and with different shapes: cylindrical, elliptical, or flat. These different fibers produce interconnected pores of different size and direction. In fact, the pore-fiber paper structure is very complex and very difficult to describe (Poulin et al. 1997).

The penetration of the coating color into the porous structure depends on the physical properties of the paper and the fluid, i.e., the porosity, which is the relative amount of empty space; the permeability, which represents the capacity of the porous media to let a liquid flow through it; and the tortuousity, which is the random arrangement of the fibers (and pores) in the paper. Furthermore, the liquid influences the penetration with its own surface tension, the contact angle in the interface liquid-solid-gas, and its rheological behavior.

Once the coating color particles have filled the surface of the paper, the fluid phase penetrates the web by flowing into the empty passages. The flow depends on the geometry of the porous structure and the physical properties of both solid and fluid material (humidity and rheology, for example). However, the factors that most influence the penetration are the adsorption of the liquid into the pores, the expansion of the fiber net, the pressure exerted by the air inside the pores and the compression of the paper (Poulin et al. 1997). When an external force is applied, the predominant mechanisms are the capillary pressure and the external force itself. The fluid rheology and the structure of the pores dominate the penetration when a high external pressure is applied, as it is often the case in coating processes (Poulin et al. 1997). The penetration plays an important role in the coating process and has a direct impact on the smoothness, opacity, gloss, and brightness of the final coated product.

1.3 Paper Coating Formulations

All paper coating colors share the main same ingredients. They are aqueous suspensions of mineral pigments (kaolin or $CaCO_3$) and binder particles (latex, starch) together with functional additives (carboxymethyl cellulose, CMC; polyvinyl alcohol, PVA; hydrophobically modified alkali swellable emulsion, HASE.) The pigment gives the paper the desired characteristics of brightness, gloss, and opacity. The binder keeps the pigment particles together and sticks them to the paper. Additives are a large group of chemicals that act as dispersants, water retention aids, pH controllers, viscosity modifiers, lubricants, brightness agents, etc.

The rheological properties of the coating fluid depend on the relative amount of each component in the formulation. The coating color rheology is defined by the solids content, the shape and size of the particles, the packing ability, the rheological properties of both polymer additives and the interaction among all of them (Engström and Rigdahl, 1990). The relative amount of each ingredient may give the coating color some specific characteristics, like shear-thinning, shear-thickening, or viscoelastic properties. A typical behavior of a coating color under pure shear is shown in Fig. 1.2.

There is no Newtonian plateau in viscosity at low shear rates, but a definite shear-thinning behavior is always seen (at steady flow conditions), which may be followed by a shear-thickening behavior at high shear rates, depending on the formulation. At very high shear rates, for instance, a clay-starch coating usually has constant viscosity, whereas a high solids content may trigger shear-thickening behavior (Roper and Attal, 1993).

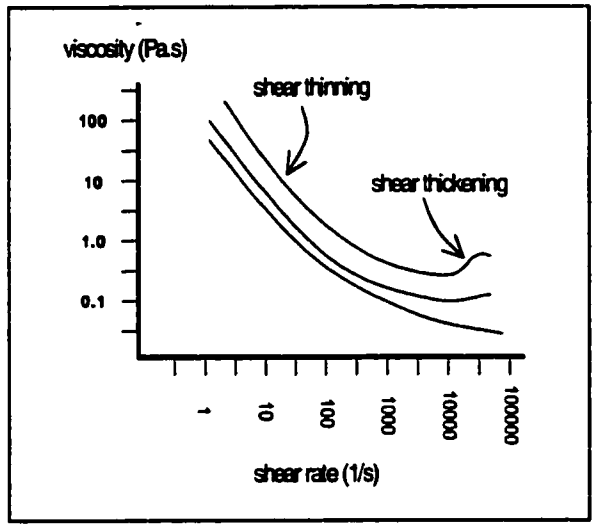

Figure 1.2 Typical rheological behavior of coating paper formulations (Roper and Attal, 1993).

1.4 Typical Film Coating Defects

The objective of any coating process is to produce a uniform coating film on a continuous web with a required dry-thickness and some specific physical properties. Any undesired property that prevents the film from serving its stated purpose is a defect. Defects in the coating layer can appear from mechanical or hydrodynamic sources, electrostatic charges, stresses that arise in drying, air motion, vibration, dust, impurities, etc. In the metering nip, the most common defects are (Fig. 1.3)

- Ribbing, the formation of uniform lines regularly spaced running downweb that may appear from hydrodynamic causes.
- Cascade, a seashore pattern running across the web produced by air entrapment in the meniscus when it is pulled through the gap by a high metering roll speed.
- Spitting, when the velocity is so high that the coating starts to be projected out of the meniscus, where the drop size is a function of the metering speed.

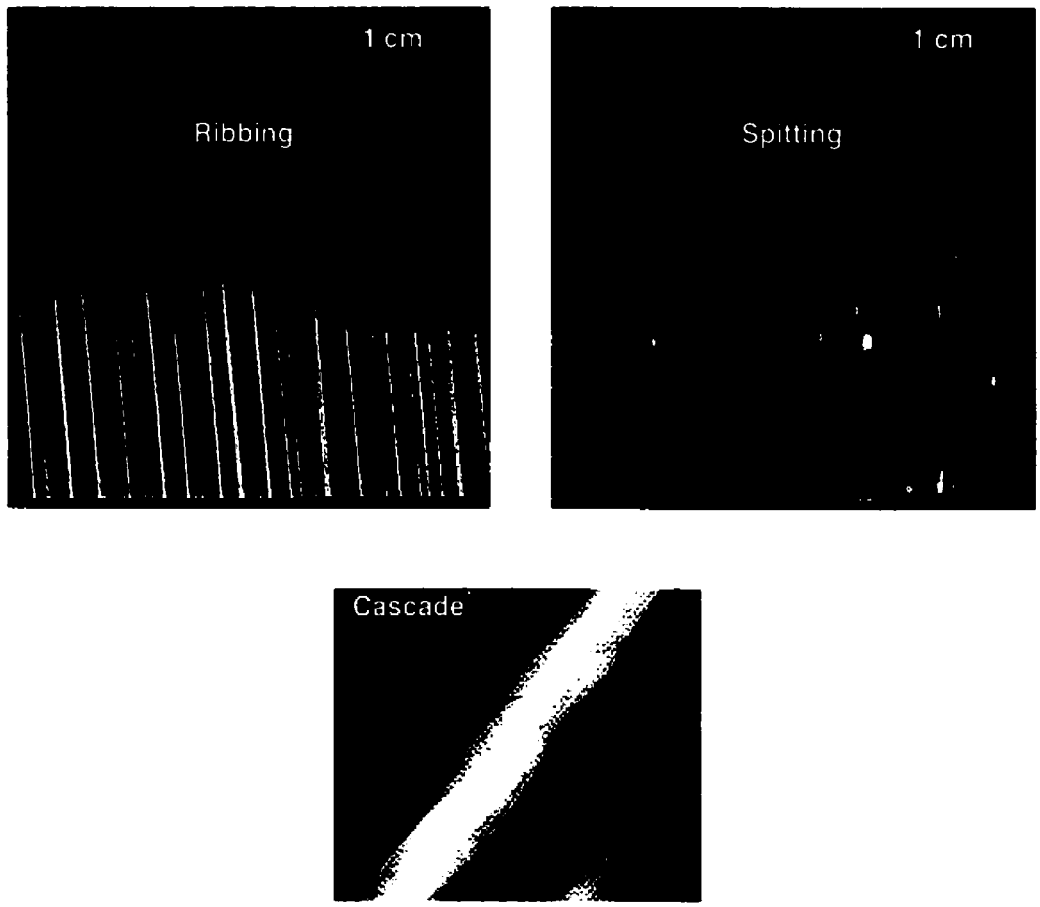

Figure 1.3 Main defects produced in the metering nip (The cascade picture is taken from Coyle et al. 1990b).

In the application nip, the most common defects are (Fig. 1.4)

- Mottle and blotchiness, which refer to defects that are usually due to coverage variations of an irregular nature caused by non-uniform base surface energies charges.
- Orange peel, a similar pattern to that of the surface of an orange that may appear due to a high solids concentration during the film splitting process.
- Misting, when the velocity is so high that the coating starts to splash out the meniscus as form of very small drops, very similar to those of a spray.

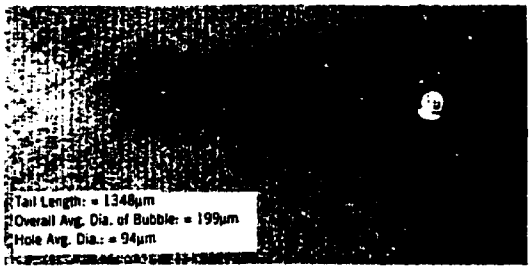

Bubble with a streak.

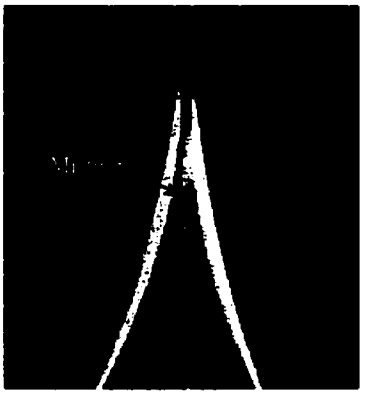

Misting.

Orange peel.

Figure 1.4 Main defects in the application nip (Roper et al. 1998).

1.5 General Objective

The requirements for a successful industrial coating operation mean creating a uniform film on the paper. Some components in the coating color tend to increase certain defects while others tend to eliminate them. Some imperfections arise because

of the sensitivity of the film quality to the process parameters. In practice, the determination of the optimal formulation for a given operating window is usually achieved by trial and error.

From a scientific standpoint, roll coating processes have widely been studied by using analytical, numerical or experimental techniques. Both analytical work and numerical models have been used to describe the hydrodynamics of the coating process. Coating formulations have been investigated to elucidate their role in the appearance of the defects in the coating film. Despite all the work done, the hydrodynamics is still not well understood, especially at high speeds and with industrially based coating colors.

The advantages of the metering process makes it a very important key to obtain a superior coated paper quality. Thus, the **general objective** of this thesis is to further examine the flow hydrodynamics of the metering film formation in the context of the metering size press with coating colors and at very high speeds. The mechanisms that trigger the film defects should be better understood, so that they can be controlled, minimized, or, if possible, eliminated. The coating color rheology is also investigated: its role in the appearance of defects on the metered film, its relevance with regard to classical rheological measurements and its behavior in the metering nip. At the end, numerical simulations are carried out to be compared to the experimental results and to deeper examine the metering nip flow in regard to coating color rheology.

CHAPTER 2

LITERATURE SURVEY

In the metering size press, the operations of film formation and film application are carried out separately. Both of them involve the manipulation of the coating fluid within small gaps between rotating rolls, as found in every roll coating process. As a result, the fluid flow hydrodynamics are governed by the principles of fluid mechanics, which are also complicated by the influence exerted by the air-liquid interfaces, static and dynamic contact lines, the non-Newtonian behavior of the coating fluids, and the deformable roll cover (Coyle, 1992).

This thesis deals with the understanding of the metering film formation. In this chapter, the available information about the hydrodynamic instabilities is presented. The rheological behavior of the coating colors is also reviewed, as well as its role in the appearance of the coating defects. At the end, the specific objectives are formulated.

2.1 Metering flow instabilities

When the speed is increased, two hydrodynamic instabilities appear in the metering nip: ribbing, a wavy film surface profile seen in the cross machine direction; and spitting, a series of little drops projected out of the nip; both defects are reviewed in this subsection.

2.1.1 Ribbing

The familiar simple case of brush marks, which appear when paint is applied to a flat surface with a paint brush, represents a similar example to the case in which a film is formed by passing a fluid through a small gap between rollers, as in the metering

nip of the metering size press. The ribbed surface often obtained decreases the final product quality. Long ago, Pearson (1960) found that the appearance of ribs in the film is a consequence of the forces acting in the film formation process. The capillary number was then defined, $Ca=\mu V_l/\sigma_T$, to measure the relative importance of viscous forces over surface tension forces. Pearson (1960) also used it to define the ribbing onset, i.e., the conditions at which the ribbing pattern appears. From a similar point of view, Pitts and Greiller (1961) arrived at a criteria for the stability of the flow (whether ribs appear or not), neglecting both inertia and gravity forces. They found that when the pressure gradient at the exit of the nip is negative, the flow is stable and uniform. Later, Greener and Middleman (1981) reported that in the reverse configuration (co-rotating rolls) ribs appear at higher speeds than in the forward mode (contra-rotating rolls). Downstream the nip, the reverse configuration keeps the pressure gradient negative at higher capillary numbers than the forward configuration (Greener and Middleman, 1981).

Since then, the capillary number has been extensively used to define the ribbing onset (Bauman et al. 1981; Carvalho and Scriven, 1997; Coyle et al. 1990a; Greener et al. 1980; Mill and South, 1967; Savage, 1984). For instance, Mill and South (1967) followed the theoretical work of Pearson (1960) and Pitts and Greiller (1961), arriving at a more general expression for the onset of ribbing because they used also several sets of rolls of different radii. Bauman et al. (1981) investigated the role of polymers on the ribbing onset, finding that elasticity is a destabilizing factor, in agreement with observations. They evidenced that large extensional stresses in a transient extensional flow may contribute to reduce the stability of the coating flow. However, the model only described qualitatively the phenomena, although the idea of roll coating as a transient process was qualitatively correct.

Savage (1984) tried to define a new mathematical theory to predict the ribbing onset by using a linear perturbation analysis with the lubrication theory, for which the proposed model agreed closely to experimental observations. Rushack (1982) also used nearly parallel flow and applied stability theory, but boundary conditions derived

from his own solution of the two dimensional flow, for which the predictions worked reasonably well. The proposed model of Ruschak (1982) was found to be effective in assessing the stability of air displaced by liquid (as it occurs in every coating process.)

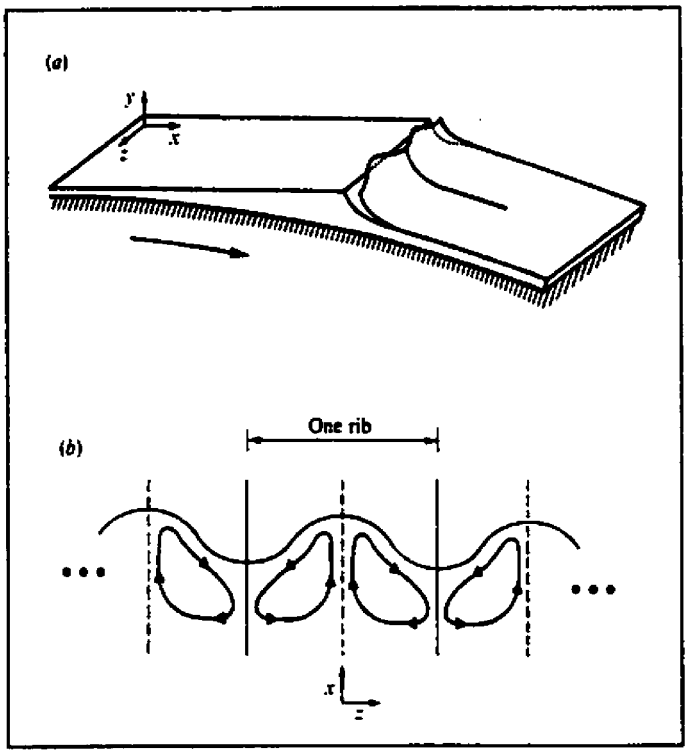

Figure 2.1 Eigenvectors for the three-dimensional perturbation in a ribbed film (Coyle et al. 1990d).

Kristler and Scriven (1984) published an asymptotic analysis of coating flows. They found that recirculations appear downstream and upstream the nip, depending on the capillary number and the speed ratio of the rolls. Coyle et al. (1986) compared that asymptotic analysis with the lubrication theory, in forward roll coating, to the solution of the 2-D Navier-Stokes equations with the finite element method. Those recirculating patterns in the film splitting region were also found. Later, Coyle et al. (1990d) analyzed the stability of the flow to three-dimensional disturbances with Fourier components. They reported that the transition to ribbing is due to end effects. Numerically, they found

that each rib contains a pair of vortices in which the liquid rotates such that the flow wells up to the free surface under the crest of the rib and descends under the trough (Fig. 2.1). Except at the symmetry plane, there is a strong downstream velocity component superimposed on the recirculating flow; consequently, fluid elements move downstream in helical trajectories under the ribs. The rotation of the liquid in each rib comes from the recirculations downstream the nip. Coyle et al. (1990d) suggested that the flow is inherently three-dimensional and ribbed, although the latter may be unimportant or imperceptible. The base flow in the meniscus is made three-dimensional by the end effects of the rolls due to a non-uniform distribution of fluid momentum at the roll edges. However, in the cases where the edges of the rolls do not play a significant role -in an 8 m wide paper film coater, for example-, ribbing is still present. As a result, the theory of end effects as the leading perturbation of the main flow may not apply to film coating.

On the other hand, Hasegawa and Sorimachi (1993) experimentally confirmed the theory of the recirculations under the meniscus as the origin of the wavy meniscus and the ribbed film. A string spanned over the gap to touch the surface of the meniscus has the apparent effect of eliminating the ribbing. Later, Decré et al. (1996) analyzed the influence of the string on the hydrodynamics of the flow. They showed that the ribbing can be delayed up to 20 times its natural onset, and that the string position controls the film splitting ratio and the total flow rate of the process (Decré et al. 1996). When in contact to the free surface, the string acts similarly to the blade, stabilizing the flow downstream the nip by delaying to higher capillary numbers the creation of the vortices.

Coyle et al. (1990b), in reverse roll coating, found experimentally that the parameters that govern the flow stability are the capillary number and the speed ratio. General stability diagrams were built (Fig. 2.2). At very low capillary numbers, the film is uniform. Ribbing develops at a critical capillary number above curve AB. If the speed is also increased, the uniform flow is replaced by the cascade instability as curve DE is crossed (air entrapment). The stability region shrinks or extends according to the nip

gap and the Reynolds number (for example, the stable area becomes smaller when the gap width decreases).

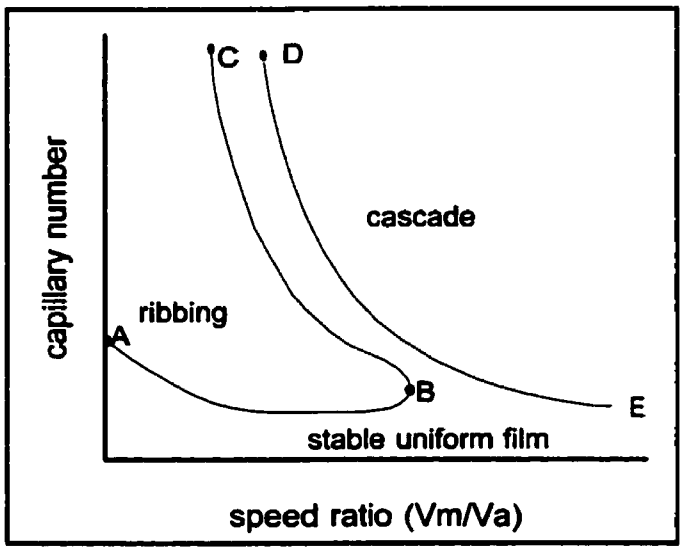

Figure 2.2 Stability diagram for reverse roll coating (Coyle et al. 1990b).

Gurfinkel and Patera (1997) employed the three-dimensional Navier-Stokes equations without inertia to investigate the ribbing instability. They found that for sufficiently large capillary numbers, the two-dimensional base flow becomes unstable to perturbations of the free surface. A small initial perturbation evolves into a finite amplitude rib (Fig. 2.3). In the meniscus region, the pressure gradient is sufficiently large for ribs to grow and develop. The meniscus shape converge to an asymptotic form, producing a ribbed film downstream the nip since the meniscus profile controls the free surface profile everywhere across the machine.

Réglat and Tanguy (1997) carried out the first investigation of the ribbing pattern at high speed (up to 1100 m/min). They showed that inertia may be important, and that the stability of the film is strongly linked to the flow hydrodynamics downstream the nip. As the velocity is increased, a transition is encountered from uniform ribs to ribs moving in the cross machine direction. Some ribs merge and divide so that the free surface

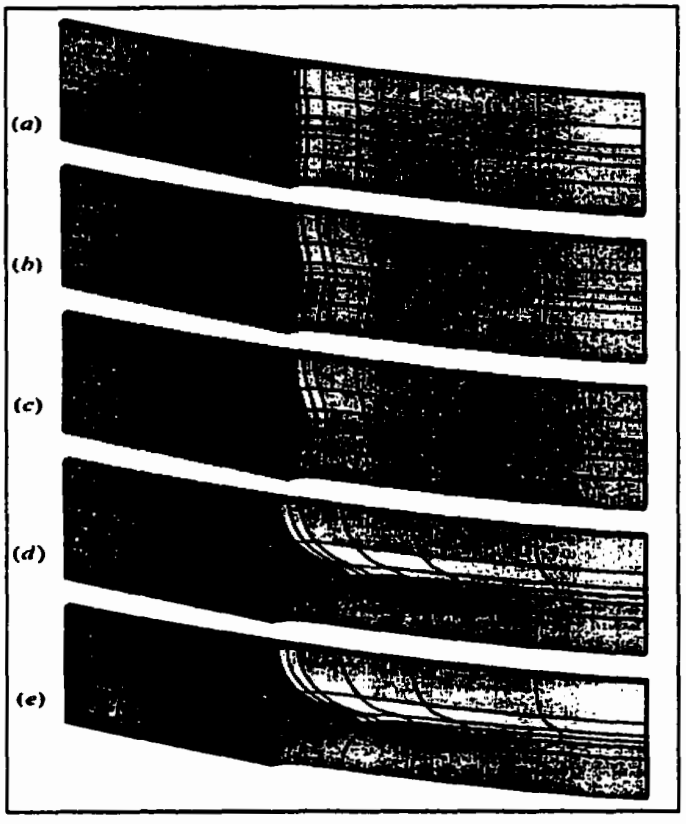

Figure 2.3 Evolution of the ribbing instability in symmetric forward roll coating (Gurfinkel and Patera, 1997).

profile downstream the nip changes continuously (Carvalho and Scriven, 1994, 1997; Coyle et al. 1990c; Réglat and Tanguy, 1997, 1998). The flow tends to be more stable if either the metering rod speed or the viscosity is increased (reducing the rib width). The same trends were seen with watery suspensions of $CaCO_3$ (Réglat and Tanguy, 1998), except that the rib width was larger than that observed with Newtonian fluids, and that the width increased when the nip gap became wider.

The extremely unstable flow with ribs appearing, disappearing and moving side to side remind what have been observed in the feeding chamber of a blade coater. Triantafillopoulos and Aidun (1990) carried out visualizations of the flow in the coating head (which had a transparent cover) and observed that if the process speed is

gradually increased, two-dimensional flow patterns appear and then evolve to a time-periodic three-dimensional flow. Toroidal eddies in the form of Taylor-Götler-like structures move side to side of the feeding chamber. Vertical band shapes are generated at the centerline and travel towards the ends, but at even higher speeds mushroom-like structures appear. The appearance of three-dimensional flow structures distributes unevenly the fluid and momentum transfer into the converging nip under the blade (Triantafillopoulos and Aidun, 1990). Furthermore, the centrifugal forces associated with those eddies may induce local particle concentration gradients, thus introducing viscosity and density variations. In theory, the blade distributes evenly the fluid on the substrate so that a uniform film should be obtained. In practice, coating defects are found when those vortices appear, like streaks and bands (Triantafillopoulos and Aidun, 1990). Three-dimensional flow patterns generate stationary streaks whose wavelength depends on the rheological properties of the coating fluid; even at higher speeds new instabilities appear in the cross machine direction and induce unstable streaks on the web (Triantafillopoulos and Aidun, 1990).

In comparison to roll coating, those recirculations exist downstream the nip (Coyle et al. 1990d; Gaskell, et al. 1998). Gaskell et al. (1998) observed those eddy in the reverse roll coating configuration. They consist of a single apparent large eddy containing two sub-eddies, one upstream, and the other one downstream the nip. The speed ratio can be decreased to move the downstream meniscus towards the nip center in order to decrease the size of the downstream sub-eddy (Fig. 2.4). A critical point is reached when the downstream sub-eddy becomes very small at the center and leaves only a single eddy attached to the upstream meniscus. The film surface profile originates at the downstream meniscus (Coyle et al. 1990d, Gurfinkel and Patera, 1997), so that the meniscus profile depends, in turn, on whether vortices are present or not. Therefore, the free surface accommodates itself according to the flow hydrodynamics of the liquid flowing beneath it so that a non-uniform distribution of momentum finally results in a uneven film. The string proposed by Hasegawa and Sorimachi (1996) somehow makes more uniform the momentum distribution under the meniscus and changes the pressure profile, stabilizing the flow. Furthermore, from the

observations of Coyle et al. (1990b), by increasing the speed ratio a transition is made from a ribbed film to a stable flow, and then to the cascade phenomena. When the metering rod speed is increased, the downstream meniscus moves towards the nip center while the downstream vortices (Gaskell et al. 1998) and the ribbing (Réglat and Tanguy, 1998) become smaller, until the meniscus arrives to the upstream side of the nip, where the possibility of air entrapment rises (cascade phenomena).

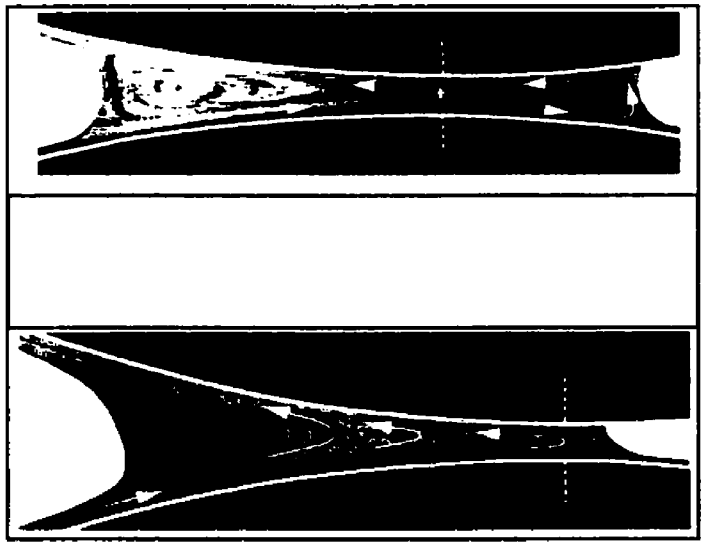

Figure 2.4 Laser illuminated dye trace of reverse-mode meniscus coating showing the co-existence of both primary and secondary recirculations (above). After an increase in speed (below), the recirculation disappears downstream the nip (Gaskell et al. 1998).

Pitts and Greiller (1961) showed the importance of the pressure profile in roll coating flows. The pressure profile can be calculated (Carvalho and Scriven, 1997; Coyle et al. 1986; Fourcade et al. 1999; Greener and Middleman, 1975) or measured (Gaskell et al. 1998; Poranen and Niemistö, 1999; Réglat and Tanguy, 1997, 1998). Fourcade et al. (1999), numerically (right), and Réglat and Tanguy (1997), experimentally (left), obtained the pressure profile shown in Fig. 2.5. Both profiles follow the same trend, but the differences are due to the assumptions implied in the numerical model (the lack of free surface downstream the nip, for instance). Still, both agree qualitatively with what has been already reported in the literature.

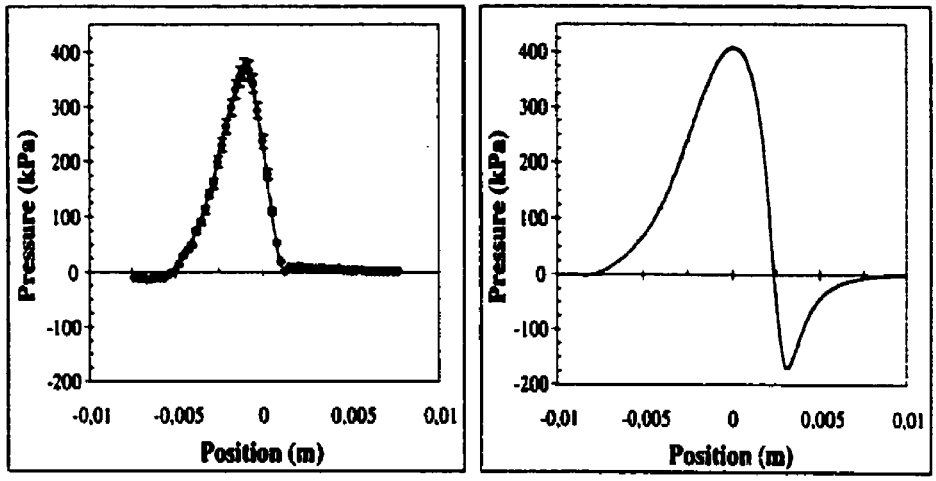

(a) Experimental data. (b) Numerical data.

Figure 2.5 Pressure profiles in the metering nip (Réglat and Tanguy, 1998).

Furthermore, in order to better understand the hydrodynamics of the flow in the metering nip, Réglat and Tanguy (1997) carried out a parametric analysis of the maximum pressure. They proposed, based on Newtonian fluids, the following relationship to describe the maximum pressure behavior in the nip as function of the operating conditions

$$P_{max} = P_{max\,0} + \frac{\Delta P_{max}}{\Delta V_t}(V_t - V_{t0}) + \frac{\Delta P_{max}}{\Delta \mu}(\mu - \mu_0) + \frac{\Delta P_{max}}{\Delta h^*}(h^* - h^*_0) \quad (2.1)$$

where the subscript "0" corresponds to a reference value obtained experimentally. They also analyzed the behavior of the maximum pressure as function of the apparent nip gap (or metering rod relative position; Fig. 2.6). Two hydrodynamic configurations were observed, the first one at narrow gaps and more sensitive to inertia effects, and the second one at wide gaps and more sensitive to capillary effects (Réglat and Tanguy, 1998).

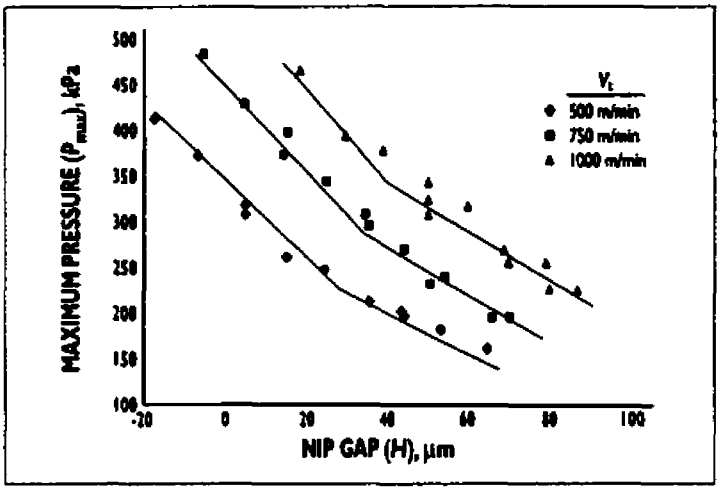

Figure 2.6 Maximum pressure as function of the metering rod position in the metering nip (Réglat and Tanguy, 1998).

2.1.2 Spitting

Spitting is a series of little drops projected out of the metering nip. It was first reported by Adachi et al. (1988), as splashing of liquid. At the edges of the rolls, there are two rings of liquid, bigger than the rest of the nip, as also reported elsewhere (Coyle et al. 1990d). The surface tension governs the size of the end ribs due the geometry of the rolls, and splashing of liquid is seen when centrifugal forces excess a characteristic limit (Adachi et al. 1988).

The film splitting region in the metering nip may be also subjected to spitting, depending on the operating conditions and formulation. It is likely that surface tension forces and the rheological properties of the coating color determine the performance of the film splitting region (Salminen et al. 1996). Grön et al. (1996) reported that a high solids content and high viscosity increase the spitting tendency, and also a low water phase viscosity and a high rod pressure; one way of alleviating the problem is to increase the metering rod speed and reduce its diameter (Rantanen, 1996; Triantafillopoulos and Smith, 1998). The fine and ball-form pigments are the worst and

plate-like pigments are the best to run without spitting (Rantanen, 1996). Soft transfer rolls and pigments with low aspect ratio also reduce spitting (Grön et al. 1996). Triantafillopoulos and Lee (1996) reported that as the vortices located downstream the nip break up when the speed increases, it causes the coating color to spit, particularly when the coating color viscosity is low. Spitting at the rod appears for colors with low polymer content and disappears with high polymer content (Grön et al. 1998). A high coating viscosity has a low solids limit for avoiding spitting at the rod (Triantafillopoulos and Smith, 1998). Despite all that information, no quantitative data about spitting, in terms of operating conditions and formulations, is available in the literature. More experiments are still needed so that the spitting phenomenon can be better understood.

2.2 Deformable roll cover

One of the changes made to the coating process in order to meet the needs of increasing speeds has been the use of a deformable roll. The principal advantages are (Carvalho and Scriven, 1993, 1997)

- To diminish the sensitivity of the coating film quality to mechanical instabilities.
- To achieve thinner coating films than those obtained with rigid rolls.
- To avoid the rolls from clashing.
- To maximize the amount of coating transferred to the substrate.

Carvalho and Scriven (1993, 1997), Coyle (1988), and Dobbels and Mewis (1978) used the lubrication approximation to describe the flow in a deformable gap. From these references, the more elastic the cover, the less pronounced the pressure profile, the more stable the flow, and the larger the ribbing wavelength. Consequently, the ribbing pattern remains longer than with rigid rolls. At a negative gap (interference between "undeformed" rolls), when the rod load increases, the gap becomes longer, narrower, and more parallel (Coyle, 1988). Carvalho and Scriven (1993) employed several models to describe the deformation of the roll cover. They found only slight

differences in the results when comparing a one-dimensional to a two-dimensional model. As a result, they suggested that the use of a one-dimensional spring-like model to describe the deformation of the roll cover would be reliable enough and also easier to adapt numerically. They additionally showed that a deformable nip can be operated at higher speeds than a rigid one without triggering ribbing (Carvalho and Scriven, 1994). Carvalho and Scriven (1997) made a stability analysis following a similar perturbation analysis of Coyle et al. (1990d), but with the lubrication theory together with a capillary-pressure-driven flow in the film splitting region. With such model they also found that in a deformable gap the ribbing pattern sets in at higher capillary numbers.

Cohu and Magnin (1997) showed that the elastic modulus of the rubber cover may be time-dependent so that it should be characterized according to the time-scale of the process. They also showed that there is a critical coating thickness under which the hydrodynamics of the flow are strongly affected. Rubber covers thinner than the contact-half nip length tend to decrease the coating thickness significantly by increasing the influence of the external load. Fourcade et al. (1999) also carried out an investigation of the metering nip flow with a deformable cover. The elastomer deformation was predicted from a static analysis considering the elastomer as incompressible and Hookean. The calculated pressure profile agreed qualitatively with the experimental results, although the differences were due to the assumptions implied in the numerical model, for instance, the lack of free surface downstream the nip (Fourcade et al. 1999). Very recently, Carvalho and Scriven (1999) applied, for the first time, a three-dimensional stability analysis of free surface flows to forward roll coating. Their main findings were that with soft covers and negative gaps the flow rate is nearly insensitive to the position of the rolls. After certain point, the film thickness becomes constant, which has been already seen in practice (Kokko et al. 1999). Furthermore, soft rolls delay the ribbing onset as much as twice the capillary number. This explain why deformable roll covers are often used in paper roll coating applications.

2.3 Coating colors rheology

Paper coating colors are aqueous mixtures of mineral pigments and binder particles along with soluble cobinder species and additives. It is usual for a coating suspension to contain up to ten ingredients. In many cases, the formulations have evolved and developed in response to the stringent requirements with respect to the paper properties, the handling properties of the coating fluid, the process speed, and the printing quality.

Each ingredient in the coating color formulation has a specific purpose. Typically, 80% to 90% of the dry formulation weight is composed of pigment. Several sorts of pigments are used, depending on the desired brightness, gloss, opacity, and the relative cost of the material. Kaolin and $CaCO_3$ are commonly used; TiO_2 is employed only for special paper grades due to its high cost. The aim of the binder is to cement the pigment particles firmly to the paper surface and to each other. The final dried coating film is not continuous, but a porous structure of pigment particles together at their points of contact. If too much binder is used, the voids begin to fill in and some light scatter capability is lost (Smook, 1997). Common binders are starch and latex, like styrene-butadiene and vinylacetate. Cobinders are used to give the coating color special characteristics. A typical example is the carboxymethyl cellulose, which increases the viscosity of the suspension and helps to avoid evaporation. A fourth category are the special additives. They are usually patented ingredients that improve the final coating paper properties. They are used to enhance the brightness, gloss, and opacity of the coated paper. Furthermore, dispersants help to make the suspension of particles during the coating makedown, bactericides kill the germs that could spoil the coating color during storage, defoamers decrease the possibility of air entrapment during coating makedown, handling and coating, and pH controllers maintain the suspension within a range of internal energy so that the fluid is more stable.

2.3.1 Coating colors characterization

The metering process subjects the coating color to a wide range of shear and extensional rates from the fluid makedown in the coating kitchen and the film formation in the metering nip to the film relaxation on the transfer roll surface. The coating color behavior under such conditions is certainly very complex. The formulation is then adapted in order to obtain some desired rheological properties so that the coating fluid performs adequately during the conditions of the coating metering film formation, the coating application, and fluid flow. Indeed, rheological measurements are always made to predict the coating color behavior in the coating process.

The viscous analysis of the coating fluid may be carried out in several ways. In the industry, Brookfield viscosimeters are usually used (Spindle # 4 at 100 rpm). Unfortunately, torque measurements in a infinite medium, where the shear rate is difficult to evaluate, is far from the actual process conditions. Still, industry uses it as a parameter of quality control in the coating makedown. On the other hand, under pure shear conditions, rheometers with a Couette geometry are usually employed to characterize the fluids in both steady state, oscillatory, and transient conditions. A tangential flow exists between two concentric cylinders, with a gap usually very small. The outer cylinder rotates so the shear rate depends on the speed of rotation. The measured torque and the gap allow to evaluate the viscosity and the elastic properties of the sample. But very high shear rates cannot be easily handled because of viscous dissipation (heating of the sample), particle migration and wall slippage. It is then when capillary rheometers are used. The sample flows through a capillary tube under steady state conditions, while a very high pressure is applied to a sample reservoir. The shear rates obtained in the tube lie usually in the same range as those experienced by the coating fluid during its metering and application. Entrance and exit effects can be used to evaluate normal stresses (Carreau et al. 1997). The extensional viscosities may be evaluated as well from using two capillaries of different length but with the same diameter (Kokko et al. 1999). However, using capillary viscosimeters require entrance and end effects corrections by using the Bagley method. In this method, data with

several capillaries with different length L but both equal radius R and flow rate Q are obtained so that the entrance pressure remains the same. Then the total pressure is plotted *versus* L/R at Q to obtain the entrance pressure loss (Macosko, 1994). Moreover, the slippage effect usually present when multi-phases systems are analyzed (particle suspensions, for example) has to be as well corrected by using the Mooney method. This technique requires measuring apparent wall shear rates $\dot{\gamma}_a$ at constant extrusion pressure (i.e., constant τ_w) for a constant L/R. τ_w is plotted *versus* 1/R in order to obtain the slip velocity v_s according to the relation $\dot{\gamma}_a = \dot{\gamma}_{a\infty} + 4v_s/R$ (Macosko, 1994).

Coating processes as with blade and rolls subject also the fluid to extensional fields that deform the coating color in the direction perpendicular to the main flow. Extensional flow rheometers have been designed to investigate the fluid rheological behavior under extensional conditions. Contrary to purely shear flow rheometers, extensional flow rheometers are mostly specially designed for the fluid under analysis. Carvalho et al. (1995), Cohu and Magnin (1995), and Fernando and Glass (1988) used a spinning fiber apparatus that sucked or extruded the sample to investigate the flow behavior under extensional conditions. Lavoie et al. (1997) designed an orifice rheometer that permitted to obtain very high deformation rates at small deformation in a mostly extensional flow. Isaksson et al. (1998) used a converging channel that extended or strained the fluid at a constant rate. Each technique has its own drawbacks since measuring the extensional viscosity requires creating a pure extensional flow, approach very difficult to achieve.

2.3.2 Coating colors shear viscosity

The most common rheological characteristic of coating colors is shear-thinning, which appears in practically all formulations. However, as the shear rate is increased, the behavior of the coating color may change according with its formulation, as in the references that follow, where the formulations used were all different (Fig. 2.7). No viscosity plateau is seen at very low shear rates. Shear-thinning behavior is found at relatively low shear rates. In most of the formulations, the viscosity tends to level off at

moderate shear rates, as shown in curve (a) (Carreau and Lavoie, 1993; Cohu and Magnin, 1995; Ghosh et al. 1997; Laun and Hirsh, 1989; Roper and Attal, 1993; Yziquel et al. 1999). Sometimes, instead of attaining a plateau, the shear viscosity continues to decrease with shear rate, as in curve (b) (Cohu and Magnin, 1995; Laun and Hirsh, 1989). Still, some of the formulations that have leveled off become shear-thickening at very high shear rates, as in (c) (Laun and Hirsh, 1989; Roper and Attal, 1993; Tsuji et al. 1990). Finally, some of the shear-thickening coating colors at high shear rates become shear-thinning at even higher shear rates, as curve (d) illustrates (Laun and Hirsh, 1989; Roper and Attal, 1993; Tsuji et al. 1990).

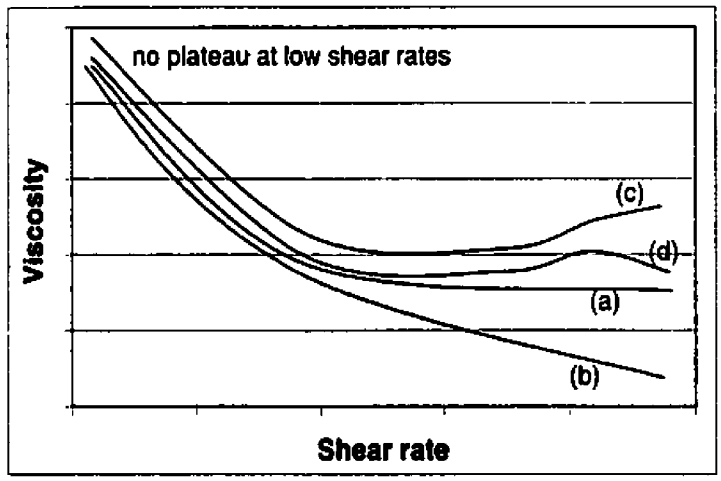

Figure 2.7 Different steady state rheological behaviors seen in coating colors (purely shear conditions).

When shear-thinning occurs, anisotropic domains align to the flow direction (Yziquel et al. 1999), and some particles links stretch and become parallel to the main flow decreasing the flow resistance and hence the viscosity. The viscosity may also decrease due to particle slippage (Tetlow et al. 1998). When all the particles are aligned and free from each other, the viscosity tends to be constant, although at even higher shear rates the particles may collide with each other and create shear induced structures (Kurath and Larson, 1990; Laun and Hirsch, 1989), increasing indeed the

viscosity of the fluid. To describe such rheological behavior of coating colors, Roper and Attal (1993) used the Cross model on the shear-thinning range and the Gillespie model to include the shear-thickening behavior of the fluid at very high shear rates, to develop the following empirical equation

$$\mu = \frac{1000}{1+K_1\dot{\gamma}^n} + \eta_\infty + \frac{K_2\dot{\gamma}}{K_3+\dot{\gamma}^2} \qquad (2.2)$$

where K_1 and n control the power-law dependent shear-thinning region, η_∞ is the viscosity plateau, K_2 controls the shear-thickening range and K_3 the critical shear rate at which shear-thickening behavior is observed.

The effect of the coating color rheological behavior in the process is vital. Coyle et al. (1990c) reported that purely viscous shear-thinning fluids differ little from the Newtonian ones at the same capillary number. An increased solids content generally increases the viscosity of the coating color; it may also trigger shear-thickening behavior at very high shear rates. Similar behavior may be seen when increasing the particle size (Roper and Attal, 1993). Purkayastha and Oja (1993) found that at low coating viscosities the predominant coating defect is spitting; at high coating viscosities the defects are streaks. Réglat and Tanguy (1998) showed that, at high speed, pigmented fluids followed the same ribbing behavior as with Newtonian fluids, except that the rib width was twice as large and increased with gap thickness.

Steady state shear viscosity tests in the laboratory have been generally used to predict the coating color rheological behavior in the process. However, the nature of the coating process requires the continuous utilization of fresh coating color, fluid that comes from the coating kitchen to the coating machine, passes through the nip, and is then applied to the paper. The coating color follows indeed a unique history from makedown to application. As a result, the conditions of the coating process may be such that steady state of the coating fluid may not be reached. All the numerical stability analysis carried out on coating processes also suggests the time as a very important

parameter (the steady state base flow is infinitesimally perturbed and its evolution is monitored as function of time to assess whether the fluid flow is unstable to that perturbation.) Therefore, the rheological properties of the coating color are also to be analyzed accordingly, i.e., under transient conditions so that the laboratory tests are closer to the actual process.

2.3.3 Coating colors extensional viscosity

Roll coating processes have a converging-diverging geometry in nature so that the fluid is compressed and stretched in a very short period of time. Indeed, the knowledge of the coating fluid behavior under extensional flow is necessary. It can be theoretically proven that the viscosity of a fluid under extensional flow, the extensional viscosity, is three times the viscosity under pure shear for Newtonian fluids (Macosko, 1994). This ratio is usually referred to as the Trouton ratio. Since coating colors are non-Newtonian, the extensional viscosity may play an important role in the process if its Trouton ratio differs from the Newtonian reference of three. Cohu and Magnin (1995) found that the Trouton ratio for several paints lied within the Newtonian range. Both Newtonian and paints showed to have a Trouton ratio of about 4.5, but the discrepancy was probably due to the shear contribution to the flow (Cohu and Magnin, 1995). Indeed, they concluded that the paints, which are suspensions similar to coating colors, behave more like Newtonian fluids under extensional flow.

Lavoie et al. (1997) designed an orifice rheometer in which deformation rates up to $5x10^5$ s^{-1} could be reached with a mostly extensional flow. The coating color behavior was found between the Newtonian reference and the elastic behavior of some polymer solutions at low Reynolds numbers, but no information about the Trouton ratio could be inferred. The difficulties lied in assessing the laminar flow for which the theoretical approach was developed, and the particle accumulation before and after the orifice. Isaksson et al. (1998) used a converging channel to evaluate the extensional viscosity of some coating colors. The shape of the channel was such that the suspension was extended or strained at a constant rate. The extensional viscosity was calculated with

the help of numerical simulations of inelastic fluids with similar viscous behavior, but neglecting the normal stress differences needed in the mathematical development due to the lack of available data. The extensional viscosity was found to decrease with strain rate and to increase when increasing the CMC concentration. The Trouton ratios that could be inferred decreased with CMC, strain rate, strain, and lied in a relatively wide range [6.1 –0.17] in a extensional rate range of [500 – 2500 s^{-1}]. This variation in the Trouton ratio suggests that both shear and extensional viscosities should be made at the shear rates of the process.

The role of the extensional viscosity in the instabilities of the coating process has also been investigated. Carvalho et al. (1995) experimented with two polymeric solutions having the same high shear rate viscosity, but one being extensional-thickening and the other one extensional-thinning, at extensional rates up to 10^3 s^{-1}. The onset of ribbing for both solutions was found at a capillary number smaller than that of Newtonian fluids. Although the Trouton ratio varied largely with the extension rate, the ribbing reduction was greater with the extensional-thickening solution, which Trouton ratio was 6 times the Trouton ratio of the extensional-thinning solution (at 1000 s^{-1}.) Indeed, high Trouton ratios may be undesirable in coating processes.

2.3.4 Coating colors viscoelasticity

Coating colors exhibit elastic behavior at low deformation (Carreau and Lavoie, 1993; Ghosh et al. 1997; Laun and Hirsh, 1989; Lavoie et al. 1997; Purkayastha and Oja, 1993; Yziquel et al. 1999). Viscoelasticity is due to particle interactions, chain formation and binder effects on the mineral particles (Engström and Rigdahl, 1990; Fadat et al. 1988; Purkayastha and Oja, 1993). Viscoelasticity is assessed by the magnitude of the elastic and viscous modulus. The elastic modulus is a representation of the level of structure of the coating color (Carreau and Lavoie, 1993), and the viscous modulus corresponds to the energy dissipated during flow.

The actual role of the viscoelasticity in the process is a controversial subject. On one hand, Bauman et al. (1981) by using a qualitative model treating the growth of a disturbance as an extensional flow, showed that elasticity is a destabilizing factor, in agreement with their own experimental observations. Greener et al. (1981) showed that viscoelastic fluids are far less stable than Newtonian fluids, with elasticity playing a mayor role in the onset of the ribbing instability. They confirmed the stability of the reverse roll coating configuration: ribbing was not observed under any reverse conditions (shear rates from 100 to 1000 s^{-1}), while in the forward configuration the elastic solutions could not be coated without ribbing at any small measurable speed. Coyle et al. (1990c) reported that elasticity decreases the film thickness, which becomes much less sensitive to speed ratio variations. Elasticity also induces irregular and time dependent ribbing. Kang et al. (1991) reported that viscoelasticity enlarges the gap width (the middle nip region of Fig. 1b), increasing the coating thickness and making the flow unstable (inducing the ribbing to appear at lower speeds.) Both shear-thinning and elastic polymer solutions produce an increased wipe ratio between rolls in the reverse configuration (Kang et al. 1991). Purkayastha and Oja (1993) showed that even at high strains (0.2) coating colors containing starch and CMC are still viscoelastic. Finally, Ghosh (1998a) reported that coating colors having low storage and loss modulus usually run without problems.

On the other hand, Greener and Middleman (1975) theoretically showed that elasticity makes only a minor contribution to the roll-separating force, and it is smaller than the corresponding negative contribution due to non-Newtonian effects. Carreau and Lavoie (1993) carried out experiments with an equipment capable of simulating the roll coating process, with its high strain rates. The coatings showed Newtonian behavior, even in the presence of CMC. Indeed, they showed that viscoelasticity may play a negligible role at very high deformation rates. This is in agreement with the fact that the storage modulus, associated with the internal structure of the suspension, decreases rapidly with increasing strain, while the loss modulus remains relatively constant. Wang et al. (1994) reported that, although not much difference was obtained in film thickness between purely viscous and viscoelastic liquids, certain anomalous

shapes of the coating bead were seen, that included concave and saw-tooth surfaces. This phenomena was observed with highly elastic fluids while still maintaining a stable film surface at speeds up to 54 m/min. Such a different conclusions about the role of viscoelasticity in the process may be due to the different coating formulations used in each case, similarly to the different shear dependent viscosity behaviors observed for a large number of coating color formulations (see Fig. 2.7).

Normal forces developed during shearing may play an important role in the process if the fluids show shear-thickening behavior. Laun and Hirsch (1989) used a cone-plate rheometer to characterize industrial coating colors. They reported that a coating color that exhibits shear-thickening behavior at very high shear rates may develop normal stresses. In transient tests, it was also shown that a shear-thinning coating color builds up a normal force when the deformation grows. The transition may be due to changes of the coating color structure with time (Laun and Hirsch, 1989); however, in a rheological test, the sample is continuously sheared (infinite deformation), but in the process, the coating color is continuously renewed and subjected to a finite deformation so that it might not be enough time to the build up a normal force.

2.3.5 Coating colors transient viscosity

In the reverse flow conditions, the complex film formation sequence of events can be simulated with step growth and step relaxation experiments. The step growth simulates the sudden increase in shear rate suffered by the coating color from the coating head to the nip, and the step relaxation mimics the sudden relaxation on the transfer roll surface after passing the nip. These tests have already been used to investigate the color behavior in coating processes (Cohu and Magnin, 1995; Laun and Hirsch, 1989; Yziquel et al. 1999). Laun and Hirsch (1989), studying industrial coating formulations at different solids contents (62% to 70%), found overshoots in viscosity during step growth tests. The overshoots diminished when decreasing the solids content, but at 4000 s^{-1} and 62% of solids, the coating colors hardly exhibited overshoots. Cohu and Magnin (1995), carrying out step growth experiments with paints,

found overshoots in shear stress. They diminished when increasing the set shear rate; at a shear rate of 7500 s^{-1}, no overshoot was observed. They concluded that, in the roll coating process, where the shear rates are much higher, one should not expect viscosity overshoots. Yziquel et al. (1999) found response overshoots when performing start-up tests with coating colors containing PVA. An overshoot in the transient viscosity was observed; it increased when the value of the initial shear rate of the experiment was increased. The same tests were performed with coating colors containing CMC, but the overshoot behavior was reversed, i.e., the overshoots decreased when increasing the shear rate.

2.3.6 Coating colors thixotropy

The investigation of the transient viscosity and the thixotropy of the coating colors are closely related, because they involve the change of the rheological properties with shear rate and time. The magnitude of shear rate is usually imposed to investigate the degree of structure of a coating color, and its duration is used to investigate the rate of destruction or recovery of the coating color. Carreau and Lavoie (1993), Cohu and Magnin (1995), and Laun and Hirsch (1989) have reported structure breakdown of the coating color, sometimes for shear rates as low as 100 s^{-1}. However, the same authors reported a characteristic recovery time that allows the structure to build up (the viscosity increases with time up to a certain value that may be the initial one). For Carreau and Lavoie (1993) and Cohu and Magnin (1995), the recovery time was found to be about 1000 s, 10^5 times longer than the lag time from the metering nip to the application nip, and about 10^3 times longer that the lag time from the application nip to the drying section (at 1000 m/min). This suggests that a large recovery time would not affect the rheological properties of the coating color film during its very short lag time on the transfer roll (from the metering to the application nip.)

Laun and Hirsch (1989) also showed how different clays results in different thixotropy. When working with English and American clays, the first one is more thixotropic than the second one. Those time-dependent shear stresses mostly have

their origin in shear-induced changes of the coating structure during flow. After a rapid change in shear rate, the coating needs some time to reach its steady state structure and state of stress (Laun and Hirsh, 1989). As the coating effective process time is of a few milliseconds, what happens before reaching its steady state may be very important.

Ghosh et al. (1997), with transient tests carried out at very small and constant shear rates, found a relationship between the appearance of defects on the film and the rheological behavior of the coating colors at both small deformation and deformation rates. Typically, the transient shear stress increases up to a maximum, which corresponds to the stress that has to be overcome so that the fluid can start to flow, and then the stress decreases. The peak in shear stress was correlated to the speed -in a cylindrical laboratory coater- at which the defects in the coated film start to appear. They found that the higher the shear stress peak, the higher the speed with a defect-free film running speed. However, it remains to be proven if this correlation applies as well in the converging-diverging geometry of a film coater.

2.3.7 Coating colors yield stress

Another common characteristic of coating colors is yield stress (Bingham fluids). The yield stress is the force needed to break down the network that is formed in the suspension so it can start to flow; it is the limit between viscoelastic solid and liquid-like behavior (Lavoie et al. 1997). Yield stress has been found in coating colors containing CMC (Engstrõm and Rigdahl, 1990; Fadat et al. 1988). Lavoie et al. (1997) reported the existence of yield stress in stress growth experiments at low shear rates. Greiffenberg et al. (1999) showed how the yield stress increases almost linearly with air content, in the same manner increasing the air and solids content increases the shear viscosity.

2.3.8 Coating color shear viscosity in the process

Although the coating process cannot be fully characterized by steady state rheological parameters (Lavoie et al. 1997), a great deal of useful information has been

obtained and applied to increase the runnability of the paper coating processes (Ghosh, 1998a,b; Hilden and Mustonen, 1998). Yet, no rheometer can reproduce the actual conditions of the film coating process. The rheological properties of the coating colors downstream from the metering nip (the rheological properties of the wet film on the transfer roll) are also needed to better understand the defects that occur in the application nip (Triantafillopoulos and Smith, 1998). Vidal et al. (1991) pioneered the investigation of coating color rheological behavior in the coating process. A viscosity was calculated in the blade nip. The pressure exerted by the fluid on the blade and the surface of contact were calculated as function of the blade deformation. The shear stress was function of the pressure distribution within the nip, whereas the shear rate was estimated from the film thickness. The viscosity of the formulations was found to decrease with the process speed, with shear rates around 10^5-10^6 s^{-1}. In these conditions, the process viscosity was found of the order of 20 mPa.s. For these same coating colors, higher values of viscosity were obtained in a capillary rheometer, although the differences were apparently due to variations in the temperature during the tests. Vidal et al. (1991), however, tried to obtain the same viscosity from both methods, rather than explain the differences.

Réglat and Tanguy (1998) investigated the viscosity of $CaCO_3$ slurries in a laboratory reverse roll coater. They defined the process viscosity as the shear viscosity of a Newtonian fluid that would yield the same maximum pressure measurement in the same flow conditions. With a pressure transducer polished to fit the surface of the metering rod, they measured the pressure profile within the metering nip. Pressure peaks for Newtonian fluids were used to build a master curve, which was then employed as a basis to evaluate the viscosity of the suspensions. They found that the process viscosity of the $CaCO_3$ slurries can be up to seven times higher than that measured in a Couette configuration. Therefore, they proved that $CaCO_3$ suspensions behave differently in the process, so that the viscosity obtained in the rheometer may not be the same that the actual viscosity in the nip. It is important to clarify if the same phenomena takes place with more complex pigmented fluids like paper coating colors.

2.3.9 Coating colors particle behavior

Particle motion is very important when a coating color flows. Hase and Bousfield (1994) proposed a model to describe the motion of a non-spherical particle suspension in a shear field. The model accurately predicted the viscosity as function of the concentration, giving a good correlation with experimental data. However, the viscosity was overpredicted when a kaolin suspension was simulated. Bousfield et al. (1996) carried out simulations of particle movement in the blade coating process, considering hydrodynamic and electrostatic forces. A stagnation region was observed with a higher particle concentration than the incoming fluid, which was explained in terms of particle-particle interactions. Particles are pushed together to the stagnation zone where they may form clusters, which, in turn, may promote the appearance of scratches, blade deposits and blade wear (Bousfield et al. 1996). Gane et al. (1997) carried out a study about particle orientation during coating. They showed that the particle alignment given in blade coating is optimized, with implications for improved runnability, coverage, and micro-smoothness. In contrast, roll coating at high solids concentrations develop disordered particle orientation; hence, producing a less smooth paper.

Numerical simulations carried out in the metering nip (Ritz et al. 1998) have shown that particle migration is also likely to occur at relatively low speeds (125 m/min). The maximum shearing occurs very near the metering rod surface, so the particles tend to move toward the transfer roll. As a result, a competition exists between the centrifugal forces provided by the transfer roll, inertia and viscous forces, and the driving forces developed by shear rate gradients. The relative importance of those driving forces determines the degree of particle migration under certain operating conditions.

2.4 Specific Objectives

The current demands for increasing speeds of the modern coating applications require a better understanding about the coating process. In the paper coating industry,

for example, more and more complex fluids are used in order to fulfil the changes in the process due to the reduced residence times that take place at very high speeds. State-of-the-art printing technology also requires new changes in the formulations so that the printing quality is improved. As a result, deeper and up-to-date studies are necessary to meet the current coating technology constraints so that the present coating problems can be better understood and, if possible, solved.

The metering nip flow hydrodynamic instabilities have been widely studied, but little is known about its behavior at the current film coating speeds. For example, the influence of the rheological behavior of the paper coating colors and the operating conditions on the high-speed ribbing pattern is still an open subject. At the same time, these same high speeds have triggered the appearance of spitting droplets in the metering nip. Although from the information of the literature it seems that the spitting phenomenon can be easily controlled, no information has yet been published about its origin and its relation to the hydrodynamic conditions of the metering nip flow.

Moreover, in order to have a improved control of the quality of the final coated paper, the understanding of the metering nip flow also requires a very good knowledge about the rheological behavior of the coating fluids. Steady state and oscillatory tests are usually performed to characterize the coating colors. In fact, these tests have given a lot of information that has been used to predict the coating color performance in the nip. However, some industries have found that certain coating formulations with very similar rheological properties perform differently in the coating process. It seems that some rheological tests are not representative of what occurs in the coating process. Thus, an investigation is needed in order to clarify the reasons of the differences.

This thesis intents to fill some of the gaps found in the literature regarding the understanding the metering nip flow. It is done by investigating the hydrodynamic instabilities triggered in the metering nip of a film coater when coating with paper coating colors and at very high speeds (up to 1900 m/min). Furthermore, the rheological behavior of the coating colors is also studied at the very same conditions of the

metering nip. We will try to clarify the reasons of the differences found between the predictions made from classical rheological measurements and the performance of the coating fluids in the coating process.

From the literature survey, we know that the film metering process is governed by the rheological behavior of the coating color and the operating conditions. The shear viscosity, specially the Brookfield viscosity in the paper coating industry, has been used as the basis to assess the quality of the coating fluid. The Brookfield viscosity is far from representing the actual transient and extensional conditions of the process; even the shear viscosity. Although some rheometers are capable of reaching the shear rates that occur in the film coating process, the shear viscosity may not be the best way to assess the quality of the coating color. It has been shown that the rheological behavior of particle suspensions in the nip is different from that observed in the rheometer. As a result, our first objective is to establish the link, if it exists, between the coating color rheological behavior determined with classical rheological tests and the rheological behavior in the process itself.

The hydrodynamic conditions of the metering process are critical from an economical standpoint. Runnability problems have been widely studied, specially the ribbing instability. However, most of the information regarding the flow hydrodynamics in the metering nip available in the literature deals with conditions less stringent than those of the current paper film coating process. Coating defects like ribbing and spitting need to be better understood. Therefore, the second objective and second paper is to further examine the hydrodynamics of the metering nip flow with respect to those instabilities. Under industrial operating conditions, the film coating defects are analyzed in relation to the rheological behavior of the coating colors. The instabilities are also evaluated with respect to the process operating conditions so that they can be minimized, or if possible, eliminated.

When the coating process operating requirements do not allow the elimination of the film coating defects, process runnability is usually controlled by modifying the

coating color rheological properties. Therefore, a better understanding of the rheology of the coating fluids in the process is crucial in controlling the quality of the final product. In this third objective and third paper, we retake the subject of coating colors rheology to further examine the coating color performance in the nip. A new method to evaluate the viscosity of the coating colors is proposed and the results are compared to rheological tests that are more representative of the metering process.

The fundamental understanding of the fluid mechanics in the metering nip is wide. In this fourth objective and fourth article, computer simulations of the metering nip flow are used to narrow this understanding by assessing the process viscosity models proposed in the previous papers. To carry out the evaluation, both maximum pressure and torque are calculated with an 2-D elastohydrodynamic model and comparisons with experimental measurements are performed.

CHAPTER 3

EXPERIMENTAL SETUP AND MEASUREMENTS

3.1 Laboratory coater

The laboratory coater (Fig. 3.1) was built in collaboration with PAPRICAN (Pulp and Paper Research Institute of Canada). It represents half a metering size press, where the role of the paper is played by a doctor blade (Réglat, 1997). The maximum transfer roll speed is 1900 m/min, the maximum metering rod speed is 100 m/min, a strip of 20 cm can be coated on the transfer roll, the radii of both transfer roll and metering rod are 0.8 m and 0.04 m, respectively, and the transfer roll cover elastic modulus is 10 MPa.

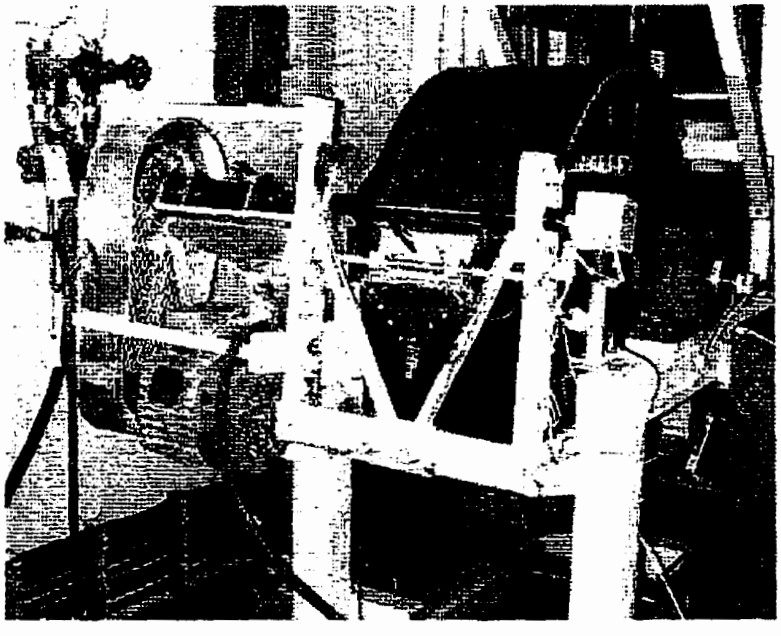

Figure 3.1 Laboratory coater.

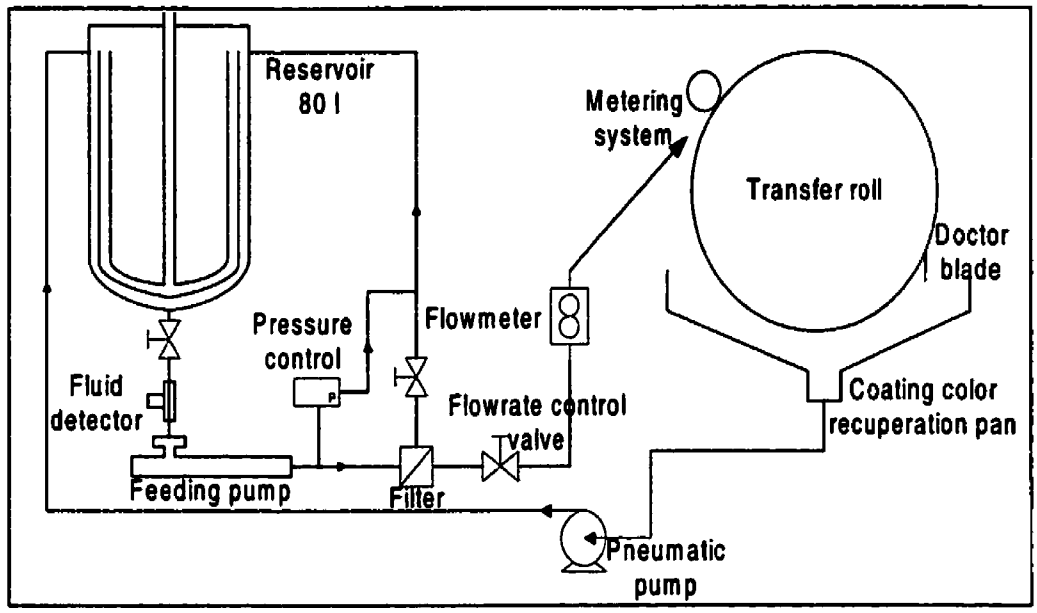

Figure 3.2 Fluid recirculation path and accesories of the laboratory coater.

Fig. 3.2 shows a diagram of the complete fluid circuit and all the accessories of the coater, namely:

- A coating circuit that feeds the coater from an 80 L reservoir.
- A progressive cavitation pump that ensures a constant flow rate (without pulses) to the coating head.
- A by-pass system that permits to adjust the flow rate arriving at the coating head.
- A flowmeter that allows to read the actual flow rate arriving at the coating head.
- A filter that holds particles bigger that 50 μm (Réglat, 1997).
- A coating head in an open configuration (Fig. 3.3a). It has a flexible blade on the transfer roll with variable width. The slot can be varied from 1 to 10 mm. A small proportion of the fluid is applied on the transfer roll, and the other is recovered in a pan below the coater and recirculated to the reservoir by a pneumatic pump.

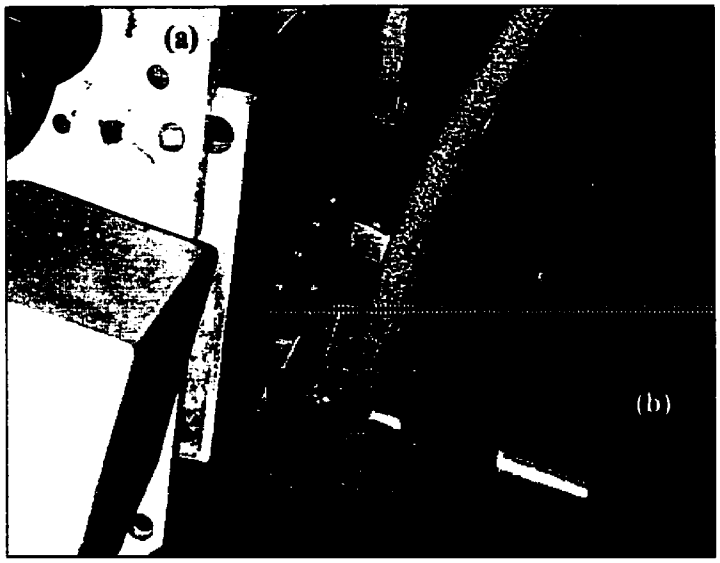

Figure 3.3 Side view of coating headbox (a) and displacement transducer (b).

The load in the metering rod is applied by a pneumatic system as shown in Fig. 3.4. The metering rod is supported at the ends by two articulated arms around an axis that is fixed to the machine frames. Two pneumatic cylinders of 38 mm of diameter allow to apply a load of up to 3 kN/m on the rod, operation that is carried out with a manual regulator.

A fluid detector has been installed before the pump. Its function is to cut off the pump and the load in the metering rod when the machine is in operation but there is no fluid in the system. It permits to avoid closing the nip gap and using the pump without fluid, eliminating the risk of damaging the elastomer coated on the transfer roll.

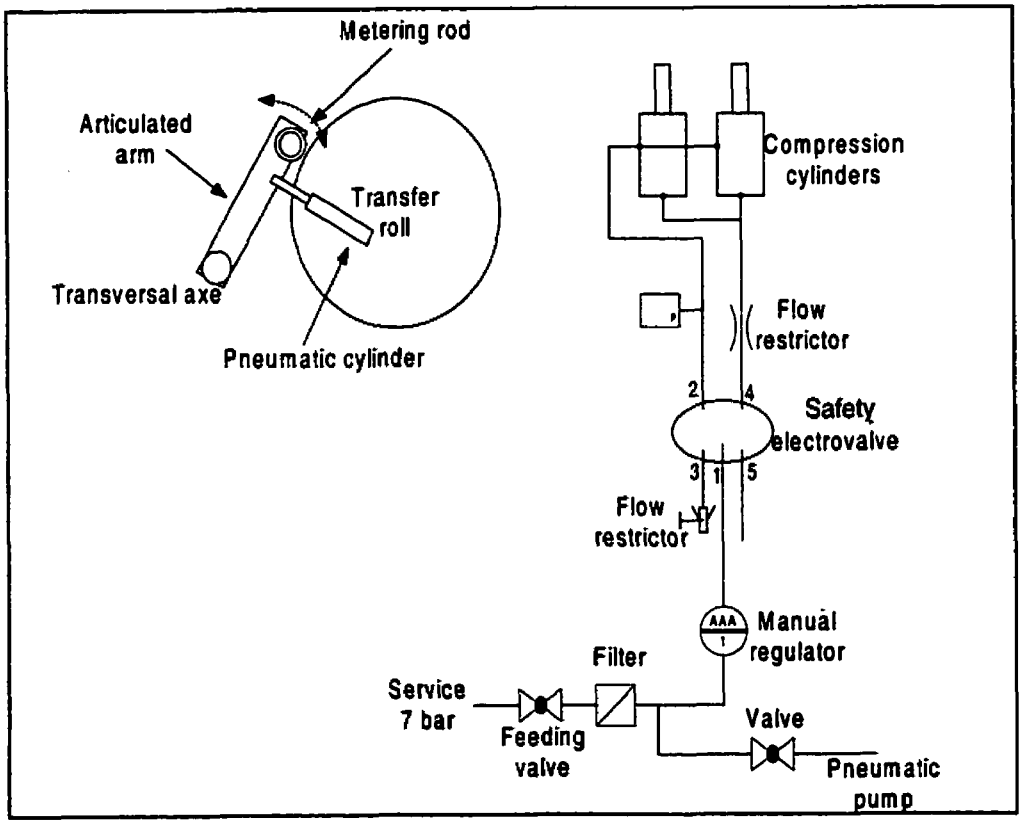

Figure 3.4 Pneumatic compression system on the metering rod.

Fig. 3.5 shows the electric circuits of the machine. The coater is equipped with three motors (AC, three-phasic, 650V), and a motor for the mixing system (AC, three-phase, 220V). Each motor has a manual speed regulator. The maximum transfer angular speed is 760 rpm, at which the transfer roll inertia is about 670 kJ. Since the control cannot dissipate the energy from decelerating the transfer roll (250 kg), an induction brake of 30 kW ensures a very good control of the stability of the speed of the roll.

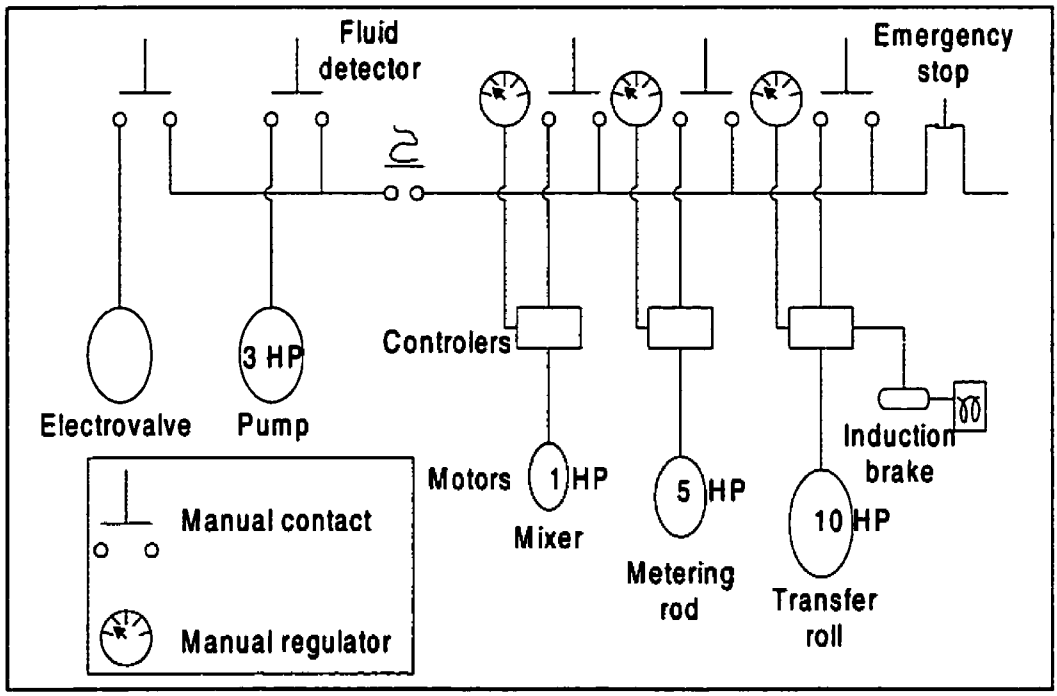

Figure 3.5 Electric diagram of the laboratory coater.

3.2 Transducers and acquisition system

The laboratory coater is properly instrumented to measure speeds, the metering rod position, pressure profile, load, torque, and temperatures:

- Two encoders (Hengestler 521 058) measure the speed of both metering rod and transfer roll. The reading speed is 200 pulses per second.
- Two displacement transducers (Omega D-500-1) measure the relative position of the metering rod from the transfer roll undeformed surface. The range of movement is 0.7 mm.
- A piezoelectric pressure transducer (Piezoelectronics PCB 205M137) on the metering rod surface measures the hydrodynamic pressure profile within the nip.
- A pressure transducer (PX613-100G5V) measures the total load applied on the metering rod.
- A torquemeter (Vibrac TQ-200) measures the torque applied on the metering rod.
- Three temperature probes measure the temperature of the fluid in the reservoir, in the feeding head, and on the metering rod surface.
- A manual infrared thermometer (Raytek ST6LSU) measures the transfer roll film temperature.

The control panel, situated next to the coater, has the switches, speed and pressure controls, and the necessary electronics of the coater (Fig. 3.6). The signals are filtered, amplified, and transmitted from the machine to an acquisition system composed of a personal computer with an acquisition card (ATMIO016E-2) and the data acquisition software Labview™ (Version 5.0). The maximum speed of sampling is 500,000 points per second. The program used to filter and treat the data, developed in Labview™, allows to read in real time (and eventually to record) the speed of the rolls, the position of the metering rod, the load, the pressure profile, the torque, and the temperatures (except the infrared temperature).

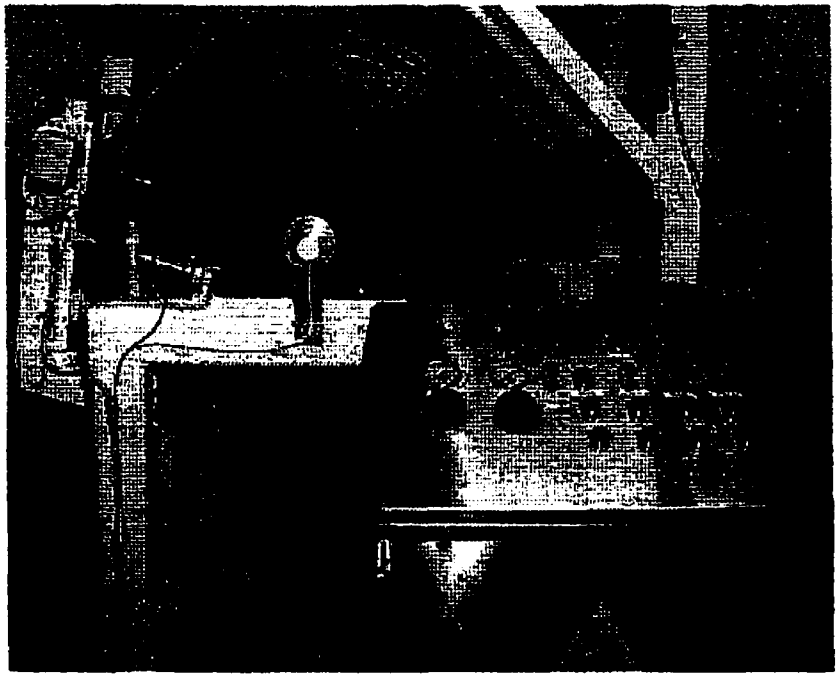

Figure 3.6 Side view of the laboratory coater and control panel.

3.3 Data processing

Once the calibration curves were obtained for the measuring devices, the uncertainty of the measurements was evaluated. Particular care was taken in treating the measurements of both displacement and piezoelectric pressure transducers.

3.3.1 Uncertainty determination

A measurement is characterized by an error. Two kind of errors can be found:

- A systematic error, or bias, that remains constant or changes predictably.
- The random error that changes unpredictably when the same measurement is made at the same conditions.

The composition of these two errors is the absolute error. The bias is generally unknown, unless it is compared to a calibration data. It includes mechanical and calibration errors that can be eventually estimated by suitable tests and judgement. The random error depends on the resolution of the measuring device and the electronic quality associated with it: stability of the electric signal, amplified signal quality, and environmental perturbations. Defined by the repeatability of the measurements, the random error can be framed within an uncertainty range as

$$P^* = \frac{\sum_{i=1}^{n} P_i}{n_s} \tag{3.1}$$

and

$$S_d = \sqrt{\frac{\sum_{i=1}^{n} (P_i - P^*)^2}{n_s - 1}} \tag{3.2}$$

for n samples of the variable measured P_i, with an average P^* and a standard deviation S_d.

The random uncertainty is then defined by

$$\Delta P^* = t_\delta \frac{S_d}{\sqrt{n_s}} \tag{3.3}$$

where t_δ is a probability coefficient, which depends at the same time on the number of samples and δ the degree of confidence given to the measurement. The value of that coefficient is given by the Fisher-Student table, from which an extract is presented in Table 3.1.

Table 3.1 Extract of the Fisher-Student table (taken from Réglat, 1997).

n_s	t_{95}	t_{99}
2	4.303	9.93
4	2.776	4.6
6	2.447	3.71
8	2.306	3.36
10	2.228	3.17
12	2.179	3.06
14	2.145	2.98
16	2.120	2.92
18	2.101	2.88
20	2.086	2.84

3.3.2 Metering rod relative position measurements

The position of the metering rod is determined by two displacement transducers located at each end of the rod (Fig. 3.3b). The edge of each transducer is spherical and made of steel. Both transducers are in direct contact with a copper ring fixed in the axis of the metering rod. In the first hours of utilization, a channel is formed on each ring due to friction with the edge of the transducer. After some time, the contact is such that there is negligible erosion in the contact point.

The errors in the position measurements are difficult to identify, although they can be accounted as (Réglat, 1997):

- The erosion of the ring (tenths of microns).
- Misalignment of the transducers (tenths of microns).
- Zero position of reference (tens on microns).

The zero position is particularly important (all the measurements should have exactly the same point of reference). The calibration of the metering rod zero position is carried out with the naked eye. Both rod and roll are marked so that they have the very same point of contact if a recalibration is required.

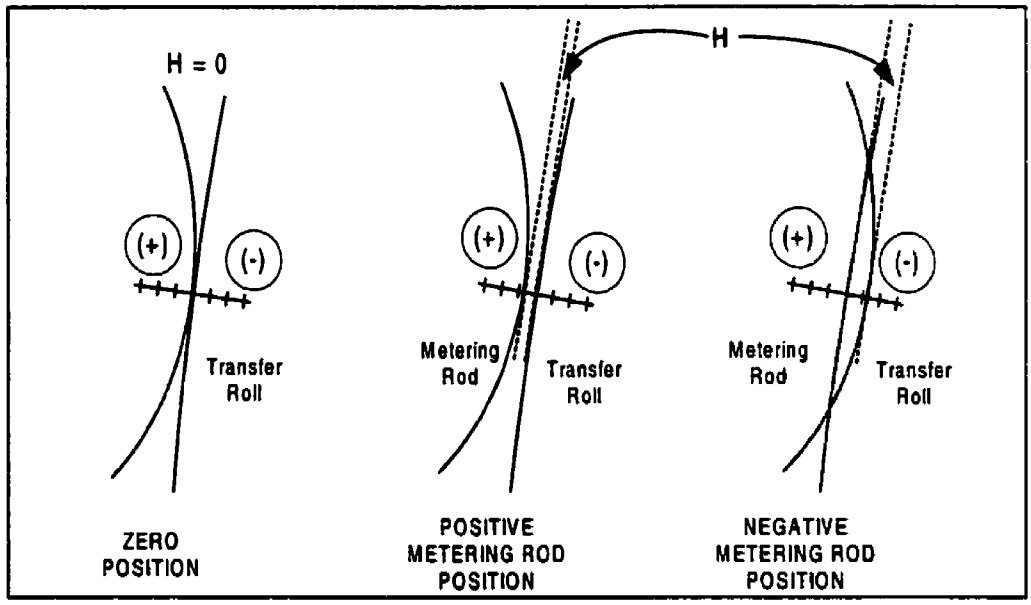

Figure 3.7 Calibration of the zero metering rod position (underformed transfer roll).

Under static conditions, the zero position is made when the surface of the metering rod is in slight contact with the *undeformed* surface of the transfer roll (Fig. 3.7). This relative position is sometimes called the apparent nip gap "H", but it is actually the metering rod relative position with respect to the location of the initial zero reference position. This apparent nip gap *does not* represent the clearance between rod and roll. When the coater is running, the fluid dragged by the transfer roll forces a clearance between rod and roll. A positive metering rod relative position means that between rod and roll there is a clearance (Fig. 3.7 center), although the hydrodynamic pressure may be high enough to deform the transfer roll soft cover so that the actual nip gap is unknown (because the transfer roll deformation cannot be measured). A negative apparent nip gap means that the rod location is intersecting the undeformed transfer roll

surface, and the soft cover is therefore deformed due to both the applied load on the metering rod and the hydrodynamic pressure generated by the flow. Again, this relative position does not give the exact rod-roll clearance because the deformation of the transfer roll is unknown.

Having the same position of zero reference is controlled in two ways:

- From a regular monitoring of the signals that correspond to that position.
- With a calibration test with well-known fluids.

The random error is followed by a systematic calculation of the difference between the measurements of the two transducers. The readings of both displacement transducers are monitored in real time, and the value of the metering rod position is considered correct when the difference between both readings is less than 15μm.

3.3.3 Pressure profile measurements

Figure 3.8 Pressure transducer.

The metering rod has a hole of 2.5 mm of diameter, where a small support for the pressure transducer is installed (Fig. 3.8). The surface of the pressure transducer

and the support have been carefully polished (± 2.5 μm) according to the metering rod curvature to minimize the rod surface irregularities.

The pressure measurements are read with a bias, which comes directly from the size of the pressure transducer, for its diameter is 2.5 mm, when the length of the pressure profile is around 13 mm. The zero corresponds to the atmospheric pressure, which is measured systematically at the beginning of every profile acquired. If that value changes a little, a re-zero readjustment can be made to correct the measurements. The range of the measurements is from –50 kPa to 650 kPa, relative to the atmospheric pressure. From the acquisition data, each stoked pressure profile corresponds to an average of ten profiles. Following the statistics procedure of above, the standard deviation can be calculated. In Fig. 3.9, the example shows a typical stoked pressure profile with its corresponding standard deviation for the ten profiles originally acquired.

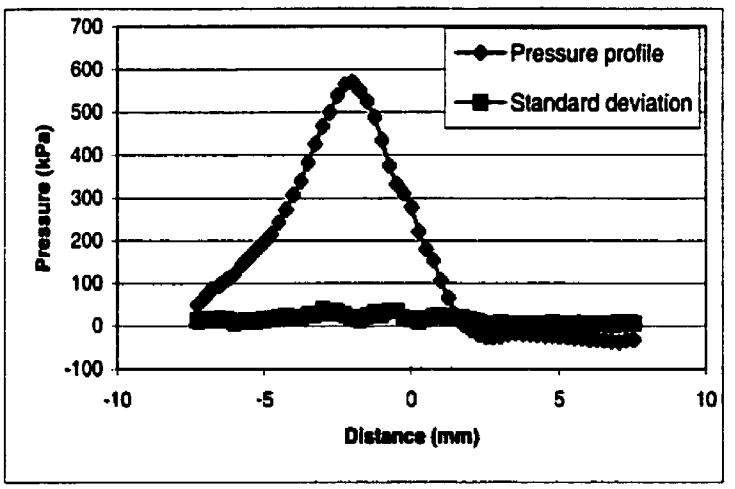

Figure 3.9 Pressure profile within the nip and the corresponding standard deviation for ten profiles.

CHAPTER 4

PROCESS VISCOSITY IN A FILM COATER: MAXIMUM PRESSURE AND TORQUE MEASUREMENTS

The conditions at which the coating process is currently running required an update of the laboratory coater, experimental setup that was developed in an earlier investigation (Réglat, 1997). The retrofitting carried out to the coater was the following:

- the metering was changed for one with a smaller diameter (0.04 m),
- the operating speed was increased up to 1900 m/min,
- a torquemeter was installed in the metering rod so that more information could be obtained,
- and the elastic cover was changed for another one stiffer (50 P&G). As before, a pressure transducer on the metering rod was used, as well as displacement transducers on the metering rod.

$CaCO_3$ suspensions exhibit a behavior in the metering nip very different from that observed in the rheometer (Réglat and Tanguy, 1998). Since $CaCO_3$ suspensions are often the basis of a more complex suspension such as a paper coating color, a question arises whether a coating color and a $CaCO_3$ suspension behave similarly in the metering nip. Thus, this first article represents the first effort of investigating the rheological behavior of paper coating colors in the metering nip.

From a theoretical point of view, the method proposed by Réglat and Tanguy (1998) is used, with some modifications. Additionally, a novel method to evaluate the process viscosity in the metering nip is proposed. This new procedure is based on a dimensional analysis carried out on the metering nip and the Metzner and Otto concept. Both procedures are fully described, and the results are compared and discussed in relation to steady state rheological measurements.

PROCESS VISCOSITY IN A FILM COATER

S. Alonso, O. Réglat, F. Bertrand, and P.A. Tanguy

NSERC/Paprican Chair

Department of Chemical Engineering

École Polytechnique

P.O. Box 6079, Station Centre-ville

Montreal, Can., H3C 3A7

Keywords: coating color, process viscosity, shear viscosity, maximum pressure, torque.

Published: Paperi ja Puu (Paper and Timber), 82(2000):1, 34-40.

4.1 Abstract

A mini film coater was built to investigate the rheological behavior of paper coating colors and the film application on a paper web at commercial speed. As for the rheological characterization, the main idea is to use measurements of metering nip pressure and torque on the metering rod to back calculate the viscosity (inverse problem). It was found that the values of process viscosity are very different from those obtained in classical rheometry. This is explained by the rheological behavior of the suspension in the nip, where it is subjected to a mix of high intensity extensional and shear deformations for a very short period of time.

4.2 Introduction

Film coating is a commercial process used to treat the surface of paper and paperboard to improve their optical and printing characteristics. In a film coater (Fig. 1.1), a thin film of a highly pigmented coating color is applied on a paper web running at very high speed (up to 2000 m/min) between two contra-rotating rolls covered with an elastomeric layer. The film is created upstream from the application nip in a metering system composed of a delivery head and a smooth metering rod. The challenge of this process is to deliver a uniform coating film over a wide range of coating thicknesses, operating conditions, and coating color formulations.

For a set of operating conditions and coating color formulations, undesirable phenomena like color spitting and coating ribs may be triggered in the metering nip during the film formation. These runnability problems can be partially eliminated by an optimal choice of the metering rod diameter and transfer roll cover (Stranger, 1995). However, once an equipment configuration has been designed, only changes in the color formulation can help reduce process instabilities. Therefore, the rheological behavior of coating colors plays a dominant role in governing runnability (Grön et al. 1996; McGenity et al. 1992; Roper and Attal, 1993; Triantafillopoulos and Lee, 1996).

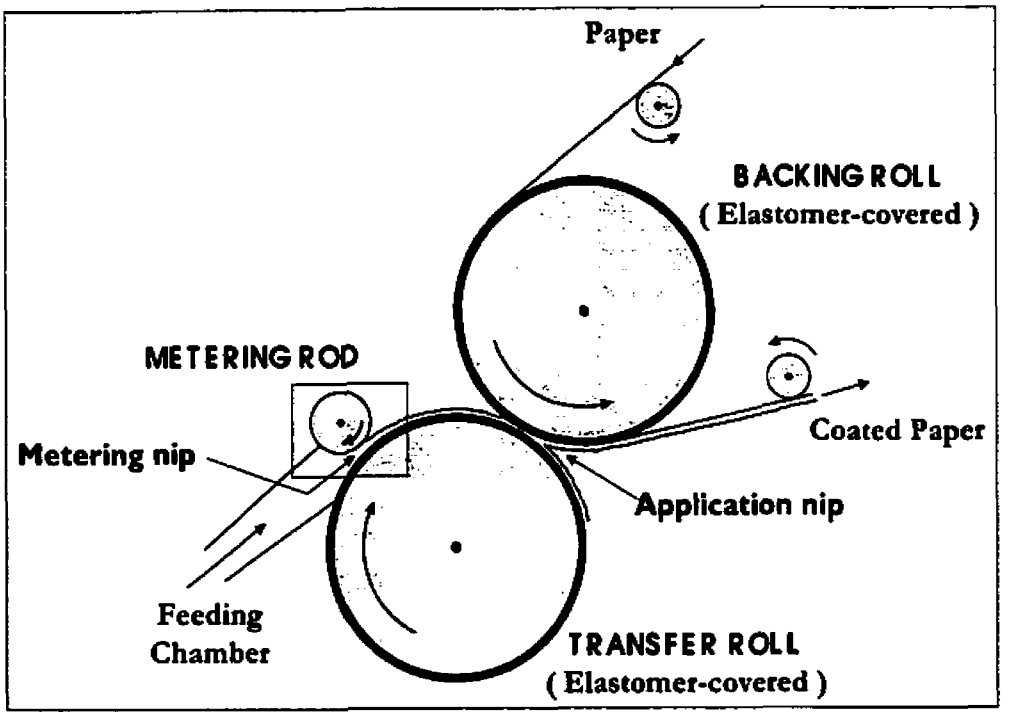

Figure 4.1 Film coating process.

From a rheological standpoint, coating colors are very complex dispersions. Classical rheometry shows that most formulations are shear-thinning at low shear rates (Carreau and Lavoie, 1993; Cohu and Magnin, 1995; Grön and Dahlvik, 1997; McGenity et al. 1992; Lavoie et al. 1996; Lavoie et al. 1997; Purkayastha and Oja, 1993; Roper and Attal, 1993), and that some of them may exhibit shear-thickening behavior at high shear rates (Laun and Hirsch, 1989; Roper and Attal, 1993). Furthermore, viscoelasticity is almost always part of the rheology; most coating colors have elastic memory when subjected to a small deformation (Grön et al. 1996; Lavoie et al. 1996, 1997; Purkayastha and Oja, 1993).

Couette rheometers are commonly used to investigate the rheology of coating colors at low shear rates (up to 10^3 s^{-1}). Higher shear rates cannot be easily handled in these systems because of heating effects (viscous dissipation), particle migration (loss of homogeneity) and wall slippage.

Capillary rheometers are used for the rheological characterization at high shear rates (10^3-10^6 s^{-1}). However, special care must be taken to correct slippage effects (Mooney method) caused by the small dimensions of the capillary. Laun and Hirsch (1989) used a gas-driven capillary rheometer to study some paper coating colors. They evidenced the importance of correcting end effects to obtain reliable results.

Although capillary rheometers are capable of reaching the shear rates levels found in the coating process, they do not account for the coating color flow history and the process time. It has been shown that a relatively low pre-shear (~ 100 s^{-1}) can be sufficient to provide a complete structural breakdown in paints, which are also complex suspensions (Cohu and Magnin, 1995). Such a level of shear rates may be exerted on coating colors when they flow through pipes, pumps, and filters from the coating kitchen to the premetering headbox (Réglat and Tanguy, 1998). Moreover, the time scale associated with rheometers is very different from that in the film coating process. In coating equipment, the fluid is subjected to large deformation rates (up to 10^6 s^{-1}) over a very short period of time (~10^{-3} s); these conditions are almost impossible to achieve in conventional rheometers. Finally, it has been shown that under steady, high shear rates, both the viscoelastic and thixotropic nature of coating colors tend to disappear (Carreau and Lavoie, 1993; Laun and Hirsch, 1989; Roper and Attal, 1993).

Classical rheometry has been extensively used to investigate the rheology of coating colors. A great deal of useful information has been obtained and applied to increase the runnability of the film coating process (Ghosh, 1998a,b; Hilden and Mustonen, 1998). However, no rheometer can reproduce the high shear and extensional rates combination existing in the film coating process. The knowledge of the rheology of coating colors downstream from the metering nip is also needed to better understand the defects that occur in the application nip (Triantafillopoulos and Smith, 1998). Vidal et al. (1991) pioneered the investigation of coating color rheology in the coating process itself. The *in situ* viscosity was evaluated using a blade coater. The pressure exerted by the fluid on the blade and the surface of contact were calculated as a function of the blade deformation. The shear stress was a function of the pressure

distribution within the nip, while the shear rate was estimated from the film thickness. Vidal et al. (1991) found that their formulations were shear-thinning for shear rates around 10^5-10^6 s^{-1}. In these conditions, the process viscosity was of the order of 20 mPa.s. For these same coating colors, higher values of viscosity were obtained in a capillary rheometer, although the differences were apparently due to variations in the temperature during the tests (Vidal et al. 1991).

Réglat and Tanguy (1998) investigated the process viscosity of $CaCO_3$ slurries in a laboratory roll coater. With a pressure transducer polished to fit the surface of the metering rod, they measured the pressure profile within the metering nip. Pressure peaks for Newtonian fluids were used to build a master curve, which was then employed as a basis to evaluate the viscosity of the suspensions. They found that the process viscosity of the $CaCO_3$ slurries was much higher than that measured with the rheometer. From a rheological standpoint, such a finding may not be surprising since, in the roll coating process, the type of deformation and time scales are completely different from those found in a conventional rheometer.

In this article, our objective is to examine, along the ideas of Réglat and Tanguy (1998), the rheological behavior of coating colors in the film coating process. Our analysis is based on pressure measurements, and a new procedure that uses the torque exerted on the metering rod to calculate the process viscosity.

4.3 Experimental

This section contains all materials and methods used in the experiments, such as the film coater features, and Newtonian and coating color formulations used. Furthermore, the rheological behavior of the coating colors is given.

4.3.1 Mini film coater

A mini film coater was built to investigate the runnability of the film coating process at commercial speed. The mini film coater (Fig. 4.2) is composed of two sub-assemblies: a) a metering section already described in Réglat and Tanguy (1997, 1998), and b) a backing roll positioned close to the transfer roll, entraining a 20 m long paper loop at the same speed as that of the transfer roll (up to 2000 m/min). The paper is coated in one revolution and dried in several revolutions. The transfer roll and the backing roll radii are 0.8 m, and that of the metering rod is 0.036 m. Both rolls are covered with an elastomer (styrene butadiene copolymer) with a hardness of 60 P&J (Young's modulus = 10 MPa) and a thickness of 15 mm. A 0.3 m wide coat strip is metered on the transfer roll with a co-rotating smooth metering rod.

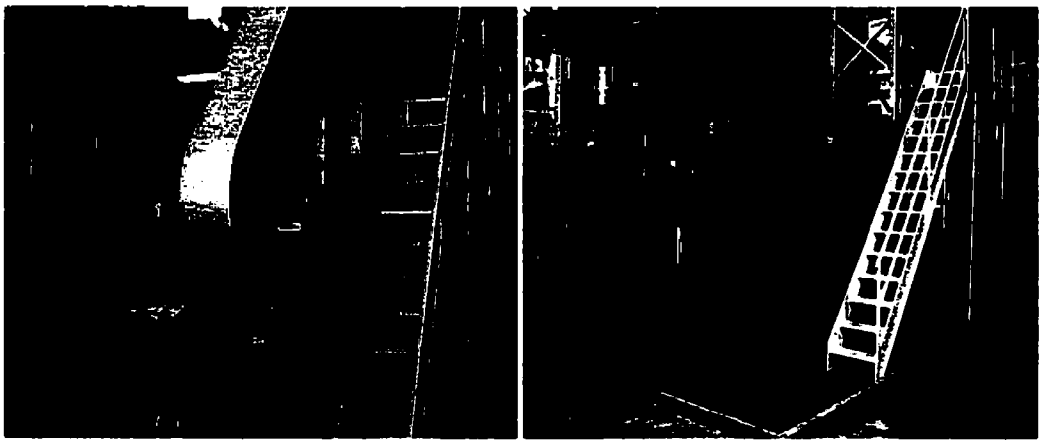

Figure 4.2 Two different views of the mini coater, including the coating kitchen (left) and a closer look at the coating section (right).

The metering section (Fig. 4.3) is fully instrumented. A wall mounted piezo transducer, located in the middle of the metering rod, allows the determination of the nip pressure profile. The range of measurements is from –50 kPa to 650 kPa (relative to the atmospheric pressure) with a response time of 250 kHz. A torquemeter and a tachometer are also connected to the shaft of the metering rod. The range of the torque

measurements is from 0 to 1.41 Nm. Two displacement transducers, located at each end of the rod, measure the position of the metering rod with respect to the undeformed surface of the transfer roll. The range of measurements is from –250 to 350 μm, and the position is given by the mean value of the two measurements; it is considered as correct if the difference is less than 15 μm. The zero position is defined by naked eye when the rod and the transfer roll are in slight contact at rest, with an uncertainty of ±20 μm. A calibration procedure makes it possible to keep the same bias for all the measurements, but repeatability gives a relative uncertainty of ±3 μm. When the coater is set in motion, the transfer roll cover deforms according to the dynamic pressure profile within the metering nip.

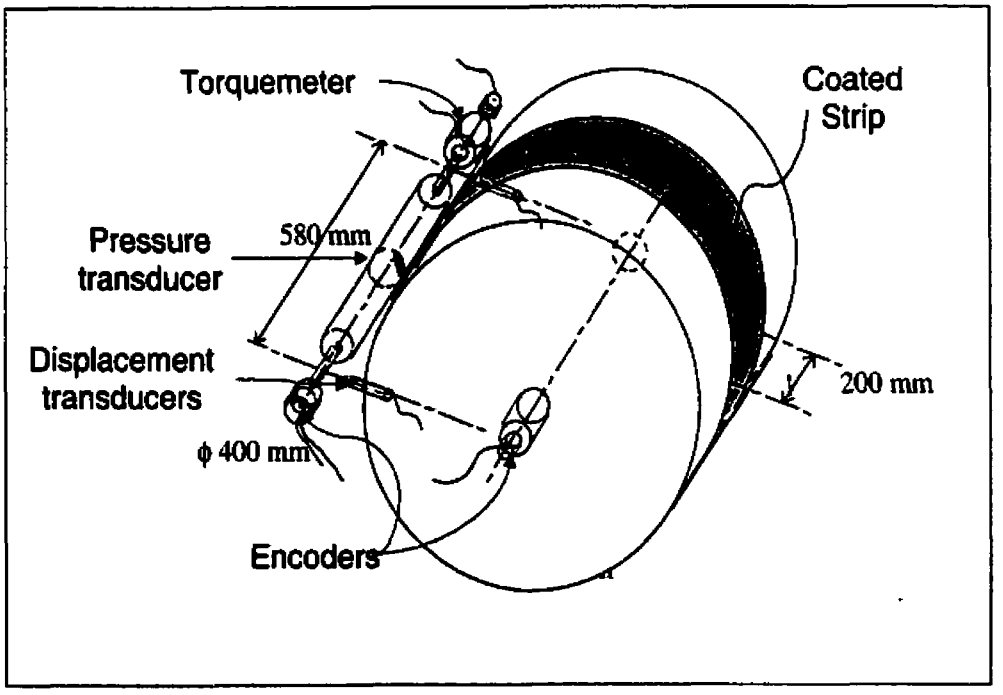

Figure 4.3 Instrumentation of the metering section of the mini coater.

4.3.2 Test fluids

Newtonian fluids were used to calibrate the pressure and torque measurements in the mini film coater. They consisted of polyethylene glycol (Hermann Ter Heli & Co. GMBH, Germany, M_W = 35000) solutions at three concentrations: 13.2%, 17%, and 18.3%, of viscosity 43 mPa.s, 84 mPa.s, and 104 mPa.s, respectively.

The formulations of the coating colors are given in Table 4.1 (100 parts of clay were used as dry basis). Engelhard Inc (New Jersey, USA) provided the kaolin pigment (HT #2). Sodium polyacrylate (DISPEX N40, Allied Colloids Canada) was used as dispersant. The coating colors also included styrene-butadiene latex, from Dow Chemicals Canada, as binder, and carboxymethyl cellulose with a degree of substitution of 0.65 (7LT, Hercules Inc.) as thickener (M_w=90000). All these ingredients were used as such.

Table 4.1 Coating color formulations.

LABEL	Clay	Dispersant	Latex	CMC	% Solids
A	100	0.04	10	0.25	61.0
B	100	0.04	10	0.5	61.0
C	100	0.04	10	1.0	61.0
D	100	0.04	10	0.5	56.3
E	100	0.04	10	0.5	61.0
F	100	0.04	10	0.5	63.3

To prepare the coating colors, the dispersant was first added to deionized water to obtain the desired solids content. The slurry was made by slowly adding the clay with a vibrating feeder. Then the latex suspension was added, followed by previously hydrated CMC. The colors were mixed for 30 minutes, and then the pH was adjusted to 8.0 by adding NaOH. At the end, the coating color was mixed for an additional hour to stabilize the pH. The mixer used for the makedown is based on two independently

driven contra-rotating impellers, one wall scraping anchor arm and one wetting/dispersing agitator (Thibault, 1999). All the coating colors were used the day following the makedown.

Steady state rheological characterization of the coating colors was carried out using a stress-controlled CVO Bolhin rheometer with Couette geometry. The variation of the viscosity with respect to the shear rate is shown in Fig. 4.4 for all formulations. All the colors were found to exhibit shear-thinning properties. The CMC concentration and solids content shift up the curve owing to an increase of the apparent viscosity, although the power index remains within a relatively narrow range (Table 4.2).

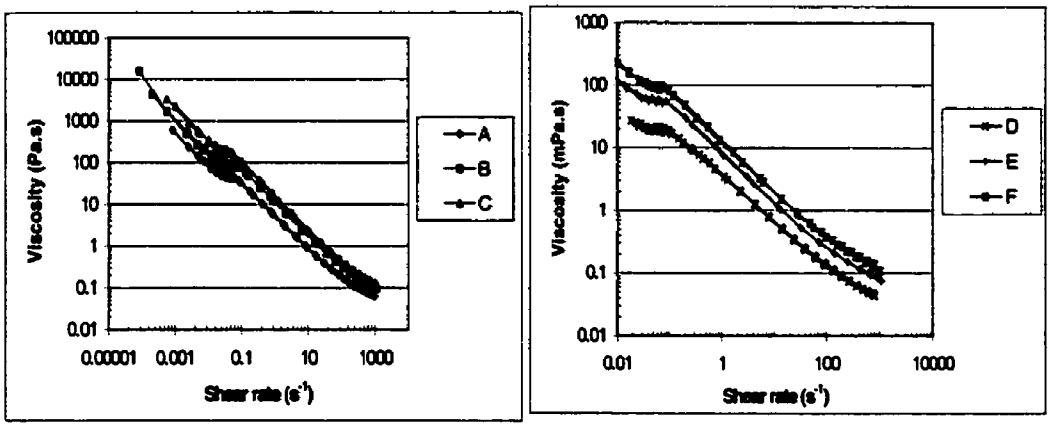

Figure 4.4 Rheology of coating colors at different CMC concentrations (left) and solids content (right).

Table 4.2 Parameters of the power law model for the coating colors.

Coating color Label	m ($Pa.s^n$)	n
A	5.0	0.220
B	10.5	0.170
C	16.0	0.145
D	3.70	0.220
E	10.5	0.170
F	11.5	0.184

4.4 Evaluation of the process viscosity

4.4.1 Nip pressure measurements

The "process viscosity" of a non-Newtonian fluid is defined as the *shear viscosity of a Newtonian fluid that would yield the same maximum pressure measurement under the same flow conditions* (Réglat and Tanguy, 1998). The operating conditions used for the analysis are given in Table 4.3. They correspond to operating conditions with good runnability (stable flow, no spitting, and no air entrapment) and are also compatible with current industrial conditions (Pauksta, 1998).

Table 4.3 Operating conditions used to evaluate the process viscosity.

V_t (m/min)	V_m (m/min)	Load (kN/m)
1250	30	1

From the dynamics of the system, following Réglat and Tanguy (1998), the maximum pressure within the nip depends on the apparent nip gap, the transfer roll speed, and the fluid viscosity:

$$P_{max} = P_{max}(\mu, V_t, h^*) \tag{4.1}$$

By differentiating we obtain

$$dP_{max} = \frac{\partial P_{max}}{\partial \mu} d\mu + \frac{\partial P_{max}}{\partial V_t} dV_t + \frac{\partial P_{max}}{\partial h^*} dh^* \tag{4.2}$$

Eq. 4.2 can be approximated by

$$P_{max} \cong P_{max0} + \frac{\Delta P_{max}}{\Delta \mu}(\mu - \mu_0) + \frac{\Delta P_{max}}{\Delta V_t}(V_t - V_{t0}) + \frac{\Delta P_{max}}{\Delta h^*}(h^* - h^*_0) \tag{4.3}$$

where P_{max0} is the reference maximum pressure measured for a Newtonian fluid of viscosity μ_0 at some reference operating conditions V_{t0} and h^*_0. The apparent nip gap h^* represents the dynamic position of the metering rod relative to its zero position at rest when the rod is in contact with the undeformed surface of the transfer roll. For the coating colors, μ becomes the process viscosity, which must be determined.

For the evaluation of the process viscosity, the reference values are chosen in the middle of the range of transfer speeds, viscosities and apparent nip gaps for a Newtonian fluid: V_{t0} = 1000 m/min, μ_0 = 84 mPa.s, and h^*_0 = -80 μm. With these reference values P_{max0} = 445 kPa.

In practice, the following strategy is proposed:

1. For each individual set of operating conditions V_{ti} and h^*_i, the maximum pressure P_{maxi} is measured for a series of Newtonian fluids of viscosity μ_i,
2. The shift factors $\Delta P_{max}/\Delta\mu$, $\Delta P_{max}/\Delta V_t$, and $\Delta P_{max}/\Delta h^*$ can then be evaluated (Table 4.4) as explained by Réglat and Tanguy (1998).
3. Eq. 4.3 can now be used to estimate the process viscosity of a coating color, $\mu = \mu_{proc}^P$, by measuring the maximum pressure $P_{max\ cc}$ together with its corresponding value of apparent nip gap h^*_{cc} at any operating conditions:

$$\mu_{proc}^{P} = \mu_o + \left[P_{max\,cc} - P_{max\,0} - \frac{\Delta P_{max}}{\Delta V_t}(V_t - V_{t0}) - \frac{\Delta P_{max}}{\Delta h^*}(h^*_{cc} - h^*_0) \right] \frac{\Delta\mu}{\Delta P_{max}} \tag{4.4}$$

where the shift factor $\Delta P_{max}/\Delta\mu$ contains the shear and extensional viscosity contributions to the flow, respectively.

Table 4.4 Shift factors.

$\Delta P/\Delta\mu$ (s^{-1})	$\Delta P/\Delta V_t$ kPa.s/m	$\Delta P/\Delta h^*$ kPa/µm
5.5×10^5	9.6	-3.5

In order to estimate the relative contribution of both shear and elongation, the level of shear and extensional rates were calculated. Flow simulations were performed using the CFD finite element software package POLY2D™ (Rheotek, Inc). Fig. 4.5 shows the fields of extensional and shear rates upstream from and within the metering nip. At the entrance, the flow is highly extensional; in the nip gap, the extensional component decreases significantly and the flow becomes shear-dominant. Under these conditions, the fluid responds with an extensional viscosity μ_{ex}, and a shear viscosity

μ_{eh}, making it necessary to know the Trouton ratio; in the case of the coating colors, it was considered equal to three (Cohu and Magnin, 1995; Ghosh, 1998b). The reader is referred to Réglat and Tanguy, (1998) for more details on this topic.

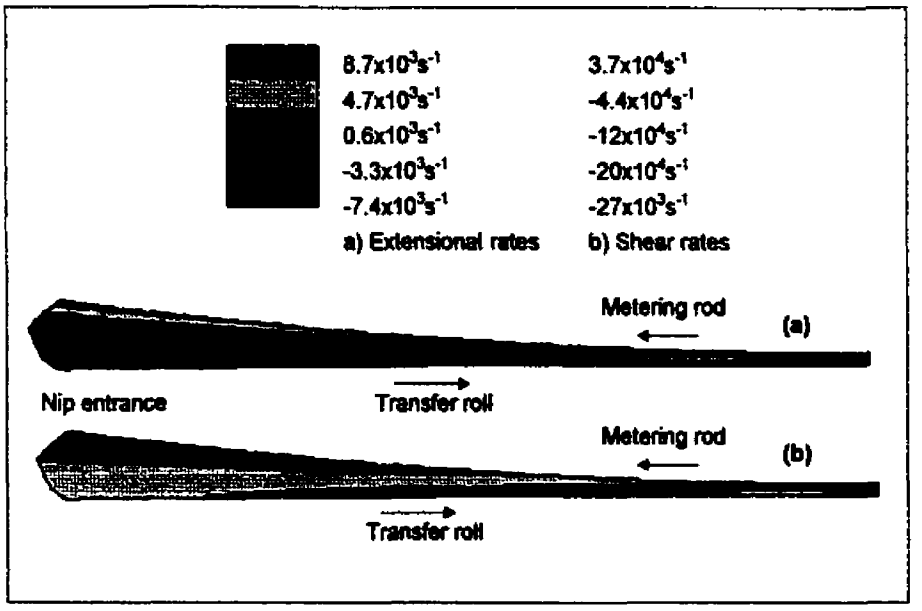

Figure 4.5 Extensional x-x (a) and shear x-y (b) components of the deformation tensor at the entrance of the metering nip at V_t = 1000 m/min, V_m = 30 m/min, μ = 110 mPa.s, and nip gap = 60 μm.

4.4.2 Torque in the metering rod

We now move on to the calculation of the process viscosity from torque measurements. First, a dimensional analysis of the flow in the metering nip is performed to obtain the dimensionless numbers describing the dynamic conditions, according to the π-theorem. The π-theorem states that the relationship between *n* variables with *m* dimensions is equal to *n-m* dimensionless π-functions which replace the original variables describing the problem (Sterbacek and Tausk, 1988).

The variables involved in the metering nip flow are V_t, V_m, T, P, μ, H, ρ, g and σ_T. The number of dimensions is three, so six dimensionless π-functions are needed. To obtain the π-functions, we have to choose a core group of three independent variables so that the other six become the dependent variables that will appear in each one of these π-functions. For the metering nip, V_t, H, and ρ can be chosen to be part of the core group; each dimensionless group will then depend on these variables and each of the remaining independent variables.

For the first dimensionless number, we obtain $\pi_1 = V_t^a H^b \rho^c T$. By substituting the dimensions of the respective variables and by comparing exponents we obtain

$$\pi_1 = \frac{T}{V_t^2 H^3 \rho} \tag{4.5}$$

By analogy with the theory of mixing (Delplace and Leuliet, 1995), it can be noticed that π_1 is nothing but the well known power number *Np*, which relates the power input of the impeller to the inertia forces on the liquid. In our case, it relates the effective torque required to rotate the metering rod at given operating conditions to the inertia forces of the liquid flowing through the nip.

The second π -function is nothing but the Reynolds number

$$Re = \frac{\rho V_t H}{\mu} \tag{4.6}$$

The other four π-functions are not considered here since they are not needed in the mathematical development that follows.

By extending further the analogy with mixing, the product of the power number and the Reynolds number yields the geometric constant *Kp*

$$Kp = Np \cdot Re = \frac{T}{V_t H^2 \mu} \tag{4.7}$$

For coating colors, which behave as power law fluids according to Fig. 4.4, the Reynolds number can be generalized as

$$Re_n = \frac{V_t H \rho}{m \dot{\gamma}_{proc}^{n-1}} \tag{4.8}$$

In the metering nip the shear rate can be approximated as

$$\dot{\gamma} = \frac{V_t}{H} \tag{4.9}$$

Following (Metzner and Otto, 1957), we introduce K_s, the constant of Metzner and Otto, to obtain an expression for the process shear rate in the nip

$$\dot{\gamma}_{proc} = \frac{K_s V_t}{H} \tag{4.10}$$

Equation 4.8 then becomes

$$Re_n = \frac{\rho V_t^{2-n} H^n}{m K_s^{n-1}} \tag{4.11}$$

and the power number can be written as

$$Np = \frac{Kp K_s^{n-1}}{Re_n} \tag{4.12}$$

where Kp is obtained from experiments with Newtonian fluids. Finally, by isolating K_s from Eq. 4.10, we get

$$K_s = \left(\frac{Kp_n}{Kp} \right)^{\frac{1}{n-1}} \tag{4.13}$$

Therefore, the process viscosity can be evaluated as

$$\mu_{proc}^{T} = m \left(\frac{K_s V_t}{H} \right)^{n-1} \tag{4.14}$$

4.5 Results and discussion

In order to test its reliability, Eq. 4.4 was used to estimate the maximum pressure measured in the case of Newtonian fluids. We compare in Fig. 4.6 the values of the estimated pressure with the experimental measurements. It can be seen that a very good agreement is obtained.

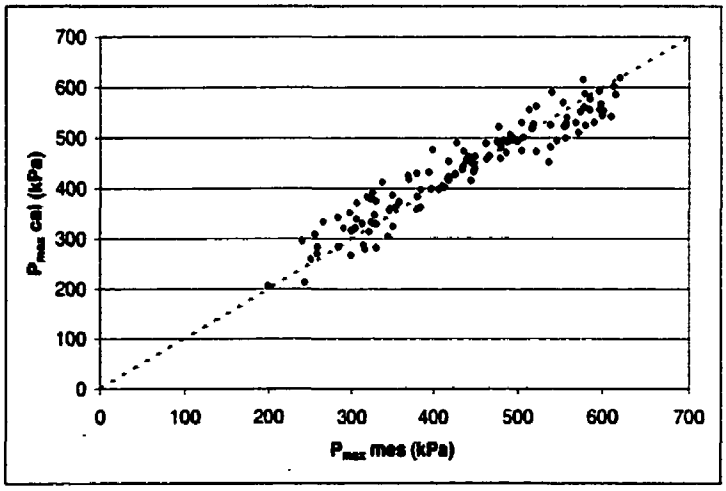

Figure 4.6 Calculated maximum pressure from Eq. 4.4 *vs.* measured maximum pressure (validation of the method).

Fig. 4.7 shows the relation between the process viscosity based on the pressure measurements and the shear (near-plateau) viscosity from the rheometer. The dotted line corresponds to Newtonian fluids, where the shear and process viscosities are equal. When evaluating the process rheology of the coating colors using Eq. 4.4, the process viscosity is much higher than the shear viscosity. Extensional and elastic effects are not considered in the values of the process viscosity. Thus, all the coating colors investigated seem to be shear-thickening at very high shear rates. Such a behavior was not seen in the Couette rheometer; in the metering nip, however, the increase in the process viscosity may be due to the effect of the particles in the fluid since it has been shown that increasing the particle size or the solids content may induce shear-thickening behavior at very high shear rates (Eriksson et al. 1990). Moreover, shear-thickening behavior has also been found elsewhere with other coating colors formulations (Eriksson et al, 1990; Kurath and Larson, 1990; Laun and Hirsch, 1989; Roper and Attal, 1995).

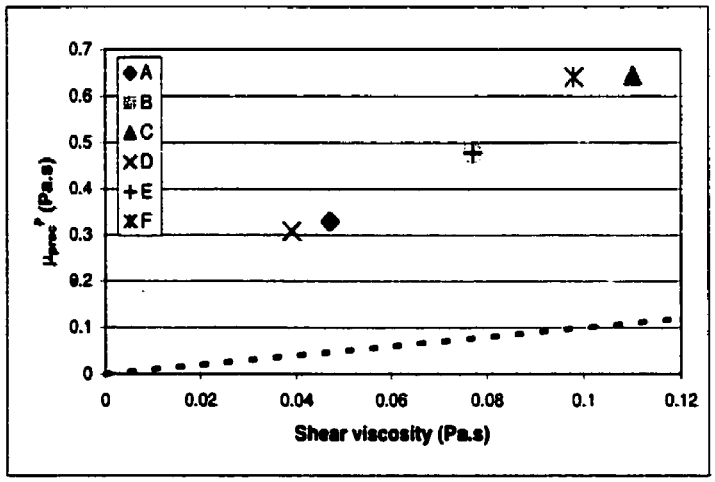

Figure 4.7 Pressure-based process viscosity *vs.* shear viscosity from the rheometer (dotted line → Newtonian fluids).

Fig. 4.8 shows the relation between the process viscosity based on the torque measurements and the shear viscosity. As before, the dotted line corresponds to Newtonian fluids. One may note that, in the case of the coating colors, the process

viscosity is closer to that measured in the rheometer. Most formulations seem to be still shear-thinning at very high shear rates, apparently in accordance with the value of their power law index, i.e., the higher the power law index, the higher the viscosity at equal consistency index and shear rate.

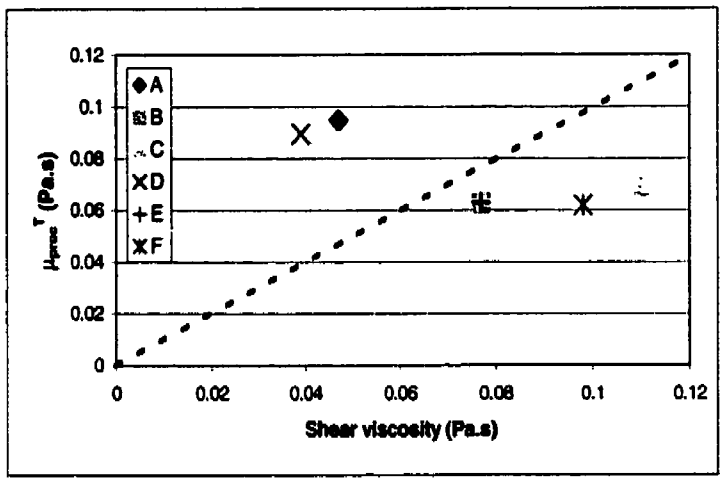

Figure 4.8 Torque-based process viscosity *vs* shear viscosity from the rheometer.

In both cases, it can be noticed that the process viscosity is not the same as the one obtained with classical rheometry. In the case of the pressure-based process viscosity, increasing the amount of CMC shifts up the curve and increases the discrepancy between process and shear viscosity. The solids content does the same, but to a lower degree. In contrast, the torque-based process viscosity apparently follows the power law index (that is, the lower the power law index, the lower the process viscosity), in agreement with the CMC concentration and solids content (see Table 4.2). The differences may be explained by the fact that, in the metering nip, the coating colors are subjected to a very different field of deformation: a high extensional flow and very high shear rates (Fig. 4.5), conditions never found in the rheometer. Moreover, the time scale is very different. Whereas in the nip the average residence time of the fluid is about 0.001 s, measurements in the rheometer take very much longer when performed at steady state. Finally, in the rheometer, the sample is always the same, though in the

process the coating color comes form the storage reservoir and is subjected to a very different shear history due to pumps, filters, pipes, etc. Consequently, the rheological behavior of coating colors within the metering nip is different from the behavior in the rheometer under simple shear conditions. Although the coating colors have a particular extensional behavior, we could not assess this effect, neither the influence of the elasticity. It would be interesting to choose some formulations with similar viscous behavior and different elastic properties to investigate this effects.

The same operating conditions were used to compare both procedures; the differences are explained by the nature of the pressure and torque measurements. The pressure represents a normal force per unit area measured at each single rotation. Although the whole pressure profile is obtained, only the maximum pressure is used in the calculations. The pressure is thus a local measurement, which depends on the normal force of the local liquid that is in contact with the transducer. The pressure may also be subjected to such cross-machine pressure variations as upstream flow instabilities (feeding open chamber), uncertainty due to the scattering of measurements, and, possibly, particle concentration gradients (Ritz et al. 1998).

In contrast to the maximum pressure, the torque represents an average tangential force measured along the nip. It is the torque required to rotate the metering rod, accordingly to the viscosity of the fluid. It is also a global measurement since it takes into account the complete nip gap width, although it does not give information about what occurs within the nip as does the pressure profile (Réglat and Tanguy, 1997, 1998). The evaluation of the nip gap represents an important issue in the calculations of μ_{proc}^{T}. What is actually measured is the relative position of the metering rod with respect to the undeformed surface of the transfer roll. In order to take into account the deformation, the physical properties of the cover and the maximum pressure were used to calculate the approximate deflection of the roll cover. As a result, H, the calculated nip gap, is only approximative since the exact nip gap profile is unknown.

4.6 Conclusions

Our objective was to investigate the rheological behavior of coating colors in the film coating process at commercial speed. For this purpose, a new mini film coater was designed and built. Two original methods that give access to the process viscosity were proposed. They are based on:

- the maximum nip pressure, which is a normal local measurement;
- the metering rod torque, which is a tangential global measurement, easier to carry out on industrial coaters.

In both cases, the process viscosity was shown to be very different from the one obtained by classical rheometry. This behavior is explained by the fact that, in the metering nip, the coating colors are subjected to a very different field of deformation. We believe that the process viscosity could be related to the occurrence of flow instabilities and air entrapment in film coating processes.

4.7 Additional comments

In the metering nip, the converging-diverging geometry gives as a result an important shear-extensional flow combination. The relative magnitudes of the calculated extensional and shear rates in the converging region of the nip were shown in Fig. 4.5. The extensional rates can be only one order of magnitude smaller than the shear rates. Thus, extensional rates play an important role on the hydrodynamics of the flow, specially if the fluid has a particular rheological behavior under extensional flow.

The metering nip flow can actually be characterized by the magnitudes of both extensional and shear viscosities. The hydrodynamic pressure profile depends on the relative magnitude of both viscosities. Thus, the shift factor $\Delta P_{max}/\Delta\mu$ gives the dependency of the maximum pressure on the viscosity of the fluid in the metering nip (Réglat and Tanguy, 1998) as

$$\frac{\Delta P_{max}}{\Delta \mu} = \frac{\partial P_{max}}{\partial \mu_{sh}} + \frac{\partial P_{max}}{\partial \mu_{ex}} \frac{\Delta \mu_{ex}}{\Delta \mu_{sh}} \tag{4.15}$$

where the left hand term is that of Eq. 4.3, the partial derivatives are the shear and extensional contributions to the maximum pressure, and the last term is the ratio of the extensional to the shear viscosity, the Trouton ratio.

The shear and extensional contributions depend on the geometry of metering nip, such as the transfer roll cover deformation and the metering rod diameter, and the speed. At any operating conditions, the relative extension and shear rates are needed in order to determine the left hand side of Eq. 4.15. Both contributions can be approximated from numerical simulations. Still, the evaluation of the first partial derivative of Eq. 4.15 requires to run tests with fluids with constant shear viscosity; similarly, the evaluation of the second partial derivative requires maintaining the first partial derivative constant. Furthermore, the Trouton ratio is also needed for the mathematical development. The evaluation of the extensional and shear contributions

to the pressure, as well as the relationship between the extensional and shear viscosities with the coating colors was beyond the scope of the investigation. The Trouton ratio for the coating colors was considered as three in the spirit of Cohu and Magnin (1995) and Réglat and Tanguy (1998) regarding the evaluation of the process viscosity from maximum pressure measurements.

The rheological behavior of the coating colors is key on its performance in the film coater. The better the rheological behavior can be predicted in the coater, the higher the possibilities to increase the efficiency of the coating process. From a rheological viewpoint, this chapter has provided new and valuable information. Still, the process efficiency need to be investigated, general topic that is the subject of the chapter that follows.

CHAPTER 5

COATING COLORS RUNNABILITY IN THE METERING NIP

Roll coating instabilities have generated a lot of the attention since the late 1950's. The new knowledge that has been published through the years has followed the process requirements of the time and the tools available to carry out the investigation. The continuous increased industrial productivity has made evolve the manner of understanding the rheological behavior of the coating fluid under the new operating conditions (subject of chapter IV) and the instabilities that are generated. This investigation started in fact with the study of the coating defects appearing with Newtonian fluids and $CaCO_3$ suspensions (Réglat, 1997). Now, paper coating colors are used under the operating conditions currently encountered in the paper industry.

Thus, this second article deals with the understanding of the film coating defects that appear in the metering nip. Both ribbing and spitting are investigated as function of the operating conditions and coating color formulation. Pressure measurements, coating film visualizations, the rheological properties of the fluids, and the operating conditions are used to interpret the experimental results. Some comparisons are made with respect to the behavior observed with Newtonian fluids and $CaCO_3$ suspensions. New knowledge emerge, however, as a consequence of the use of the coating colors, the high speed, the additional instrumentation adapted to the laboratory coater, the new smaller metering rod, and the application of the novel knowledge available in the literature.

HYDRODYNAMIC INSTABILITIES IN THE METERING NIP OF A FILM COATER

S. Alonso and P.A. Tanguy

NSERC/Paprican Chair

Department of Chemical Engineering

École Polytechnique

P.O. Box 6079, Station Centre-ville

Montreal, Can., H3C 3A7

Keywords: metering nip flow, coating color, ribbing, spitting, pressure profile, stability.
Submitted: TAPPI Journal, May 2000.

5.1 Abstract

The hydrodynamic instabilities triggered in the metering section of a high-speed film coater are investigated using industrial paper coating formulations. Both ribbing and spitting are analyzed by image analysis of video recordings of the metered film. It is shown that the metering rod speed, the load on the metering rod, and the coating color rheological behavior have a dominant role in reducing both ribbing and spitting. Furthermore, it is revealed that the sub-ambient pressure downstream the nip is strongly related to the stability of the flow. The coating colors makedown system is also found to influence the color quality and therefore the coating color runnability. Finally, it is shown that standard rheological tests do not fully correlate with film coater runnability.

5.2 Introduction

Film coating is an industrially attractive process to coat mechanical or recycled paper grades with little stress on the web at high machine speeds. In a film coater, the film formation and film application processes are achieved in separate steps. The film is first created in the metering nip. The coating layer is then conveyed to the application nip, where it is finally transferred to the paper. The challenge of the process is to deliver a uniform coating film on the paper web with the desired coating thickness.

The film transfer technique allows to meter very uniform films, but usually at speeds lower than with a blade coater. At present, the film coating speed is limited to around 1500 m/min due to runnability problems (Pauksta, 1998). Indeed, at high speed, flow instabilities appear in the metering section, like ribbing and spitting (Fig. 5.1), and in the application section, like misting and orange peel, affecting the final coated paper quality.

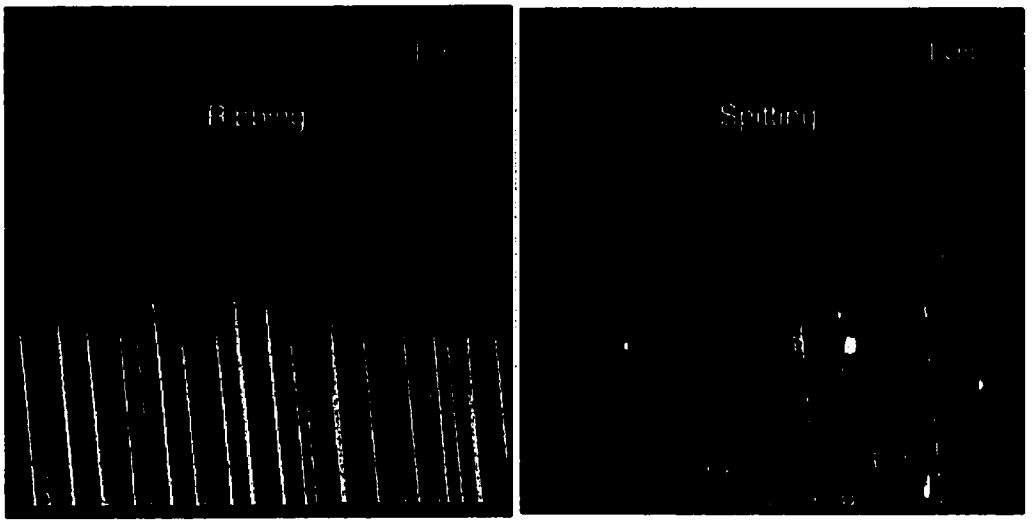

Figure 5.1 The two most common instabilities in the metering nip.

The uniformity of the metered film on the transfer roll depends on the stability of the flow. It has been found to be a function of the pressure profile within the metering nip (Pearson, 1960; Pitts and Greiller, 1961). In 1960, Pearson showed that the pressure gradient in the film splitting region governs the stability of the flow. Pitts and Greiller (1961) noted that as long as the pressure gradient near the film splitting region is negative, the flow is stable and uniform. When it is positive, the flow is unstable and ribs appear. Ribbing results from an equilibrium between the viscous forces through the nip and the surface tension forces at the meniscus (Pearson, 1960), and it can be correlated with the capillary number ($Ca = \mu V / \sigma_T$).

The capillary number has been extensively used to define the ribbing onset (Bauman, et al. 1981; Coyle, et al. 1990a; Greener, et al. 1980; Mill and South, 1967; Pitts and Greiller, 1980; Savage, 1984). Coyle et al. (1990a) showed that in reverse roll coating both the ribbing and cascade instabilities depend on the capillary number, the speed ratio, and nip gap. They introduced operating windows to identify the stable regions. In essence, ribbing is observed at low speed ratios, cascade at high speed ratios, but at intermediate speed ratios a stable uniform film can be obtained. In forward

roll coating, Coyle et al. (1990b) investigated numerically the stability of the flow by applying linear stability theory. According to their study, the transition to ribbing is due to perturbations triggered by end effects. They could accurately predict the capillary number at which the flow becomes unstable, and found that the Reynolds number stabilizes the short wavelengths (or rib widths), and destabilizes the long ones. Each rib contains a pair of vortices in which the liquid rotates so that the flow wells up to the free surface under the crest on the rib and descends under the trough. This phenomenon starts at the edges of the rolls, where the three-dimensional flow triggers a rib instability that grows when the speed is increased, destabilizing the flow. In industry, a coater can reach 8 m wide so that the roll edge geometry may not play a significant role. Still, ribbing is always present.

Hasegawa and Sorimachi (1993) showed that ribbing could be eliminated if a string was spanned over the gap so as touching the surface of the liquid meniscus. However, Decré et al. (1996), studying the fluid dynamics of the flow under the influence of a string, observed that the string does not eliminate ribbing buy only delays its appearance (up to 20 times its natural onset in the range of capillary numbers of 0.19-13.57), and that it controls the film splitting ratio and the total flow rate through the nip. Gurfinkel and Patera (1997) found that once the flow is unstable, the pressure gradient normal to the meniscus free surface is sufficiently large for ribs to grow and develop until the ribs converge to an asymptotic form. As a result, the downstream film also becomes ribbed so that the rib amplitude depends directly on the irregular meniscus form and the leveling due to surface tension forces. Gaskell et al. (1998) performing visualization experiments showed that internal eddy appear in both forward and reverse configurations for relatively wide gaps. They also showed that, in the reverse configuration, if the metering speed is increased, the meniscus moves towards the center of the nip. As a consequence, the size of the downstream eddy decreases, until disappearing, but at the same time increasing the possibility of air entrapment if the meniscus moves to the upstream side.

In the metering nip, the gap between the rolls is extremely small (~20 μm). In order to achieve such thin gaps, a deformable cover on the transfer roll is essential. Additional advantages of a soft roll cover include a lower risk of roll clashing, a reduction of the ribbing pattern, a decrease of the load that must be applied to the metering rod (Coyle, 1988; Dobbels and Mewis, 1978), and thinner films that can be transferred almost completely to the substrate (Carvalho, et al. 1993). Due to the deformation of the cover, the nip gap cannot be imposed; it results from an equilibrium between the elastic forces due to the deformation of the cover, the load applied to the metering rod, possibly flow normal stresses induced in the nip contraction, and more importantly, the hydrodynamic pressure generated by the flow (Réglat and Tanguy, 1997). Carvalho and Scriven (1997) used the lubrication theory coupled to the assumption of a capillary pressure driven flow in the film splitting region (viscocapillary model) together with a spring model to simulate the flow between deformable rolls. Their model predicts that the ribbing wavelength decreases when the capillary number increases, and that the deformation of the roll cover delays the onset of ribbing to higher speeds as compared with rigid rolls. However, coating with deformable rolls produces wider ribs, which are more difficult to level. Carvalho and Scriven (1999) carried out a three-dimensional stability analysis following the perturbation analysis of Coyle et al. (1990a). With such model they corroborated their own findings, i.e. in a deformable gap the ribbing pattern sets in at higher capillary numbers than in a rigid one.

Réglat and Tanguy (1997) analyzed the ribbing pattern in a laboratory film coater with a deformable cover. The instabilities were studied under industrially realistic operating conditions, i.e., small nip gap, and high speed (up to 1000 m/min). They evidenced the existence of an inertia regime at high speed and showed that the stability of the flow is strongly linked to the nip exit flow. Furthermore, the flow tends to be more stable if either the metering rod speed or the fluid viscosity is increased (reducing the rib width). The same trends were found when using non-Newtonian $CaCO_3$ suspensions, (Réglat and Tanguy, 1998), except that the rib width was twice as large as with Newtonian fluids, and that the rib width increased when the nip gap became

wider. As coating colors are much far complex than those fluids, further experimental study is necessary to describe their effect on the coating process.

Another instability associated with high coating speed is spitting. Adachi et al. (1988) reported for the first time the existence of little drops projected out of the nip. At the edges of the rolls there are two fluid rings, which are thicker than the inside liquid film, as reported by Coyle et al. (1990b). Spitting is seen when the centrifugal acceleration exceeds a characteristic limit for the liquid located on the roll edges, which depends on the surface tension and the density of the fluid (Adachi et al. 1988).

The film splitting region in the metering nip may be also subjected to spitting, depending on the operating conditions and the formulation. It is likely that surface tension forces and the rheological properties of the coating color influence the triggering of spitting (Salminen et al. 1996). Grön et al. (1996) reported that high solids content and high viscosity increase the spitting tendency. The same was found with a low water phase viscosity and high rod pressure. One way of alleviating the problem is to increase the metering rod speed and reduce its diameter (Rantanen, 1996; Triantafillopoulos and Smith, 1998). The pigment shape seems to play a role as well. For example, the fine and ball-form pigments are the worst to run in a coater and plate-like pigments are the best to run without spitting (Rantanen, 1996). Soft transfer rolls and pigments with low aspect ratio also reduce spitting (Grön et al. 1996). Triantafillopoulos and Lee (1996) reported that the vortices located downstream the nip break up when the speed increases. It causes the coating color to spit, particularly when the coating color viscosity is low. Spitting at the rod appears for colors with low polymer content and disappears with high polymer content (Grön et al. 1997). Despite all that information, no quantitative data about spitting, in terms of operating conditions and formulations, is available in the literature. An experimental investigation is needed so that spitting can be quantitatively assessed.

The coating color runnability can also be characterized with creep flow rheological measurements (transient rheological tests at very small constant shear

rates). Ghosh et al. (1997) found that the appearance of defects on the film in a blade coater is related to the rheological behavior of the coating colors at both small deformation and deformation rates. Typically, the shear stress under transient conditions increases up to a maximum, which corresponds to the stress that have to be overcome so that the fluid can start to flow, and then it decreases. The peak in shear stress can be correlated to the speed at which the defects in the coated film start to appear. Ghosh et al. (1997) found that the higher the transient shear stress peak, the higher the speed with a defect-free film running speed (the work was carried out in a cylindrical laboratory coater). Nevertheless, since the nip geometry of a film coater is significantly different, it is still unsure if that relationship remains valid.

In summary, ribbing has been extensively studied, although little work has been devoted to paper coating processes at very high speed. In contrast, spitting has attracted much less attention, especially from a quantitative standpoint. The objective of this paper is to address the general problem of flow instabilities in the metering nip of a film coater. Ribbing and spitting will be experimentally studied in the context of the paper coating processes. Paper coating formulations will be used to assess the operating conditions at which instabilities are minimized or eliminated. The role of mixing on the runnability of industrial coating colors will be also analyzed, as well as the runnability of basic coating colors in relation with their rheological behavior at low deformation.

5.3 Experimental

5.3.1 Measurements

A laboratory film coater was used to investigate the runnability of the coating colors. To evidence the instabilities in the process, a visualization technique coupled with image analysis was employed (Réglat and Tanguy, 1997, 1998). Briefly, a source of light is used to illuminate the film on the transfer roll surface in contraposition with a camera, so shaded and bright areas are seen (Fig. 5.2). The shadows correspond to

the trough of the ribs, and the bright parts are the crests. The striation area can be decomposed in a spectrum of light intensity peaks by an image analysis software, so the ribs can be counted and measured. The same criteria are used to assess all the ribbing patterns, so the variation in the results depends mainly on the unstable ribbing pattern obtained. The spitting instability is assessed with the same video recordings, where the spitting onset is defined at the speed at which it is first seen on the video.

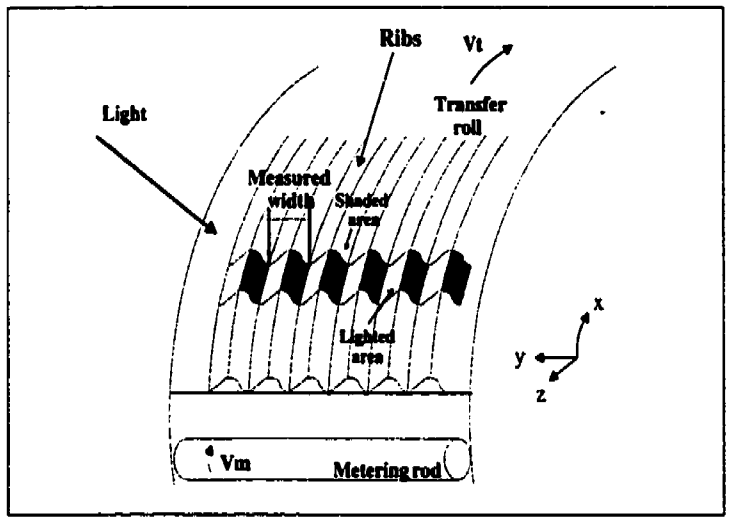

Figure 5.2 Visualization of the rib pattern.

The film coater is also instrumented with a wall-mounted fast response time piezo transducer located in the middle of the metering rod. This sensor allows the determination of the nip pressure profile, which is used to assess the stability of the flow. The range of measurements is from –50 kPa to 650 kPa (relative to the atmospheric pressure). Furthermore, two displacement transducers, located at each end of the rod, measure the position of the metering rod with respect to the undeformed surface of the transfer roll. The range of measurements is from –250 μm to 350 μm, and the position is given by the mean value of the two measurements. It is considered as correct if the difference is less than 15 μm. The zero position is defined by naked eye when the rod and the transfer roll are in slight contact at rest (without deformation of the

transfer roll cover), with an uncertainty of ±20 μm. A calibration procedure, however, makes it possible to keep the same bias for all the measurements. Repeatability gives a relative uncertainty of ±5 μm. When the coater is set in motion, a load is applied on the metering rod in order to change its position, i.e., to increase or decrease the roll-rod clearance (nip gap). The actual value of the clearance is always unknown for the transfer roll cover deforms according to the hydrodynamic pressure generated by the flow.

5.3.2 Test fluids

Several coating formulations (100 parts of clay used as dry basis) were prepared for this work (Table 5.1) according to the following procedure. The dispersant was first added to the amount of deionized water necessary to achieve the target solids percentage. The slurry was made by slowly adding the clay with a vibrating feeder. The suspension was thoroughly mixed during half an hour to ensure homogenization. Then, the latex suspension was added, followed by the CMC previously hydrated, with continuous agitation. The color was next stirred for another 30 minutes, and then the pH was adjusted to 8.0 by adding NaOH. At the end, the coating color was further stirred for one hour to stabilize the pH. A similar procedure was carried out for the makedown of the industrial coating colors.

Table 5.1 Coating color formulations (pph of clay basis).

LABEL	Regular clay	Calcined clay	Dispersant	Latex	CMC	% Solids	Mixing system
A	100	---	0.04	10	0	61.3	1
B	100	---	0.04	10	0.25	60.0	1
C	100	---	0.04	10	0.50	61.0	1
D	100	---	0.04	10	0.75	60.8	1
E	100	---	0.04	10	1.0	61.0	1
F	100	----	0.04	10	0.5	56.0	1
G	100	---	0.04	10	0.5	63.3	1
ICC1	90	10	Non available			60.0	1
ICC2	90	10	Non available			60.0	2

All coating colors were made in a laboratory coating kitchen. Two different mixing systems were used: a low shear rate system (called mixing system 1 in the forthcoming) based on a new coaxial mixer composed of a scraping anchor arm and a wetting/dispersing agitator (Thibault, 1999), and a high shear rate system (mixing system 2) commonly used in industry, consisting of a saw tooth (Cowles) turbine, rotating at very high speed. All suspensions and coating colors were used within 24 hours following the makedown.

The steady state rheological characterization was carried out with a stress-controlled CVO Bolhin rheometer and a Couette geometry. Small amplitude oscillation shear experiments were performed in the linear viscoelastic region, which was predetermined by a strain amplitude sweep at constant frequency. Creep flow tests were also performed on the CMC-containing coating colors to assess the role of the transient shear stress on the runnability in the laboratory roll coater. A RFXII rheometer, from Rheometrics Inc., was used for the creep flow tests.

5.4 Results and discussion

5.4.1 Fluid properties

Fig. 5.3 show the flow curves for the coating colors. They all exhibit shear-thinning behavior which can be well described with a power law model with a plateau viscosity at high shear rates, namely $\eta = m\dot{\gamma}^{n} + \eta_{\infty}$ (Table 5.2). Several remarks can be made regarding the viscous behavior. The power law index remains within a relatively narrow range but decreases slightly with the CMC concentration and solids content. The consistency index is also proportional to the thickener concentration and solids content. The viscosity changes drastically when the water-soluble polymer is added, shifting up the flow curve by about one decade. The thickener concentration determines the structure level in the coating color, since the highest viscosity appears in the more concentrated suspension with respect to CMC (Yziquel et al. 1999). Both power and consistency index of the industrial coating colors lie within the range of the other colors but have higher plateau viscosities at high shear rates. Color ICC1 has a slightly higher viscosity at high shear rates than color ICC2 due to the relative low shear rate imposed by mixing system 1, producing a coating color with apparently larger aggregates. No constant viscosity at low shear rates and no shear-thickening behavior at high shear rates were observed with any formulation.

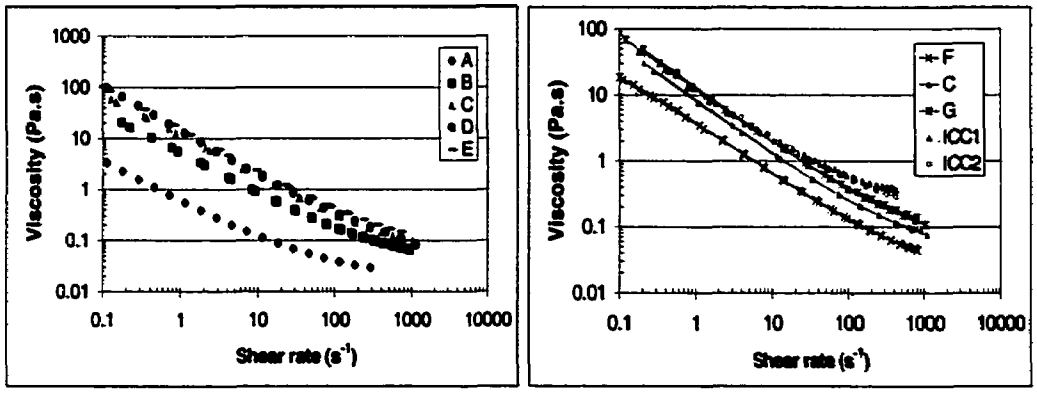

Figure 5.3 Shear viscosity of coating colors at different CMC concentrations (left), industrial and at different solids contents (right).

Table 5.2 Rheological parameters of coating colors.

Coating color Label	m	n	η_∞
A	0.58	0.225	0.022
B	5.0	0.220	0.044
C	10.5	0.170	0.063
D	16.5	0.160	0.079
E	16.0	0.145	0.090
F	3.70	0.220	0.027
G	11.5	0.184	0.088
ICC1	12.5	0.185	0.280
ICC2	13.6	0.180	0.200

Figs. 5.4(a,b) show the variation of the elastic modulus *vs* frequency at a deformation of 0.005 (within the linear viscoelastic region) for all coating colors. It can be seen that the elastic modulus increases with the polymer concentration, solids content, and frequency. The elastic modulus decreases slightly at low frequencies. The viscous modulus is about an order of magnitude lower than the elastic modulus, and the phase angle is less than 15° in all cases (not shown), meaning that all the samples are elastic at very small deformation.

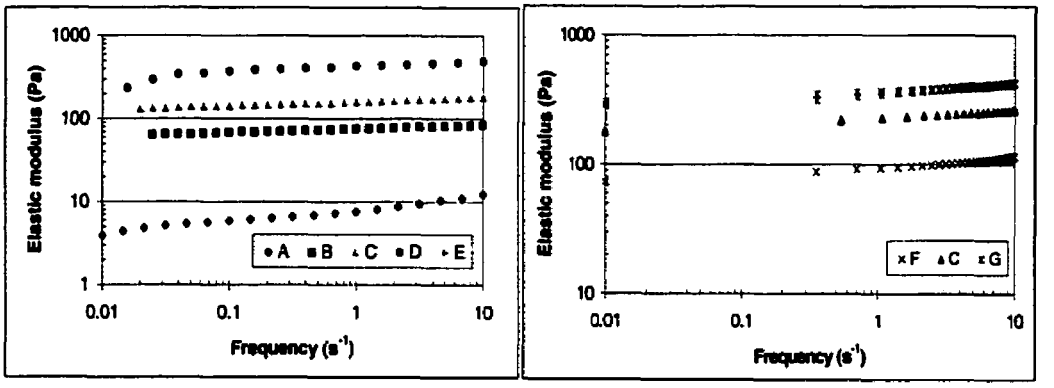

Figure 5.4(a) Elastic modulus of the coating colors at different CMC concentrations (left) and solids contents (right).

As with the shear viscosity, the elasticity is proportional to the thickener concentration and solids content (color E has higher elastic modulus than color D, although the logarithmic scale makes them appear almost equal). An increase in the polymer concentration results in stronger bindings among particles (Yziquel et al. 1999). A similar behavior is seen when the solids concentration increases. Although the polymer concentration is constant, there are more particles to bridge, resulting in a more elastic suspension. For the industrial coating colors, the elastic modulus is similar to that of coating color C. The elasticity of color ICC2 is slightly higher at low frequencies, but at high frequencies the data superpose. As a result, oscillatory tests do not differentiate the two industrial coating colors.

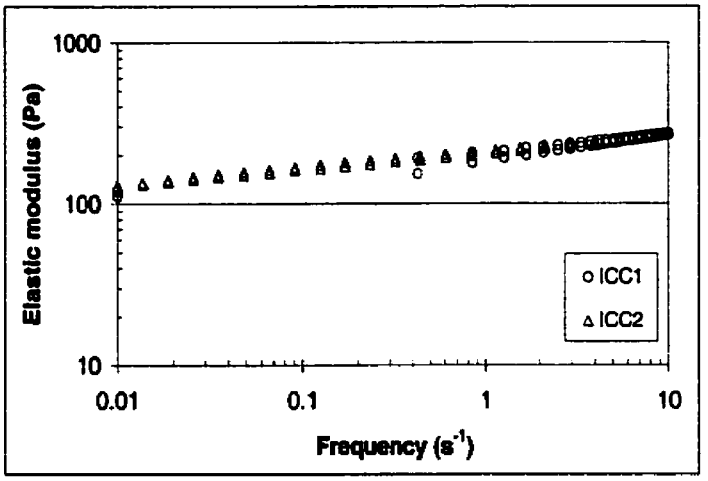

Figure 5.4(b) Elastic modulus of the industrial coating colors.

5.4.2 Ribbing

Ribbing is a series of waves formed on the film surface. Most of the ribbing patterns obtained in this investigation were time dependent, so special care was taken in selecting the most representative ribbing profiles. No information could be inferred about the height of the ribs so that only the rib width is presented.

The ribbing pattern behavior in this investigation follows some of the trends found with more simple fluids. For Newtonian fluids, an increase in viscosity increases the rib width, but it shows no dependency on the nip gap (Réglat and Tanguy, 1997). For $CaCO_3$ suspensions and coating colors, the rib width increases with particle and/or polymer concentration, but it decreases when decreasing the roll-rod clearance (Réglat and Tanguy, 1998).

Although the coating colors have higher high shear rate constant viscosities than $CaCO_3$ suspensions (Réglat and Tanguy, 1998), the coating colors yield consistently smaller ribs. The rib width for the coating colors decreases smoothly when narrowing the nip gap (Fig. 5.5a). As an illustration, the rate at which the rib width decreases with

$CaCO_3$ (inelastic) suspensions is very sharp, from 1.47 mm at a metering rod position of 70 μm, to 0.98 mm at 10 μm, while with coating colors the decrease is of only 0.1 mm in the same range. The smoother reduction in the rib width may be attributed to three factors:

a) The smaller metering rod used in the present investigation gives a less curved meniscus downstream the nip, stabilizing the flow due to the increased diverging angle of the roll surfaces (Rushack, 1985).
b) The reduction is affected by the higher degree of shear-thinning behavior of the coating colors with respect to the $CaCO_3$ suspensions (Réglat and Tanguy, 1998).
c) The role that elasticity may play in the process (Coyle et al. 1990c).

In the case of the transfer roll speed, its influence on the rib width is barely noticeable at high speeds (Fig. 5.5b). The rib width observed lies within the range expected by Carvalho and Scriven (1997) at very high capillary numbers, where the effect of surface tension is very low. At the same time, the Reynolds number is not negligible, so that an equilibrium between the capillary number (a viscous stabilizing factor) and the Reynolds number (an inertia destabilizing factor) takes place, specially in the upstream nip region. The Reynolds number is defined there as $Re = \rho V_t H/\mu$, where ρ is the density, V_t the transfer speed, H the nip gap, and μ the viscosity (Réglat and Tanguy, 1997, 1998). When the speed is increased, the capillary number rises, enhancing the viscous effect on the flow, but at the same time, the Reynolds number rises as well, increasing the inertia effects. Both effects are in competition. Wide gaps are more sensitive to capillary effects, while narrow ones are dominated by inertia (Réglat and Tanguy, 1998).

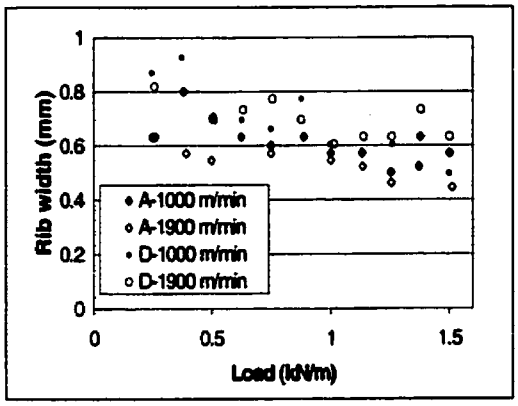

Figure 5.5(a) Rib width as a function of load on the metering rod at two transfer roll speeds.

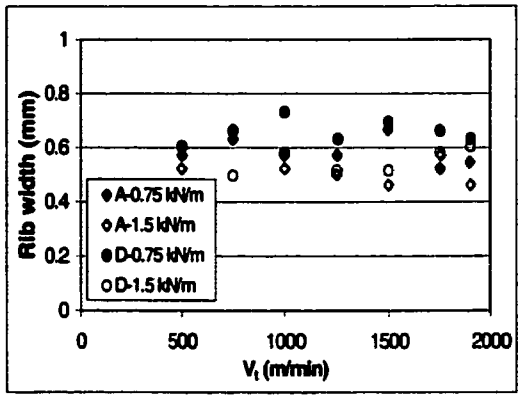

Figure 5.5(b) Rib width as a function of the transfer roll speed at two different loads on the metering rod.

High transfer speeds require high metering loads to maintain a suitable coating thickness. At high transfer speeds and loads, the influence of the metering speed on the ribbing pattern is reduced (Fig. 5.5c), contrary to what occurs at relatively low speeds, where an increase of the metering speed decreases the rib width. This observation might be explained by slippage phenomena on the metering rod, which would make it more difficult to move the downstream meniscus towards the center of the nip to decrease the size of the downstream recirculations.

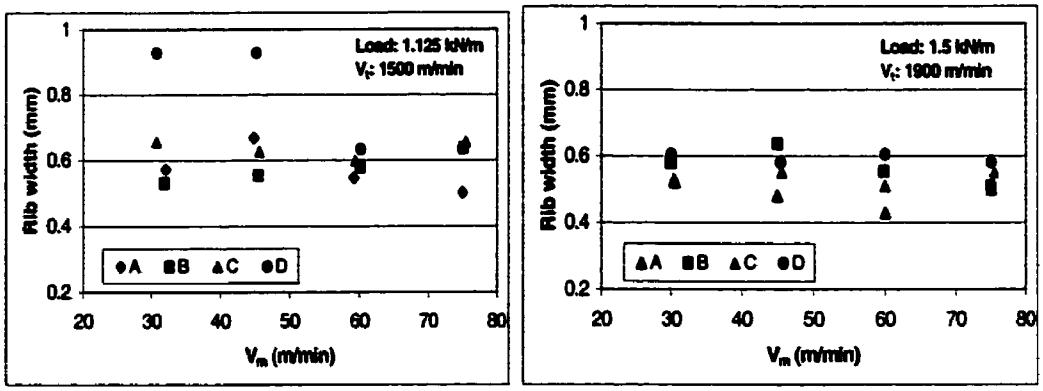

Figure 5.5(c) Rib width as a function of V_m for different CMC concentrations.

For the two industrial coating colors, which exhibit the same elastic behavior at small deformation but different high shear viscosities when compared to the other coating colors, the ribbing pattern behaved as follows:

- When the transfer speed is increased, the rib width increases with the more viscous industrial coating color (ICC1), but it remains relatively constant with the other one (ICC2).
- When the metering speed is increased, the rib width remains relatively constant with the more viscous color (ICC1), but it decreases with the other one (ICC2).
- At high metering speeds, when the transfer speed is increased, the rib width remains relatively constant for both industrial coating colors.
- The rib width is consistently larger with the more viscous coating color (ICC1).
- The rib width decreases when reducing the nip gap and is consistently smaller than that of the model coating colors, even if they have higher shear viscosities.

Thus, the hydrodynamic behavior of both industrial coating colors is quite different from one another under identical operating conditions (Fig. 5.5d). This shows how important the coating mixing may be (Persson et al. 1997). Coating color ICC2 is, a priori, better dispersed, due to the higher shear rates employed in the makedown and the lower high shear rate viscosity obtained in the rheometer. It gives better ribbing runnability as smaller ribs are easier to level; even better runnability than the model coating colors, showing how the inertia effects are reduced (decreased Re number) and the viscous effects increased (increased Ca number) when the shear viscosity is increased. In terms of the final coated paper quality, it has been suggested (Persson et al. 1997) that aggregation of particles may increase the gloss of the final coating film, so a lower gloss may be expected from ICC2.

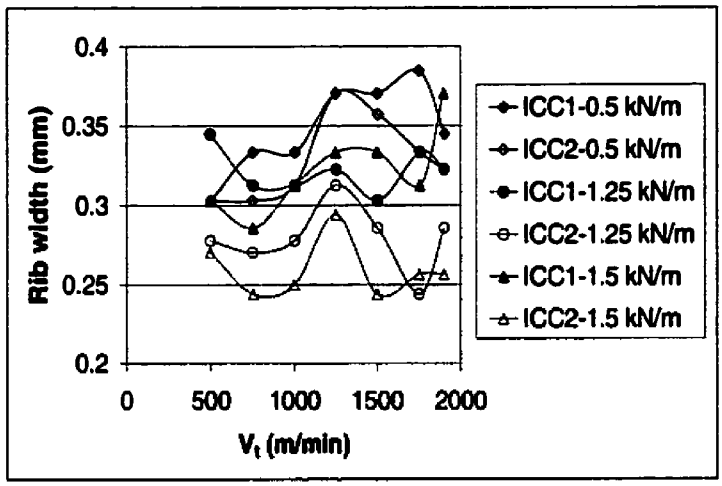

Figure 5.5(d) Rib width as a function of V_t for the two industrial coating colors.

5.4.3 Spitting phenomenon

Spitting is a series of small drops projected out of the nip. It usually starts at the edges, and it then propagates toward the center of the nip. Fig. 5.6(a) shows the conditions at which spitting occurs. Three hydrodynamic regions are clearly identified as in Réglat and Tanguy (1997, 1998):

a) at wide nip gaps, spitting is always present and can be very significant due to air entrapment.
b) at intermediate nip gaps, spitting may or may not be observed. This region is more sensitive to capillary effects and corresponds to the wide-gap region reported earlier (Réglat and Tanguy, 1997, 1998).
c) at narrow nip gaps, spitting may also appear. This region is more sensitive to inertia effects and corresponds to the narrow-gap region in Réglat and Tanguy (1997, 1998).

As the load on the metering rod is increased, the first change in slope in Fig. 5.6(a) determines when the air stops entering the nip, although spitting continues. Even

after the second change in slope, the instability is still observed. Within the narrow gap region, spitting stops while the slope remains constant for each coating color. This constant slope, independent of the spitting phenomenon, means that this instability is not related to the nip gap, but more likely to the coating formulation and the hydrodynamics of the flow. Yet, if the load is further increased, spitting may reappear. This spitting pattern was observed only with the more viscous formulations (E and G), including the two industrial coating colors.

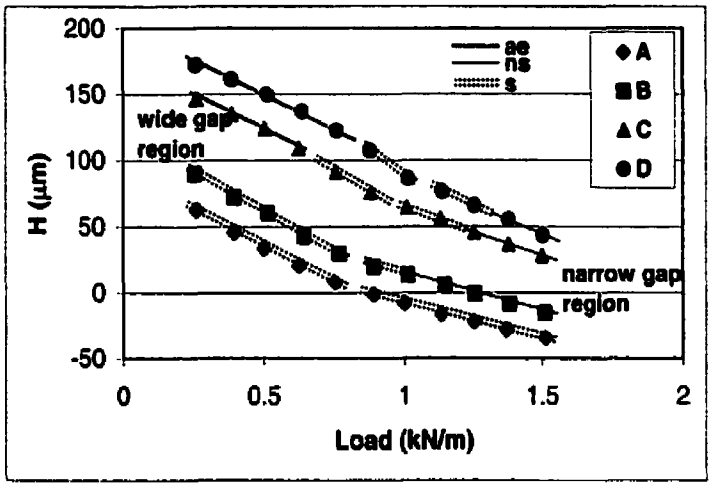

Figure 5.6(a) Apparent nip gap as function of the load on the metering rod (s = spitting present, ns = no spitting, and ae = air entrapment).

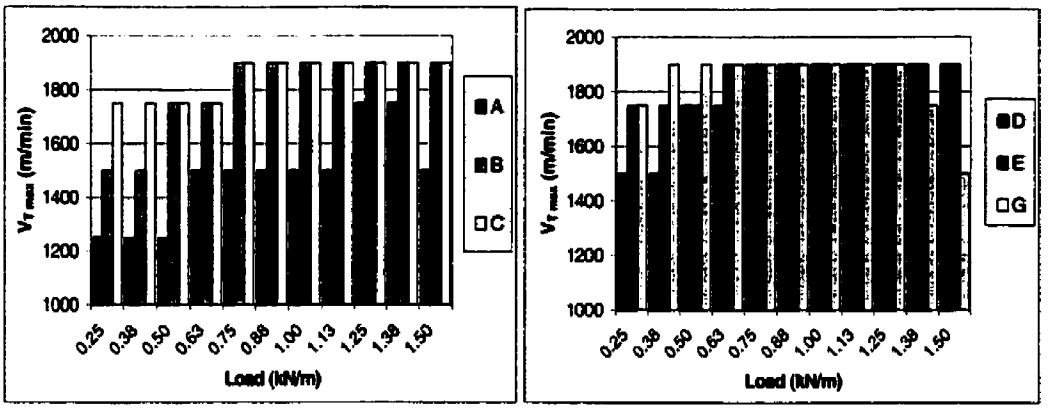

Figure 5.6(b) Speed range at which spitting could be avoided (the maximum speed of the laboratory roll coater is 1900 m/min).

We now continue with the analysis of the influence of the coating formulation on the spitting phenomenon (Fig. 5.6b). Spitting is seen at lower speeds with lower contents of either CMC or solids. This may be explained by the low water phase viscosity (Grön et al. 1996). At high thickener and/or solids concentrations, spitting sets in at higher speeds, which also correlates with the viscosity of the fluid. In the case of the industrial coating colors, Fig. 5.6(c) shows that the spitting onset is lower at a metering speed of 30 m/min with color ICC1. However, at 60 m/min the behavior is reversed. This suggests again that the coating color homogeneity may significantly influence the coating color runnability. Additionally, it has been shown that the coating color makedown can significantly affect runnability (Persson et al. 1997), as it is the case here since both industrial formulations were identical but made with different mixers. This confirms the importance of the rheological behavior of the coating formulation in the occurrence of spitting.

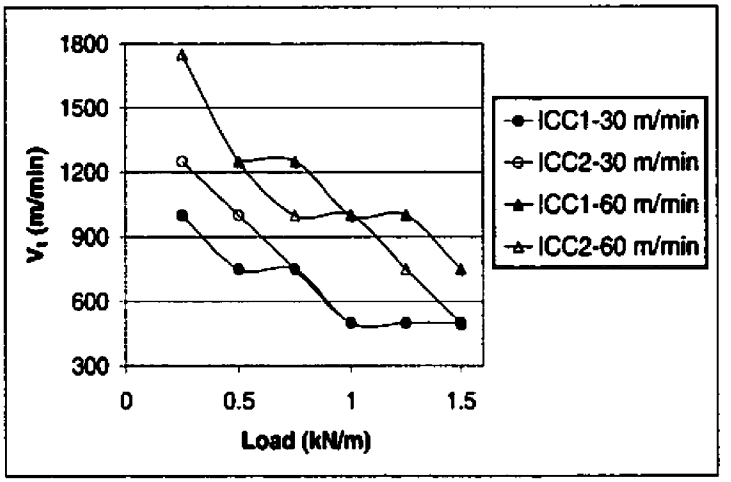

Figure 5.6(c) Spitting onset as a function of load and the metering rod speed for the two industrial coating colors.

Centrifugal forces may also play an important role in the occurrence of spitting (Adachi et al. 1988) in a similar way as it may explain misting in the application nip (Roper et al. 1998). The eddies located downstream the nip are subjected to centrifugal forces provided by the transfer roll rotation. When the transfer speed is increased, these centrifugal forces are also increased. At the point where they get higher than both surface tension and viscous forces (Adachi et al. 1988), the vortices discharge as spitting and reformed again (Coyle et al. 1990b; Triantafillopoulos and Lee, 1996). When the metering speed is increased, the opposite rotation of the rod may dampen the centrifugal forces by reducing the size of the recirculations as the downstream meniscus moves towards the nip center (Gaskell et al. 1998). This is readily seen in the experiments as a size reduction of the spitting drops until they disappear.

Additional information can be obtained from the instabilities in terms of the transfer speed and creeping flow rheological measurements. Following Ghosh et al. (1997), transient shear stress (σ^+) measurements were performed as function of strain (the product of the shear rate and time). A constant shear rate of 1.85×10^{-2} s^{-1} was applied to the coating colors after equilibrium (without prior important deformation). This value was chosen to decrease the noise sometimes observed during creep flow

rheological tests. For each color, a peak in the stress response was obtained. The critical strain at which the shear stress is maximum represents the limit between solid-like and liquid-like behavior; the maximum stress can then be interpreted as an energy barrier that has to be overcome so that the fluid can start to flow (Ghosh et al. 1997).

The critical maximum transient stresses σ^+ obtained are plotted in Fig. 5.7. σ^+ increases with CMC concentration and solids content. The maximum transfer speed V_{Tmax} at which the coating color could be run without spitting is also shown. In a cylindrical laboratory coater (CLC), the runnability is proportional to the maximum transient shear stress (Ghosh et al. 1997). In this investigation, the thickener increases the value of σ^+, whereas the ribbing pattern shows wider ribs; the tendency for proportionality between σ^+ and the runnable speed without spitting holds except for coating color D. In terms of solid content, σ^+ follows the same general tendency, i.e. it increases with solids content, although wider ribs would be expected. When comparing coating colors altogether, it is observed that runnability does not always correlate with the maximum value of σ^+. The more likely explanations may be the influence of the diverging geometry at the exit of the nip in film coating that does not exists in blade coating and the similarities between the conditions of deformation in the blade nip with the purely shear conditions existing in a conventional rheometer.

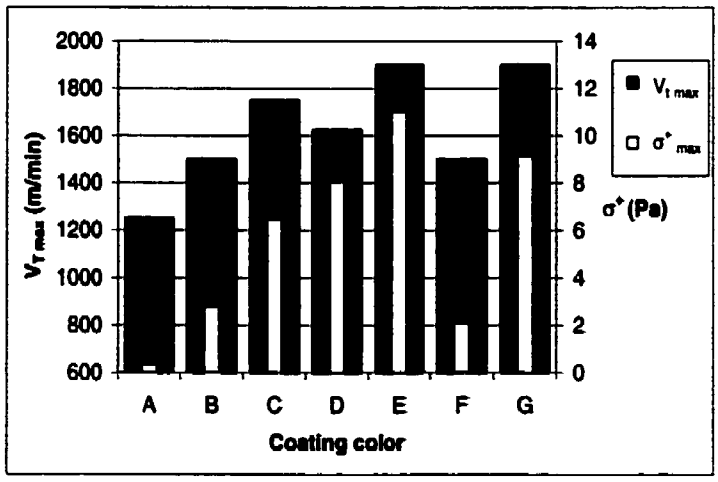

Figure 5.7 Runnability of coating colors.

5.4.5 Pressure measurements

The stability of the flow can also be assessed in terms of the pressure profile (Fig. 5.8a). When the flow is stable to spitting, profile (b) is obtained; however, once spitting is present, profile (a) is more likely to be measured. Both pressure profiles show the same general trend, with a remarkably lower standard deviation for profile (a) due to the more stable flow hydrodynamics, increasing the flow conditions reproducibility.

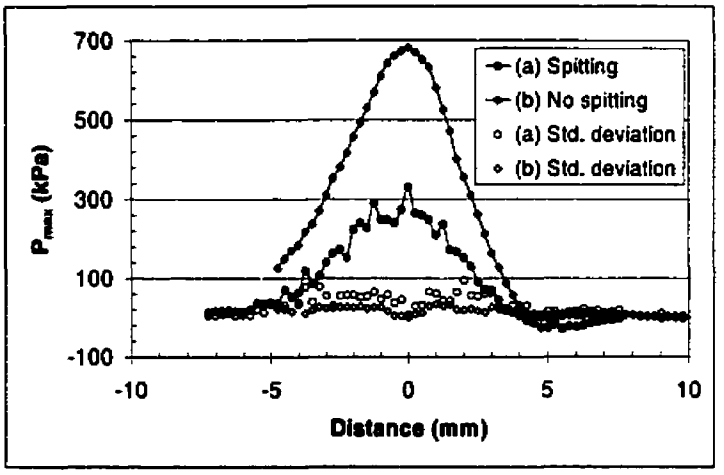

Figure 5.8(a) Pressure profiles with and without spitting (the maximum pressure is arbitrarily set at distance zero).

The stability of the flow has been also confirmed by analyzing the sub-ambient region of the pressure profile (Fig. 5.8b). When the transfer speed is increased, the downstream meniscus is farther from the nip center. As a result, there is more room for the recirculations to grow and develop, and the sub-ambient pressure is lower, so there is more tendency to spit. On the other hand, an increased metering rod speed shortens the length of the downstream part of the nip, minimizing the size of the recirculations (Gaskell et al. 1998) and increasing the minimum pressure, stabilizing the flow (the metering speed decreases the size of the drops projected as spitting until disappearing). When the load is increased, spitting stops but reappears at very high loads. The behavior of the minimum pressure is not as clear as when changing the

speed due to the deformation of the roll cover (the rod-roll clearance may not change significantly at very high loads). The minimum pressure seems to be low with either too high or too low loads, as when spitting is observed.

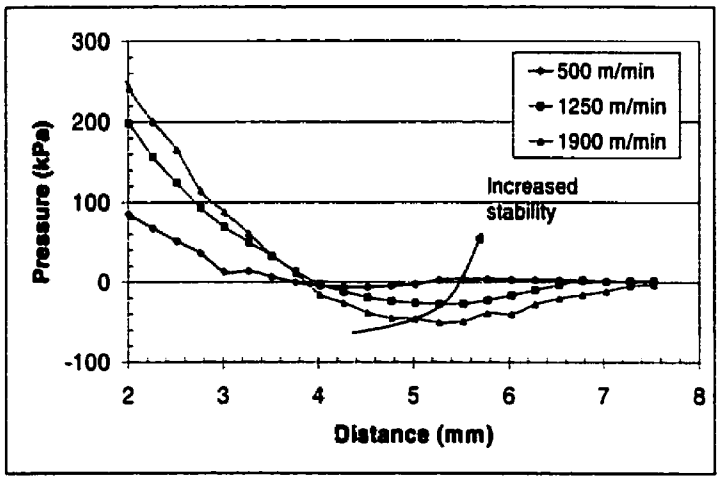

Figure 5.8(b) Subambient pressure profiles as function of the transfer speed for coating color C.

5.5 Conclusion

The general problem of flow instabilities in roll coating has been investigated. The coating color rheological behavior and the metering rod speed play an important role in the hydrodynamics of the flow and the instabilities that are generated. The ribbing pattern is a function of the operating conditions and the rheological properties of the coating color. Two spitting regimes have been observed, one at low loads and the other one at high loads. It has also been found that increasing the metering rod speed decreases the spitting drop size until spitting disappears. Furthermore, pressure profile measurements indicate that the stability of the flow is strongly linked to the sub-ambient pressure downstream the metering nip. The use of a high-shear coating color makedown increases the runnability of the metering coating process. Finally, creeping

flow tests performed in the coating colors have shown that in film coating runnability and transient shear stress rheological measurements do not always correlate.

5.6 Additional Results

5.6.1 Maximum pressure with coating colors

The pressure profile that was obtained with coating colors followed the overall trends already found experimentally with Newtonian and pigmented fluids (Réglat and Tanguy, 1997, 1998):

- The maximum pressure increases with transfer speed, load, and viscosity, i.e., CMC concentration and solids content.
- The two hydrodynamic configurations observed in Réglat and Tanguy (1997, 1988) can also be observed (Fig. 5.9).
- The length of the nip decreases with load but increases with transfer speed and viscosity.
- The minimum pressure decreases with transfer speed but increases with viscosity.

The decrease in the metering rod diameter from 8 cm to 4 cm has yielded a metering nip geometry with a steeper converging-diverging geometry (Réglat, 1997). As a result, there is more room for the recirculations, specially upstream the nip, and the nip length have increased. The maximum pressure is now lower, with a larger high-load region. The shift factors (sensitivity coefficients) are lower with the smaller rod diameter, indicating a diminished sensitivity of the maximum pressure with respect to the metering rod position, the viscosity of the fluid, and the coating speed (Alonso et al. 2000a; Réglat and Tanguy, 1997, 1998).

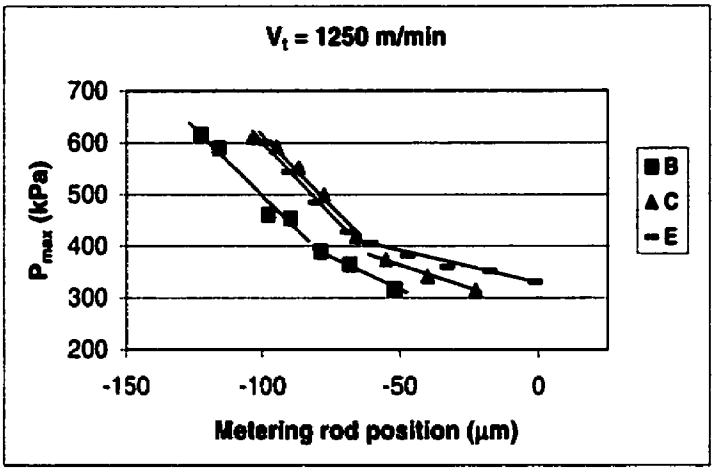

Figure 5.9 Maximum pressure within the nip as a function of the relative position of the metering rod.

5.6.2 Viscous dissipation in the metering nip

Viscous dissipation is the heat generated due to excessive friction between fluid layers when the fluid flows, i.e. mechanical energy is degraded into thermal energy. In the limit of parallel plates for flow of Newtonian fluids, the heat generated depends on the local velocity gradient and the viscosity of the fluid (Bird et al. 1960), namely

$$S_v = -\tau_{yz}\left(\frac{dv_y}{dx}\right) = \mu\left(\frac{V}{b}\right)^2 \tag{5.1}$$

where S_v is the rate of viscous heat production per unit volume. The conditions encountered in the metering nip (small nip gaps and high speeds) may induce heat generation in the fluid, specially near the metering rod surface, where the maximum velocity gradients occur.

The Brinkman number is a measure of the importance of the viscous dissipation in relation with the heat flow resulting from the temperature difference between the walls. When Br is higher than 2, there is a maximum temperature somewhere between the two walls

$$Br = \frac{\mu V_t^2}{K(T_b - T_0)} \tag{5.2}$$

For the metering nip, we assume a temperature difference of 3°C to evaluate the Br number and obtain the range of [10-52]. There is a maximum in temperature in the nip, but since the dwell time of the fluid is very short, the heat generated will be almost immediately carried away by conduction and convection. The product of the Pr·Re measures the ratio of heat transport by convection to heat transport by conduction (Bird et al. 1960) as

$$\Pr \cdot Re = \frac{\rho C_p V_t H}{K} \tag{5.3}$$

In the metering nip, the product Pr·Re is in the range [20-150], which means that the generated heat will be mostly transferred by convection. The heat will be transferred either as an increase in temperature on the metering rod or through the surroundings, since the thermal conductivity of the elastomer is low. The dissipation of the generated heat depends on the heat transfer convective coefficients fluid-rod and fluid-air. In the metering nip, temperature measurements on the rod may provide some information about the degree of viscous dissipation. Respect to the free surface, the high speeds at which the process is carried out involves a large amount of air being dragged by the transfer roll. In such a case, this is a forced convection problem with a high air-fluid convective heat transfer coefficient *h*. The heat transfer coefficient *h* depends in a complicated way on many variables such as the conductivity, the density, the viscosity, the specific heat coefficient of the fluid, the system geometry, the flow velocity, and the temperature of the system (Bird et al. 1960); thus, the prediction of that coefficient in the metering nip is in reality a complicated task.

In order to analyze the significance of viscous heat generation in the metering nip, the temperature was monitored in several locations of the laboratory coater, including the film temperature on the transfer roll. Although all temperatures were measured at all operating conditions, Fig. 5.10 shows only the more critical ones at which viscous dissipation was more likely to occur for the more viscous color (coating color C). The results correspond to test that take about seven minutes to be carried out. Fig. 5.10 (a) shows that the temperature of the fluid decreases in both tank and headbox due to the cooling effect of the whole coating machine system. At low speeds similar trends are observed on the metering rod and the film, but at high speeds both rod and film temperatures increase. At very high speeds, the viscous dissipation is slightly higher than the cooling effect of the air dragged by the transfer roll. Fig. 5.10 (b) depicts similar quantitative behavior: relatively low temperatures at very low loads but slight heating effects at high loading. Nevertheless, for both cases, the maximum temperature difference on the film and metering rod are of the order of 1.5°C in the more extreme conditions (very small temperature difference when compared to the variations observed in the coating makedown: up to 8°C in mixing system (1) and 30°C in the mixing system (2) during the coating makedown). It might be possible that other formulations with a higher viscosity, specially those which are shear-thickening, trigger higher temperature variations in the nip.

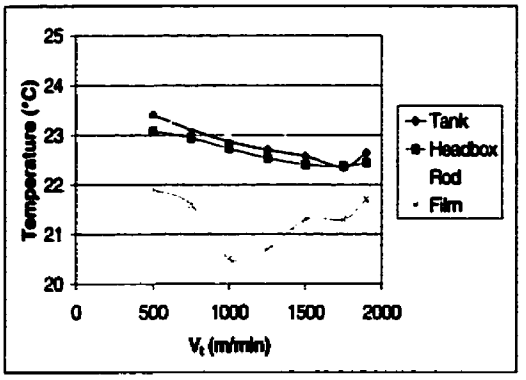

Figure 5.10(a) Temperatures from the coating reservoir to the final film on the transfer roll at 1.5 kN/m.

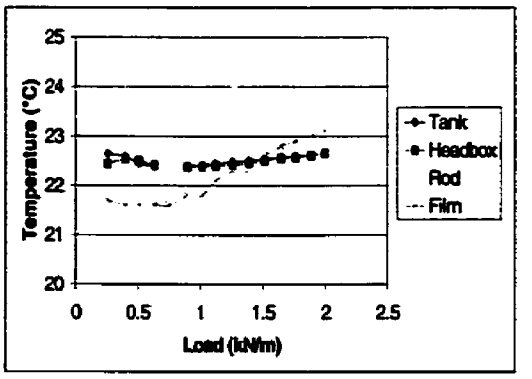

Figure 5.10(b) Temperatures from the coating reservoir to the final film on the transfer roll at 1900 m/min.

5.7 Additional Remarks

With our coating formulations, the possible effect of elasticity could not be separated from the viscous effects. Rheological measurements showed that the CMC and the solids content increased both viscosity and the elastic modulus. We observed that the effect of the solids content and thickener was similar in terms of runnability problems. New formulations with similar viscous behavior but different elasticity could give new insights about the effect of elasticity on the process instabilities. The investigation of Ghosh et al. (1997) showed how similar viscous behavior (equal viscosities) but different elastic behavior results in different runnability. However, from what we have seen in the experiments, a slight change in the plateau viscosity (even as low as 15 mPa.s) can be enough to change the runnability of that color in a film coater. We believe that the small differences in the plateau viscosities of the coating colors of Ghosh et al. (1997) may have influenced somehow its runnability in the blade coater, although that effect when compared to the elastic effects due to the CMC could have been small.

The origin of the spitting phenomena is still unclear. Pressure measurements could give further information to elucidate if the spitting drops come from cavitation effects in order to support or eliminate the theory of centrifugal forces. In this investigation, the pressure measurements were obtained mainly to read the maximum pressure (the range of the measurements of the pressure transducer does not allow to focus on both maximum and minimum pressures simultaneously, except in some cases of both medium speeds and loads.) Further experiments would be required, focused in measuring sub-ambient pressures to link them to the spitting phenomena. In some cases in our experiments, we were capable of measuring negative pressures up to 60 kPa. The big size of the pressure transducer with respect to the length of the region of negative pressure might be of importance in the sense that lower minimum pressures may take place but the current pressure transducer does not allow to measure them.

CHAPTER 6

PROCESS VISCOSITY IN REVERSE ROLL COATING

The results obtained in Chapter IV motivated the reexamination of the process viscosity of the coating colors. The uncertainty with respect to the influence of the extensional contribution to the flow and the extensional behavior of the coating color in the nip represents a formidable challenge. As a result, we propose a new process viscosity model evaluated in a region of primary shear flow. In this sense, the uncertainty with respect to the converging-diverging geometry of the nip would be reduced. The comparison with the results from the rheometer would be more representative than before since in the rheometer only pure shear is accounted for. Furthermore, step growth tests in the rheometer were chosen as a reference state since they represent in a closer manner the transient nature of the metering nip flow. Transient tests in the rheometer also allow to consider the shearing history to which the coating colors are always subjected before arriving to the metering nip. At the same time, the proposed method is simplified by avoiding both the use of Newtonian reference fluids and relying on the evaluation of the experimental nip gap. In summary, a new evaluation of the process viscosity is proposed and a more complete rheological characterization is made in order to better understand the coating colors rheological behavior in the metering nip.

PROCESS VISCOSITY IN REVERSE ROLL COATING

S. Alonso, O. Réglat, F. Bertrand, L. Choplin, and P.A. Tanguy

NSERC/Paprican Chair

Department of Chemical Engineering

École Polytechnique

P.O. Box 6079, Station Centre-ville

Montreal H3C 3A7

Canada

Keywords: metering nip, lubrication theory, coating color, transient viscosity, process viscosity.

Submitted: Trans. IChemE., May 2000.

6.1 Abstract

The rheological behavior of paper coating colors is investigated in the metering section of a laboratory reverse roll coater. The objective is to combine measurements of pressure in the metering nip and torque on the metering rod to calculate the process viscosity. Classical rheological tests and nip flow numerical simulations are also required to complete the process viscosity evaluation. This viscosity is compared with that measured from step growth experiments in a rheometer. The discrepancy observed between these two viscosities is mainly attributed to the rheological properties of the coating fluids. Furthermore, structure breakdown at relatively low shear rates suggests that steady state may not be reached in the metering nip. From numerical simulations, the pressure-driven contribution to the flow in the center of the metering nip has been found constant in the case of Newtonian fluids, dependent on the shear-thinning index in the case of non-Newtonian fluids, and independent of inertia effects.

6.2 Introduction

Reverse roll coating is a technique commonly used in the coating industry to meter a thin fluid film on a moving substrate. During the film formation, the fluid is subjected to very high shear and extensional rates over a very short period of time. The fluid domain changes as function of the hydrodynamic pressure within the nip as a result of the deformable cover usually used on one of the rolls. The free surface also adds more complexity to the flow due to the force equilibrium in the fluid-gas interface. Last of all, the rheological behavior of the coating fluid is usually non-Newtonian, so the metering flow hydrodynamics is finally very difficult to describe.

For many years now, researchers have used the lubrication theory as well as the full Navier-Stokes equations (CFD models) to investigate reverse roll coating flows (Coyle et al. 1990a,b,c; Fourcade et al. 1999;Greener and Middleman, 1981; Kang and Liu, 1991; Poranen and Niemistö, 1999). For the lubrication theory, the main hypothesis is that inertia effects are neglected. When applied to reverse roll coating flows, it also assumes that the flow between the rolls is nearly parallel, so that $P = P(x)$, $V_x >> V_y$, and

$\partial/\partial x << \partial/\partial y$, where P is the pressure and V_x the velocity in the main flow direction. Under these assumptions, the lubrication flow can be represented by (Greener and Middleman, 1981)

$$\frac{dP}{dx} = \mu \frac{\partial^2 v_x}{\partial y^2} \tag{6.1}$$

The main difficulty in solving Eq. 6.1 is that of the specification of correct inlet and outlet boundary conditions. Greener and Middleman (1981), using both vanishing pressure and pressure gradient as boundary conditions, predicted the coating thickness on the transfer roll for a relatively narrow range of metering rod to transfer roll speed ratios, although the flow rate deviated from the predictions of the model due to some recirculations upstream from the nip. However, investigations of the complete metering flow indicated that lubrication theory should be accurate in that region (Benkreira et al. 1981; Coyle et al. 1990a,b). Coyle et al. (1990a) showed that the metered nip flow deviates from the lubrication theory predictions at high speed ratios and capillary numbers: the dynamic wetting line moves towards the nip center, the nip length shrinks, and the film thickness passes through a minimum. In another investigation, Coyle et al. (1990b) numerically showed, for a half-flooded nip, the existence of secondary flow downstream from the nip. This recirculation becomes smaller and finally disappears when the speed ratio is gradually increased, which has also been experimentally shown by Gaskell et al. (1998). Coyle et al. (1990b) found that the lubrication theory can be safely applied for speed ratios lower than about 0.5, and when gravity effects can be neglected. They also showed that the recirculations that apparently made the results of Greener and Middleman (1981) to deviate were not determinant in the flow rate calculations. The recirculations were always located in the same region, so that if the speed ratio was decreased, the free surface rose to accommodate the recirculations beneath it.

Kang and Liu (1991), following experimental observations, reported that the speed ratio below which inertia effects can be neglected is a function of the capillary number, namely

$$S_R = 0.29Ca^{-0.54} \quad (6.2)$$

where S_R is the speed ratio of the metering rod to the applicator roll and Ca the capillary number ($V_i\mu/\sigma_T$) which measures the ratio of viscous forces to surface tension forces. According to the authors, Eq. 6.2 is valid for a Reynolds numbers ($\rho V_i h/\mu$) between 0.3 and 30.4.

The influence of the rheological behavior of the coating fluids on the flow hydrodynamics has also been investigated in reverse roll coating flows; the final conclusions reasonably agree. Greener and Middleman (1981) showed that the behavior of elastic liquids fits well with the Newtonian theory at low shear rates (100 to 1000 s^{-1}). Benkreira et al. (1981) reported that the behavior of purely shear-thinning fluids should be slightly different from that observed with Newtonian fluids. Coyle et al. (1990c), when working with elastic and inelastic shear-thinning fluids, showed that, from theoretical and experimental standpoints, the non-Newtonian rheological behavior of a liquid should have little effect on the flow hydrodynamics. For highly elastic fluids, however, the flow can be strongly affected. In particular, they noted that elasticity decreases the film thickness, and the ribbing instability becomes irregular and time dependent. Furthermore, a small amount of polymer additives in the fluid can increase the wipe ratio and stabilize the flow if a long-chained polymer molecule is used (Kang et al. 1991). Finally, particle suspensions and Newtonian fluids behave differently at high speed in terms of the instabilities that are generated. For particle suspensions, the ribbing is smaller and more sensitive to the operating conditions (Réglat and Tanguy, 1998).

Reverse roll coating flows find important applications in the paper coating industry; specifically, the metering operation on a film transfer coater (Metering Size Press) is nothing but a high-speed reverse roll coating process. Most publications on the hydrodynamics in reverse roll coating flows have focused on low speeds and one-phase liquids. On the contrary, paper coating processes require the application of highly concentrated suspensions, that is, fluids which exhibit a complex rheological behavior.

shear-thinning is commonly observed at low shear rates; at high shear rates (above 1000 s^{-1}), the color may be either Newtonian or shear-thickening, depending on the formulation (Alonso et al. 2000a; Laun and Hirsch, 1988; Réglat and Tanguy, 1998; Roper and Attal, 1993); and finally, elasticity is usually seen at low deformation (Laun and Hirsch, 1989).

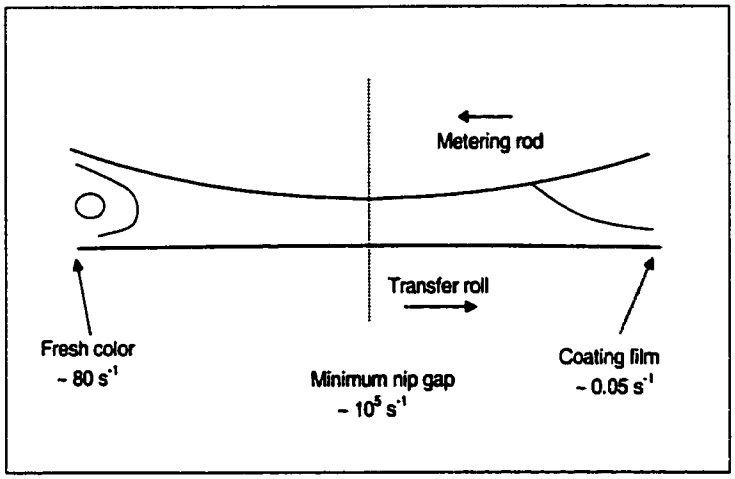

Figure 6.1 Typical shear rates in the metering nip.

In the reverse flow conditions of the metering nip of a MSP, the film formation obeys a series of steps that makes the history of deformation very complex: the liquid is subjected to a moderate level of deformation rates during the preparation process; then, to a sudden increase of shear rate as it passes through the nip, and finally to very low shear rates during leveling (Fig. 6.1). In classical rheometry, the closest tests to simulate the film formation mechanisms are the step growth and step relaxation experiments. They have already been used to investigate the color behavior in coating processes. Laun and Hirsch (1989), when studying industrial coating formulations at different solids contents (62% to 70%), found that such experiments led to an overshoot in viscosity that increased with solids content. Nevertheless, at a shear rate of 4000 s^{-1} and solids contents lower than 62%, the coating colors hardly exhibited any overshoot. Cohu and Magnin (1995), when carrying out step growth experiments with paints, observed overshoots in shear stress that diminished when increasing the imposed

in the roll coating process, where the shear rates are much higher, one should not expect viscosity overshoots. Yziquel et al. (1999) found response overshoots when performing start-up tests with coating colors containing PVA. An overshoot in the transient viscosity was observed; it increased when the value of the initial shear rate of the experiment was increased. The same tests were performed with coating colors containing CMC, but the overshoot behavior was reversed, i.e., the overshoots decreased when increasing the shear rate.

The rheological behavior of paper coating colors can be investigated *in situ* by using the coater itself as a viscometer. By doing so, all the factors contributing to the behavior of the suspension can be better accounted for: shearing history, field of deformation, and speed. Vidal et al. (1991) were to our knowledge the first ones to determine the coating color viscosity directly in a blade coater. They evaluated the shear stress a as function of the blade deformation, and the shear rate as function of the coating thickness. They found that the colors exhibited shear-thinning behavior in the process, but a viscosity slightly different from that in a capillary rheometer. Réglat and Tanguy (1998), in reverse roll coating, investigated the rheological behavior of $CaCO_3$ suspensions and compared the process viscosity within the nip with that in a rheometer. By means of a pressure transducer fitted to the surface of the metering rod, they measured the pressure profile within the metering nip. By using different Newtonian fluids, the maximum pressure was employed to build a master curve, which they used to evaluate the viscosity of suspensions. They found that the process viscosity was much higher than that determined in a classical rheometer at steady state (Couette geometry), which may be due to the shear-thickening behavior at high shear rates usually developed by aqueous suspensions (Thibault, 1999). Alonso et al. (2000a) proposed a new procedure to obtain a coating color process viscosity from torque measurements, method which requires the construction of a calibration curve with Newtonian fluids. Furthermore, they compared it with that based on pressure measurements (Réglat and Tanguy, 1998). Although both procedures gave different results, they confirmed the irrelevance of the viscosity values obtained from classical rheometry to describe the color rheological behavior in the nip gap between rolls. These

results are in agreement with what had been suggested earlier by Kistler and Scriven (1984): fluids behave differently in conventional rheometers and within coating nips.

This paper is a further contribution to the evaluation of process viscosity in paper coaters. The objective is to propose a novel method that combines both torque and pressure, and steady state rheological measurements to evaluate the coating color process viscosity. The method is based on the lubrication theory, which is applied in the nip center region. No calibration curve is required as with former. The process viscosity is compared with that measured in transient conditions in a rheometer, a more realistic method to study the hydrodynamics of the metering nip.

6.3 Experimental

A laboratory reverse roll coater is used for the measurements (Fig. 6.2). A full description of this apparatus is given by Alonso et al. (2000a) and Réglat and Tanguy (1997). The metering rod of this coater (Fig. 6.3) is fully instrumented with a wall-mounted piezoelectric transducer (response frequency of 250 kHz) to obtain the nip pressure profile. A torquemeter is directly connected to the shaft of the metering rod. Two displacement transducers, both located at the rod extremities, measure the position of the metering rod with respect to the undeformed surface of the transfer roll.

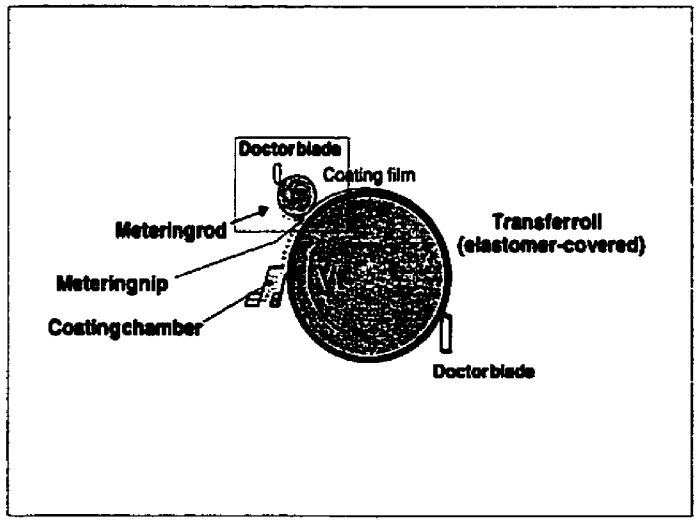

Figure 6.2 Laboratory reverse roll coater.

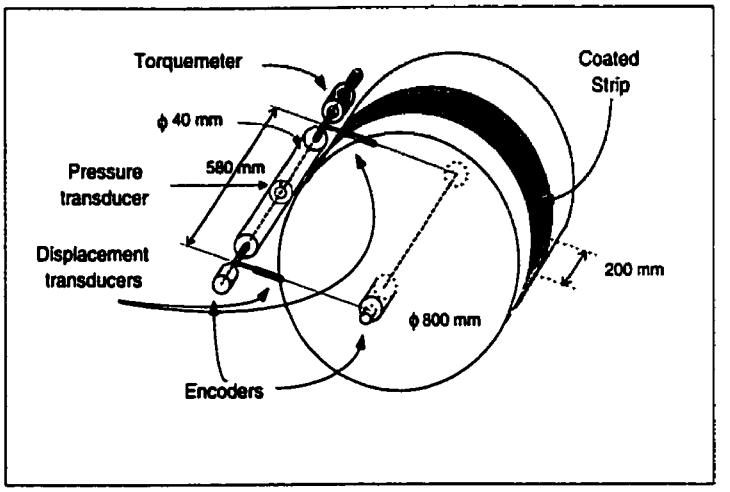

Figure 6.3 Instrumentation of the metering section of the laboratory coater.

Several coating formulations (100 parts of clay used as dry basis) were considered in this work (Table 6.1). To prepare the suspensions, the dispersant was first added to the amount of deionized water necessary to achieve the target solids percentage. The slurries were made by slowly adding the clay with a volumetric feeder. Then, the latex suspension was added, followed by (previously hydrated) CMC, under continuous agitation. The colors were mixed for a minimum of 30 minutes before the pH was adjusted to 8.0 by adding NaOH. At the end, the coating colors were mixed for an additional 60 minutes to stabilize the suspension.

Table 6.1 Coating color formulations (pph of clay basis).

LABEL	Clay	Dispersant	Latex	CMC	% Solids
A	100	0.04	10	0.25	61.0
B	100	0.04	10	0.50	61.0
C	100	0.04	10	1.00	61.0
D	100	0.04	10	0.50	56.0
E	100	0.04	10	0.50	63.3

6.4 Theoretical basis of the process viscosity

The theoretical development is based on the lubrication theory (straight streamlines and inertia effects neglected) applied in the nip core region (Fig. 6.4). It is delimited by the two dotted vertical lines between which the pressure gradient is essentially constant as shown in Réglat and Tanguy (1997, 1998). In this section, inertia forces are negligible and the streamlines are almost parallel (Coyle, et al. 1990a,b; Greener and Middleman, 1981). In addition to the above realistic assumptions, we further suppose that the deformation of the transfer roll is such that the nip gap is almost constant (Carvalho and Scriven, 1997; Fourcade, et al. 1999).

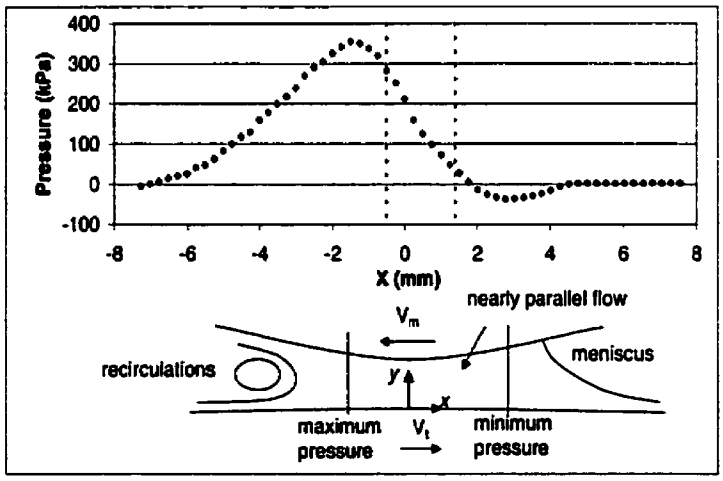

Figure 6.4 Characteristic pressure profile in the metering nip.

Since both torque and pressure measurements take place on the surface of the metering rod, we apply the lubrication theory (Eq. 6.1) on the rod. There, we approximate the shear rate as

$$\left.\frac{\partial v_x}{\partial y}\right|_{wall} \equiv \frac{V_t}{h}\alpha \tag{6.3}$$

where V_t is the transfer roll surface speed and h the nip gap.

Eq. 6.1 implies that the velocity profile is parabolic, with a combination of Couette and Poiseuille flows (Carvalho and Scriven, 1997; Cohu and Magnin, 1995). The parameter α is defined as the contribution of the Poiseuille flow on the resulting Couette velocity gradient evaluated at the wall, namely

$$\alpha = \left. \frac{\left. \frac{dv_x}{dy} \right|_{Couette + Poiseuille}}{\left. \frac{dv_x}{dy} \right|_{Couette}} \right|_{wall} \tag{6.4}$$

Using Eq. 6.1 and Eq. 6.4, the process viscosity can be expressed as (see Appendix)

$$\mu_{proc} = \frac{T^2}{V_t \cdot \frac{dP}{dx} \cdot (S \cdot R)^2 \cdot \alpha} \tag{6.5}$$

The procedure by which Eq. 5 was obtained does not require a Newtonian fluid to be used as reference like in previous studies (Réglat and Tanguy, 1998; Alonso et al. 2000a). The evaluation of the process viscosity can be made directly from torque and pressure measurements combined with the rheological characterization of the fluid at steady state and numerical simulations of the metering nip flow (to evaluate the parameter α). In the limit of pure Couette flow, dP/dx = 0, and the method cannot be applied.

Numerical simulations were carried out to evaluate the parameter α since it is not accessible experimentally. The commercially available CFD software POLY2D™ was used for this purpose. The nip is fully flooded, deformable, and the metering rod speed is 0.5 m/s rotating in reverse mode. The two-dimensional Navier-Stokes equations were solved with the finite element method. Let us mention that POLY2D™

was adapted to solve the deformation of the transfer roll (see details in Fourcade et al. 1999). About 4000 quadratic triangular elements with six nodes in velocity and one in pressure were used in each simulation for the fluid domain. The solid domain required about 5000 elements. Each simulation was carried out by first solving the fluid problem and considering that the coating colors obey the Cross model. The pressure and stresses fields were then calculated and used to deform the transfer roll surface. As a result, a new fluid domain was created and remeshed, and the fluid problem was solved again. This iterative procedure was used until convergence of the solid-fluid interface (Fourcade et al. 1999). At the very beginning, the mesh was tested and refined so that the results were not dependent on the mesh size. In the center, at layer of 5 elements was required to obtain accurate calculations of the Poiseuille contribution α.

6.5 Results and discussion

To investigate the coating colors rheological behavior through the nip, stress growth tests were carried out to mimic the metering nip flow conditions. A Rheometrics RFX II rheometer was used for that purpose. The tests started (continuous line) with an initial pre-shear of 80 s^{-1} during 30 s, a typical value induced by the flow in the coating make-down step (Réglat and Tanguy, 1998). It was followed by a abrupt rate increase to 1000 s^{-1} (stress growth), which was maintained during two seconds; these two parameters were the best compromise that could be obtained with the rheometer to describe the nip hydrodynamics. At the end of the experiment, the shear rate was brought down to 0.05 s^{-1} (stress relaxation) to simulate the rate of leveling of the film on the transfer roll (Macosko, 1994).

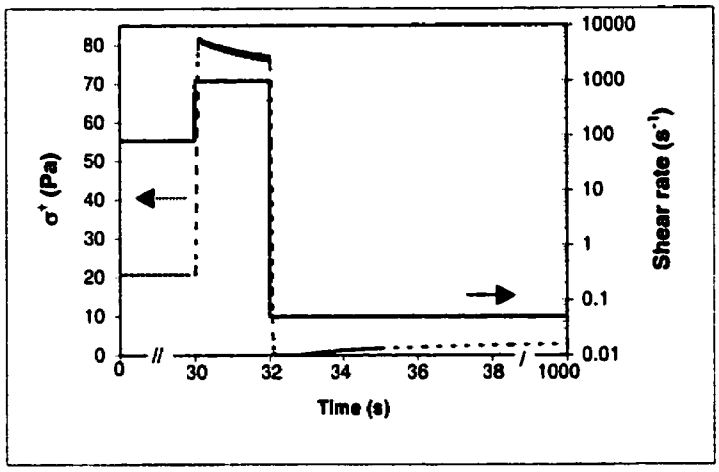

Figure 6.5 Transient shear stress response of the coating colors.

The transient stress σ^+ response (dotted line) of the coating colors is shown in Fig. 6.5. At the end of the pre-shearing stage, the steady state is already reached. The sudden stress growth results in a small overshoot in shear stress, which is attributed to shear-induced rearrangements of the coating structure in the gap (Laun and Hirsch, 1989). After the two second lapse, the stress relaxation produces a rapid decrease of the transient shear stress because of the reduction in the shear rate; however, σ^+ increases slowly with time, and so does the transient viscosity η^+ due to the structure build-up of the coating color at very low shear rates. In this work, we observed that the overshoots increased with shear rate, CMC concentration, and solids content. The overshoots were found at short times, as expected (Macosko, 1994), but the response times were significantly larger than those occurring in the metering nip, which suggests that steady state may not be reached in the metering nip. The overshoots were observed with all formulations, similarly to what has been observed with other coating color formulations (Laun and Hirsch, 1989; Yziquel et al. 1999).

Following the same procedure as in Fig. 6.5, tests were performed on all coating colors, but with different stress growth levels (the shear rates varied between 100 s^{-1} and 1500 s^{-1}). The results in Fig. 6.6 (for coating formulation C) show that the higher the shear rate imposed in the stress growth step, the lower the transient viscosity after the

two seconds of shearing –which is explained by the shear-thinning behavior of the samples– and the lower the eventual value of η^+ (measured 1000 s after the stress relaxation step). The recovery time seems to be proportional to the stress growth level and appears to be very large. Consequently, the Deborah number (the ratio of the fluid relaxation time to the characteristic process time) is also expected to be large, so that elastic stresses are expected to dominate.

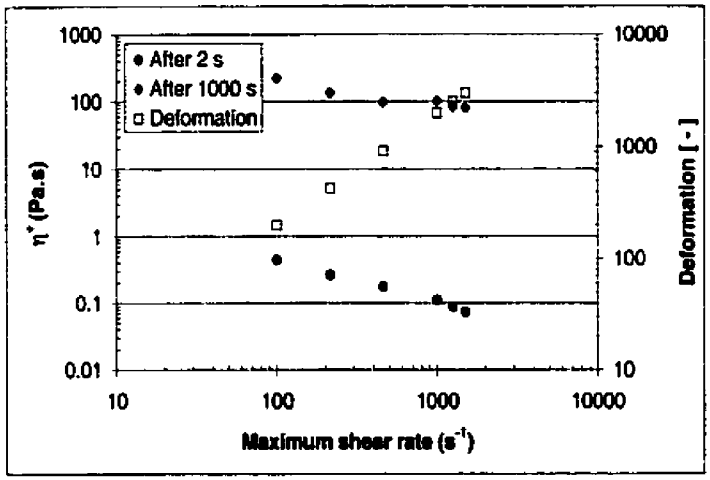

Figure 6.6 Rheological behavior of coating color C.

The coating process can also be analyzed in terms of deformation (the product of shear rate and time). From a theoretical standpoint, there is a critical deformation above which the internal structure in the fluid is completely destroyed so that steady state is reached. The smallest deformation (evaluated after the 2 seconds of the step growth experiment) shown in Fig. 6.6 is about the same order of magnitude as that expected in the process, a deformation level at which coating color breakdown may have already started. At higher deformations, the coating color takes more time to recover. Complete structure breakdown is not reached at very large deformations and the process viscosity becomes a relevant parameter in the process. Therefore, the viscosity of the coating colors arriving in the application nip is very likely lower than that shown in Fig. 6.6, since the shearing in the metering nip is very significant ($\sim 10^5$ s^{-1}), and the time the coating color film has to relax under a shear rate of about 0.05 s^{-1}, from

the metering nip to the application nip, is substantially lower (~0.04 s at 1250 m/min); in fact, it may be very close to its viscosity just after leaving the metering nip.

In Fig. 6.7, the transient viscosity η^+ measured after the stress relaxation step is compared with the steady state values μ_{ss} at low shear rate (0.05 s^{-1}) obtained without pre-deformation of the samples. The viscosity of the coating colors, those that were subjected to the shearing history, is consistently lower. Indeed, some structure breakdown occurred during the tests (Cohu and Magnin, 1995; Laun and Hirsch, 1989).

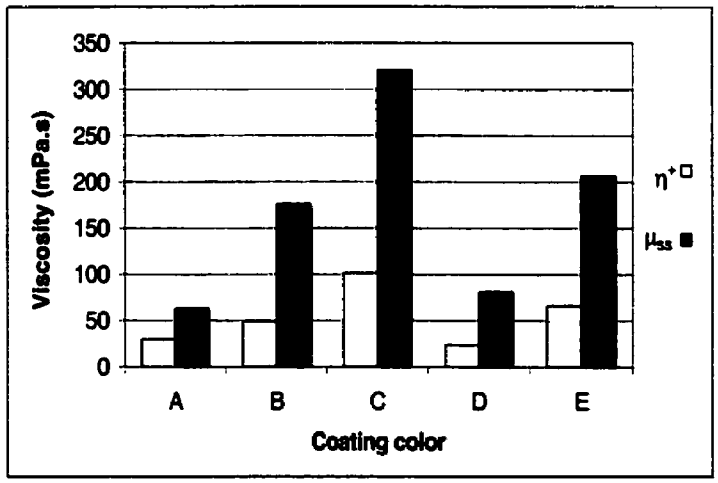

Figure 6.7 Comparison of transient viscosity η^+ (after 1000 s) with steady state viscosity μ_{ss}.

To further characterize the coating colors, steady state shear rate measurements and small amplitude oscillatory shear tests within the linear viscoelastic region were also performed. All coating colors are shear-thinning at low shear rates (Fig. 6.8), and for all of them, the viscosity levels off at high shear rates (Yziquel et al. 1999). The power law fits fairly well with a viscosity plateau at very high shear rates (Table 6.2), where the coating colors behave as Newtonian. Furthermore, as shown in Fig. 6.9, the storage modulus G' increases with the CMC concentration, solids content, and frequency, and it is one order of magnitude larger than the loss modulus G" (not shown). Such a response is typical of a solid-like behavior, where the strong particle-

particle interactions, the break-up and build-up of structures, and the particle alignment govern the coating color behavior (Carreau and Lavoie, 1993). The corresponding phase angle was found always lower than 15°, confirming the elastic behavior of the formulations at very small deformation.

Table 6.2 Parameters of coating colors following the power law model $\mu = m\dot{\gamma}^{n-1} + \eta_\infty$.

Coating color Label	m (Pa.s^n)	n	η_∞ (Pa.s)	$\lvert(\mu_{exp}-\mu_{pl})/\mu_{pl}\rvert$
A	5.0	0.220	0.044	0.056
B	10.5	0.170	0.063	0.072
C	16.0	0.145	0.090	0.081
D	3.70	0.220	0.027	0.058
E	11.5	0.184	0.088	0.073

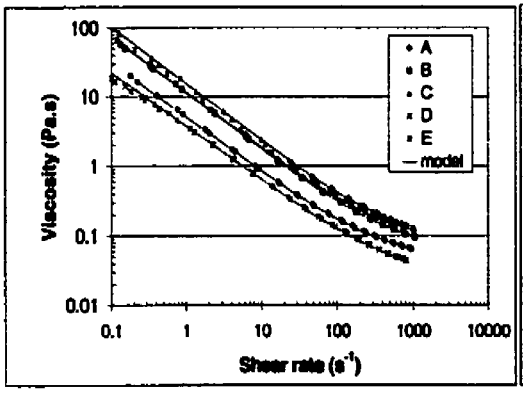

Figure 6.8 Shear viscosity of the coating colors.

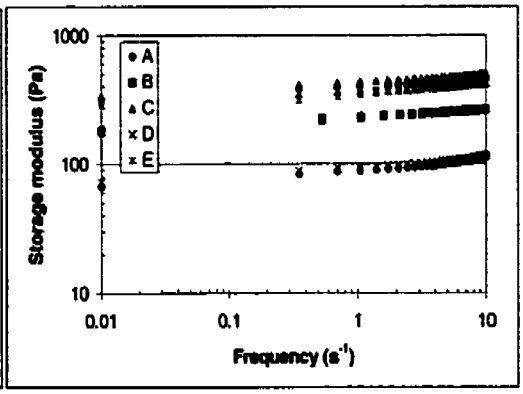

Figure 6.9 Storage modulus of the coating colors.

6.6 Evaluation of the process viscosity

In order to evaluate the process viscosity, the laboratory coater was operated with the following parameters:

- Transfer roll speed: 1250 m/min.
- Metering rod speed: 30 m/min.
- Load per unit width: 1 kN/m.

These conditions correspond to an operating range where good runnability was obtained (no spitting, no air entrapment). They are also fully compatible with current industrial paper coating operating conditions (Pauksta, 1998). Furthermore, the minimum critical speed ratio calculated from Eq. 6.2 lies just above the speed ratio used in this work ($V_m/V_t = 0.024$), but all these cases correspond to Reynolds numbers in the range [9.04 - 27.13], below the upper limit of 30.4 (Kang and Liu, 1991). Strictly speaking in terms of the speed ratio (from Eq. 6.2), lubrication theory cannot be applied to our problem; however, that lower limit arose because it was the lower speed ratio for which the experimental apparatus was designed, not from limitations in the applicability of the lubrication theory (Kang and Liu, 1991). Therefore, we assume that Eq. 6.2 still applies to our problem.

The physical meaning of the pressure-driven contribution α is now discussed. Eq. 6.5 implies that all the measurements are to be made on the wall of the metering rod, where both torque and pressure are actually measured. The dotted line in Fig. 6.10 represents the Couette contribution to the global flow. The parameter α, the Poiseuille contribution, added to the Couette flow gives the parabolic profile shown. Since the Poiseuille contribution to the flow is not accessible experimentally, numerical simulations were carried out at different nip gaps, Newtonian viscosities, and transfer roll speeds. Table 6.3 shows the values for the different operating conditions; α at the wall is practically constant in all cases and independent of viscosity for the conditions considered in this work. Therefore, in the region of nearly constant pressure gradient, the flow is equivalent to a Couette flow with a constant pressure-driven contribution

(Carvalho and Scriven, 1997), independent of the Newtonian viscosity, nip gap and speed.

Table 6.3 Numerically-evaluated ratio of Poiseuille to Couette contributions to the flow in the center of the metering nip for Newtonian fluids.

α	*Nip gap (μm)*							
	25		*50*		*75*		*100*	
	Newtonian Viscosity (mPa.s)							
V_t (m/min)	**84**	**104**	**84**	**104**	**84**	**104**	**84**	**104**
1000	1.93	1.94	1.94	1.95	1.95	1.93	1.92	1.93
1250	1.93	1.93	1.95	1.96	1.96	1.94	1.95	1.94
1500	1.93	1.94	1.95	1.96	1.96	1.95	1.96	1.95

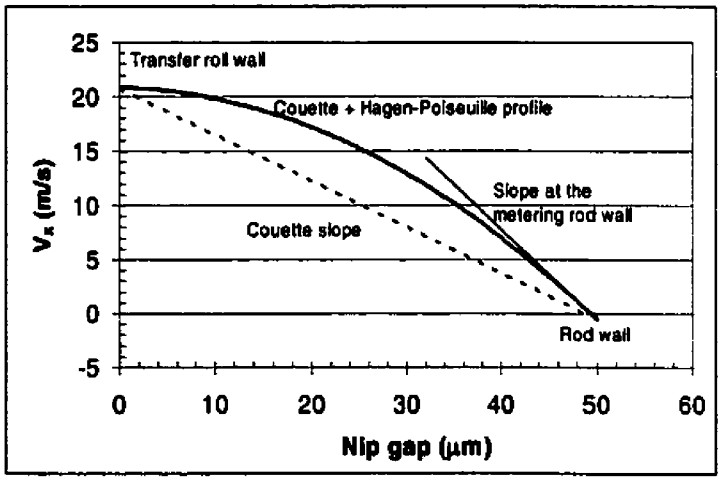

Figure 6.10 Numerical velocity profile in the center of the metering nip (V_t = 1250 m/min, μ = 75 mPa.s, V_m = 0.5 m/s, nip gap = 50 μm).

For the coating colors, the same numerical procedure was carried out with the Cross model since the power law model leads to infinite viscosities at low shear rates, which cause computational problems (Roper and Attal, 1993). The low shear-rate

viscosity plateau η_o was imposed at 500 Pa.s, since lower values did not affect significantly the global hydrodynamics of the flow. The Cross model rheological parameters for the coating colors are shown in Table 6.4. The parameter α increases with respect to the shear-thinning index p as shown in Table 6.5, but then it reduces to nearly the Newtonian limiting value. At high values of p, the shear rates developed in the center of the nip are such that the rheological behavior of the coating colors is that of the Newtonian plateau at very high shear rates.

Table 6.4 Parameters of coating colors obeying the Cross model
$\mu = \eta_\infty + [\eta_o - \eta_\infty]/[1 + (t\dot{\gamma})^p]$

Coating color Label	t (s)	p	η_o (Pa.s)	η_∞ (Pa.s)	$\lvert(\mu_{exp}-\mu_{Cross})/\mu_{Cross}\rvert$
A	290	0.80	500	0.044	0.062
B	87	0.84	500	0.063	0.083
C	62.5	0.83	500	0.082	0.095
D	1100	0.76	500	0.028	0.081
E	83	0.82	500	0.080	0.094

Table 6.5 Numerically-evaluated ratio of Poiseuille to Couette contributions to the flow in the center of the metering nip at different rheological parameters.

α	p					
V_t (m/min)	0.2	0.4	0.6	0.7	0.8	0.84
1000 (t = 87)	2.11	2.39	2.10	1.99	1.99	1.99
1500 (t = 87)	2.07	2.15	2.07	2.02	2.01	2.00
1250 (t = 62.5)	2.08	2.21	2.07	2.00	1.98	1.99
1500 (t = 62.5)	2.07	2.20	2.07	2.01	1.99	1.98

Another important result from the simulations was that the values of α shown in Tables 6.3 and 6.5 were independent from inertia forces. Certainly, inertia does affect the hydrodynamics of the flow upstream and downstream from the nip by changing the

location and the shape of the recirculations, but in the center of the nip, inertia effects are unimportant.

From the numerical simulations, another correction had to be made with respect to the torque. The torquemeter used in the experiments implicitly measures the integral of the stress forces exerted by the fluid on the rod surface. Eq. 6.5 requires the torque, but only the integral of the stress forces over the region within which the pressure gradient is constant. A typical torque profile (the nodal shear stress times the rod radius) is shown in Fig. 6.11 (the numerical model included in every case the rheological parameters of Table 6.4.) Since the deformation of the roll and the nip gap are the result of an equilibrium of hydrodynamic forces (Alonso et al. 2000b; Réglat and Tanguy, 1997, 1998), the pressure peak was used as a reference parameter to categorize the flow hydrodynamics. The experimental and calculated torque values were compared when the maximum pressure was equal. The total torque applied on the rod corresponds to the integral of the curve in Fig. 6.11, i.e., the summation of the positive and negative areas. The total torque values were first compared, and then the local torque in the region of interest was inferred (the integral of the torque in the small region around which the maximum torque is located and the pressure gradient is almost constant). The measured torque in the experiments overpredicted the tangential force in the region of almost constant pressure gradient, depending on the coating color (Table 6.6). The experimental torque measurements were accordingly corrected.

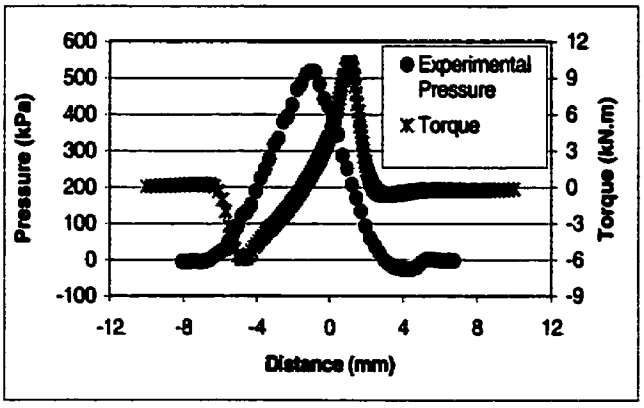

Figure 6.11 Calculated tangential force and its experimental pressure profile for coating color D (V_t = 1250 m/min, V_m = 30 m/min, numerical nip gap = 35 μm).

Table 6.6 Correction factors of the experimental torque measurements.

Coating color Label	Correction
A	0.90
B	0.85
C	0.85
D	0.9
E	0.85

To verify the validity of Eq. 6.5, Newtonian fluids were used. They consisted of polyethylene glycol solutions at three concentrations (w/w): 13.2%, 17%, and 18.3%, yielding viscosities of 43 mPa.s, 84 mPa.s, and 104 mPa.s, respectively. The differences between the shear viscosity and the process viscosity evaluated from Eq. 6.5 are less than 11%. We believe that the disagreement is due to experimental errors, the assumptions underlying the analytical development of Eq. 6.5, and the assumptions implicit in the numerical model when calculating the parameter α and the torque corrections.

We show in Fig. 6.12 the results of the process viscosity μ_{proc} against the transient viscosity 0.1 s after the stress growth at 1000 s^{-1}, where the overshoot in shear stress is maximum (the interval of 0.1 s corresponds to the time it takes the rheometer to change the shear rate from 80 s^{-1} to 1000 s^{-1}; during this period the actual shear rate is unknown). Both transient and process viscosities increase almost linearly with the CMC concentration (the dotted line represents the case when the process viscosity equals η^+). Since all coating colors are below the dotted line in Fig. 6.12 (left), it follows that the higher shear rates encountered in the process broke down more rapidly the coating structure than the step growth experiments, with a shear-thinning degree higher than that deduced from rheological measurements. The proportional increase of both process and transient viscosities can be seen as the effect of the

viscous behavior of the coating colors. The separation from the dotted line may be explained by the increased shear-thinning behavior in the nip.

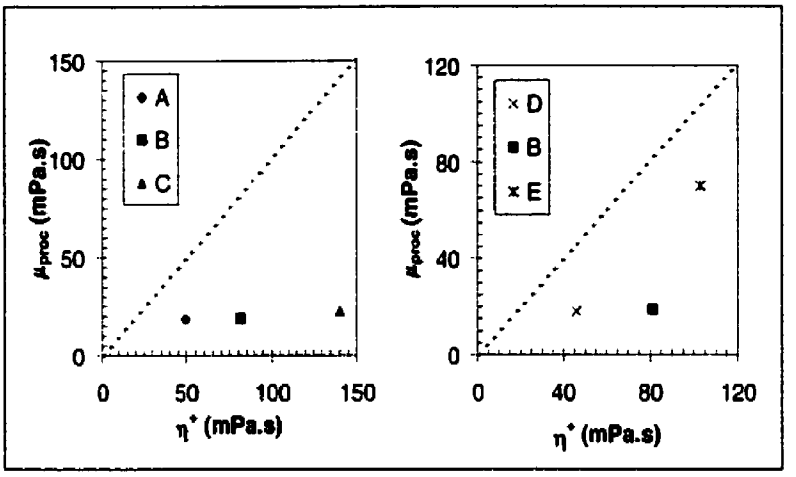

Figure 6.12 Process viscosity for the coating colors at different CMC concentrations (left) and solids contents (right).

Fig. 6.12 (right) shows the influence of the solids content. When there are more particles, the values depart from the dotted line, a behavior also encountered when increasing the thickener concentration (Fig. 6.12 left). Within the metering nip, the amount of solids plays a dominant role in the behavior of coating color E by increasing its process viscosity. Although coating colors C and E have comparable rheological properties as inferred from classical rheological measurements, the increased shear rate in the nip may appreciably reduce the shear-thinning degree of coating color E. As a result, the viscosity of coating color E is higher in the metering nip than that predicted from classical rheology.

Elasticity may contribute to that separation if normal stresses are important. Since the overshoots increase with shear rate, but they occur at short times, very high changes in shear at very short times -very high deformation rates as those in the metering nip- may maintain the coating colors within the viscoelastic region, before reaching its steady state. Under those circumstances, the corresponding normal stresses would affect both torque and pressure. The torque is lower than 1 Nm, so that

an increase in its value would actually decrease the process viscosity (see Eq. 6.5). The same response would be seen if the total pressure within the nip were increased. Elastic stresses developed by the flow are believed to be unimportant (Carreau and Lavoie, 1993) since the samples did not show any shear-thickening behavior, which has been shown to induce normal stresses at very high shear rates (Laun and Hirsch, 1989).

6.7 Conclusions

Our objective was to investigate the rheological behavior of coating colors in reverse roll coating. We carried out rheological measurements to represent what actually occurs in the metering process. A laboratory coater was used and a new method was proposed to evaluate the coating colors viscosity in the metering nip. Two important parameters in reverse roll coating were used in the procedure: the pressure gradient and the metering rod torque signal; additionally, classical rheological measurements and numerical simulations were performed. Lubrication theory was applied in a region where the pressure gradient is almost constant, relatively far from the location of the instabilities. The method proposed in this work made it possible to evaluate the process viscosity, which was found different form that obtained by transient tests in a classical rheometer. The process viscosity was found 2.5 to 6.3 times lower than the transient viscosity, depending on the coating color formulation. It was also shown that the structure breakdown of the coating color may be such that steady state is not reached in the metering nip. Moreover, the viscosity of the coating colors arriving in the application nip is probably very close to that leaving the metering nip. Finally, numerical simulations showed that there is a constant pressure-driven contribution to the flow in the center of the nip, where inertia effects do not play a significant role.

6.8 Additional remarks

Only a few works reported in the literature have considered inertia effects when dealing with roll coating processes (Benjamin et al. 1994; Kang and Liu, 1991; Klostermann and Mewes, 1998). In terms of coating thickness, when the capillary number increases, the region where lubrication theory applies shrinks; however, increasing the Reynolds number enlarges the lubrication region (Klostermann and Mewes, 1998). As pointed out by Réglat and Tanguy (1998), there is a competition between capillary and inertia effects; capillary effects are more important at wide nip gaps, but inertia at narrow nip gaps. Quantitatively speaking, little is known about the relative influence of these dimensionless numbers at very high Reynolds and capillary numbers. From the simulations performed here, it was observed that inertia does affect the flow by changing the position and size of the recirculations upstream the nip, becoming smaller, flatter, and nearer the metering rod. However, their location and size at high Reynolds numbers seemed not to affect the flow in the center of the nip. We believe so because the Poiseuille contribution to the flow in the center of the nip was found the same whether inertia effects were considered or not. As a result, we believe that the application of the lubrication theory in the center of the nip, even at high speeds, is correct.

From the values of the process viscosity, none coating color behaved as expected from classical rheological measurements, but with higher shear-thinning degrees, depending on the formulation. Therefore, the process viscosity becomes relevant in understanding the metering nip flow. We believe that the viscosity of the fluid arriving in the application nip is the process viscosity in the metering nip, since the relaxation time is about six magnitude orders longer than the residence time on the transfer roll. As a result, the process viscosity may give new insights in understanding the runnability of the coating colors in the application nip. Runnability problems in the application nip may also be better understood. For example, by knowing the viscosity of the coating colors in the metering nip, it would be possible to predict the premetered film coating thickness (Grön et al. 1998); thus, the specific pressure on the application

nip, according to the base paper properties, could be specified for a desired film transfer ratio (Grön et al. 1998). Another example would be the implementation of new rheological measurements such as the viscosity of the coating colors water phase in order to comprehend the degree of polymer chain adsorption in the coating color (Kokko et al. 1999). Finally, creep flow rheological tests can relate runnability to coating color formulation (Ghosh et al. 1997). Thus, apart from the process viscosity, more rheological tools are needed in order to better understand all the phases of the paper film coating process such as the process viscosity.

6.9 Appendix

We present here the complete mathematical development carried out to evaluate the process viscosity. Neglecting inertia effects in the Navier-Stokes equations, the momentum balance for the lubrication flow is (Greener and Middleman, 1981)

$$\frac{\partial^2 v_x}{\partial y^2} = \frac{1}{\mu}\frac{\partial P}{\partial x} \tag{A6.1}$$

Eq. A6.1 implies that the velocity profile is parabolic. It is in fact a combination of Couette and Hagen-Poiseuille flows (Carvalho and Scriven, 1997; Cohu and Magnin, 1995). Integrating Eq. A6.1 we obtain

$$\frac{\partial v_x}{\partial y} = \frac{1}{\mu}\frac{\partial P}{\partial x} y + C_1 \tag{A6.2}$$

If we assume a small velocity gradient on the surface of the transfer roll (y = 0), then (see Fig. 6.10)

$$C_1 \equiv 0 \tag{A6.3}$$

and Eq. A6.2 becomes

$$\frac{\partial v_x}{\partial y} = \frac{1}{\mu}\frac{\partial P}{\partial x} y \tag{A6.4}$$

If we now consider the small speed ratio used in reverse roll coating paper applications (metering size press), and if we assume that the roll curvature is very small near the region of nearly constant pressure gradient (around the center of the nip), we can approximate the shear rate on the wall of the metering rod by

$$\left.\frac{\partial v_x}{\partial y}\right|_{wall} \cong \frac{V_t}{h}\alpha \tag{A6.5}$$

where V_t is the transfer roll speed, h the nip gap, and α represents the contribution of the Hagen-Poiseuille flow on the resulting velocity gradient evaluated at the wall near the center of the nip. By combining Eq. A6.4 and Eq. A6.5 we obtain

$$\alpha \frac{V_t}{h} = \frac{1}{\mu}\frac{\partial P}{\partial x} h \tag{A6.6}$$

Solving for μ in Eq. A6.6

$$\mu = \frac{1}{\alpha V_t}\frac{dP}{dx} h^2 \tag{A6.7}$$

Now we are going to establish the relation between Eq. A6.7, which expresses the dependence of the viscosity on the nip flow conditions, and the torque exerted by the metering rod on the fluid. From the Newton's law of viscosity

$$\sigma|_{wall} = \mu \left.\frac{\partial v_t}{\partial y}\right|_{wall} \cong \mu \frac{V_t}{h}\alpha \tag{A6.8}$$

where $\sigma|_{wall}$ is the shear stress on the rod evaluated in the almost constant pressure gradient region. This shear stress is related to the measured torque T exerted by the rod by

$$\sigma|_{wall} = \frac{T}{SR} \tag{A6.9}$$

In this equation, S is the wetted area on the metering rod surface, R its radius, and T the torque exerted only at the center of the nip around the region of almost constant pressure gradient. Solving for h in Eq. A6.8 and substituting into Eq. A6.7 yields

$$\mu = \frac{1}{\alpha V_t}\frac{dP}{dx}\left(\frac{\mu V_t}{\sigma|_{wall}}\right)^2 \tag{A6.10}$$

By using Eq. A6.9, μ becomes the process viscosity that can be expressed as (Eq. 6.5 in the text)

$$\mu_{proc} = \frac{T^2}{V_t \cdot \frac{dP}{dx} \cdot (S \cdot R)^2 \cdot \alpha} \tag{A6.11}$$

where α depends on the rheological behavior of the fluid and can be estimated numerically.

CHAPTER 7

A CFD ASSESSMENT OF FILM COATING PROCESS VISCOSITY MODELS

Three process viscosity models have been proposed in this thesis. Although they all are based on measurements of the hydrodynamic pressure and torque in the metering nip, each one follows a different theoretical approach. The results obtained from each model suggested that a better understanding of the process viscosity was needed. In this fourth article, numerical simulations of the metering nip flow are used to assess the process viscosity models. This is carried out in order to identify the reasons of the disagreement, but more importantly, to distinguish the best method which represent in a better manner, from a rheological viewpoint, what occurs in the metering nip. On the metering rod, both maximum pressure and torque are calculated and comparisons with experimental measurements are performed. The numerical complexity associated with coupling an elastohydrodynamic model with a free surface algorithm is avoided by considering a fully flooded nip. This two-dimensional model maintains the main features of the nip flow and is numerically more manageable than the entire representation of the free surface elastohydrodynamic reverse roll coating problem in three dimensions.

A CFD ASSESSMENT OF FILM COATING PROCESS VISCOSITY MODELS

S. Alonso, F. Bertrand, and P.A. Tanguy

NSERC/Paprican Chair

Department of Chemical Engineering

École Polytechnique

P.O. Box 6079, Station Centre-ville

Montreal H3C 3A7

Canada

Keywords: process viscosity, metering nip, maximum pressure, torque, pressure gradient, coating color.

Submitted: The Canadian Journal of Chemical Engineering (August, 2000).

7.1 Abstract

Computer fluid dynamic simulations of the metering nip flow were used to assess the process viscosity of the coating colors. The numerical solution was based on a Galerkin/finite element technique that included the deformation of the roll cover to better represent the flow elastohydrodynamics. The Navier-Stokes prediction was compared with experimental measurements of torque and pressure in the metering nip. From the comparisons, the process viscosity determined in a region of shear-dominated flow is the one, among the three models analyzed, that can better describe the hydrodynamics of the metering nip flow. To improve further the fluids flow numerical description, this process viscosity was combined with an adapted transient Cross model. This new semi-analytical rheological model decreased the differences between the numerical and experimental results. The findings also suggested that the model requires further enhancements, topic that will be addressed in future work.

7.2 Introduction

The film coating technique is used for the surface treatment of fragile webs, as very little stress is applied to the substrate, contrary to blade coating. Film coating is also known to produce a contour-like coating with superior coverage even at high process speeds (Wickström and Grön, 2000). These advantages are achieved due to the use of a pre-metering step, in which a thin coating film is first formed in a metering section, before being applied to the substrate. In the metering nip, the film is formed between a small smooth metering rod and a large-diameter soft transfer roll. The metered film characteristics depend on the coating formulation and the nip flow conditions that are governed mainly by the load exerted on the roll by the rod, the speed, and the roll cover hardness. Since the metered film is an essential part of the final product, a thorough understanding of the metering nip flow is central to the better design of film coating equipment.

In coating processes, thin films of the order of a few tens of microns are produced. In order to obtain such thin coatings and to avoid roll damage, a deformable

cover on the transfer roll is essential. The use of an elastic cover results in a fluid-solid boundary that changes according to the hydrodynamics of the flow. In practice, the fluid domain, which is influenced by the equilibrium between flow and elastic forces, is difficult to describe. Coyle (1988) used the lubrication theory to model such fluid domain and described the deformation of the roll cover as simple Hookean springs. He reported that the maximum pressure is lower than that with rigid rolls. In terms of coating thickness, he identified two load regions of different slopes, similar to those observed experimentally at high speed with Newtonian fluids and suspensions (Alonso et al. 2000b; Réglat and Tanguy, 1997, 1998). Carvalho and Scriven (1993) compared three methods to describe the deformation of the elastic cover. Since the one proposed by Coyle (1988) gave results similar to those of the other models, Carvalho and Scriven (1993) concluded that the spring model was reliable enough for practical design considerations. Lubrication theory, however, does not account for the effect of the hydrodynamic stresses on the deformation, and the spring model does not allow for sideways displacements or incompressible covers.

Fourcade et al. (1999) proposed a novel model for the deformation of a Hookean incompressible cover that allows for sideways displacements generated by fluid stresses. For Newtonian fluids, the calculated maximum pressure was compared to that measured experimentally. The results showed similar trends although quantitative differences were observed. They were attributed to the uncertainty associated with the measurement of the metering rod position relative to the transfer roll (apparent nip gap), and three-dimensional and free surface effects (Fourcade et al. 1999).

An improvement in flow simulations has been achieved by including the free surface downstream from the nip. Carvalho and Scriven (1997), using the lubrication theory, adapted a viscocapillary model for the free surface to a spring-like model for the roll deformation. They found that the deformation of the cover reduces the pressure and delays the onset of the ribbing pattern to higher capillary numbers. Carvalho and Scriven (1999) improved the numerical treatment of the forward roll coating problem by carrying out a three-dimensional flow stability analysis, together with a spring-like model

for the roll deformation. Their results confirmed that the deformable cover decreases the pressure gradients and delays the onset of instabilities.

In reverse roll coating flows, the numerical treatment of the free surface is very complex. The three-phase dynamic wetting line leads to a non-integrable stress singularity, so that a slip hypothesis must be implemented (Coyle et al. 1990; Hao and Haber, 1999). The dynamic contact angle needs to be known as well. The uncertainties about the conditions prevailing at the dynamic wetting line make uncertain the reliability of the quantitative predictions of the flow field (Coyle et al. 1990). From experiments, Ghannam and Esmail (1997) showed that, for rotating rolls, the contact angle depends on the geometry of the wetted surface and the capillary number. Numerically, Hao and Haber (1999) found that the contact angle and the slip distance have a strong influence on the location of the three-phase line and the coating thickness. As a result, the numerical solution depends strongly on the conditions of the dynamic wetting line, and matching a set of experimental conditions to the numerical model requires specific values of the slip coefficient, slip length and dynamic contact angle.

In numerical simulations, considering the cover deformation results in a better approximation of the flow hydrodynamics (Carvalho and Scriven, 1997; Fourcade et al. 1999). Consequently, parameters that are particularly sensitive to the nip elastohydrodynamic forces such as the torque acting on the rotating rod become natural candidates for the assessment of the reliability of computational models. Torque measurements are at the basis of rotational rheometry (Carreau et al. 1997; Macosko, 1994), and they can also be adapted to mixing process rheometry (Brito et al. 1998). Although it is relatively simple to measure the torque on a rotating roll, only a few works have dealt with this issue (Alonso et al. 2000a,c). From a fluid mechanics viewpoint, the torque signal may provide relevant information about the rheological conditions of the fluid in the metering nip, in the spirit of what has been obtained from experimental pressure measurements (Alonso et al. 2000a,c; Réglat and Tanguy, 1998). Thus, the objective of this article is to assess the process viscosity models developed in Film Coating by means of Computer Fluid Dynamic simulations of the metering nip flow. Newtonian fluids and paper coating colors are used under the typical conditions of a

paper film coating process. Numerical simulations that consider the deformation of the roll cover as in Fourcade et al. (1999) are carried out. On the metering rod, both maximum pressure and torque are calculated and comparisons with experimental measurements are performed. In order to avoid the numerical complexity associated with coupling an elastohydrodynamic model with a free surface algorithm, the nip is considered fully flooded. This simple two-dimensional model maintains the main features of the nip flow and is numerically more manageable than the entire representation of the free surface elastohydrodynamic reverse roll coating problem in three dimensions.

7.3 Physical and Numerical Experiments

The laboratory reverse roll coater used in the experiments is described in Alonso et al. (2000a). Briefly, the metering rod is instrumented with a wall-mounted piezoelectric transducer to obtain the nip pressure profile at each revolution (Fig. 7.1). A torquemeter is directly connected to the shaft of the metering rod so that the torque signal is continuously monitored and recorded. Two displacement transducers, both located at each end of the rod, measure the relative position of the metering rod with respect to the undeformed surface of the transfer roll. The zero position is set when both rod and roll are in slight contact while being at rest.

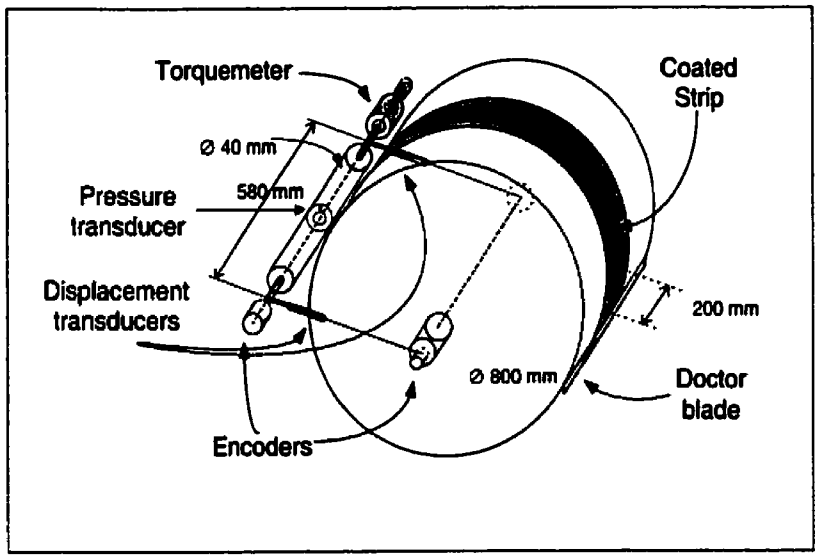

Figure 7.1 Instrumentation of the metering section of the laboratory coater.

Polyethylene glycol solutions at three concentrations (13.2%, 17% and 18.3% w/w) were used as Newtonian fluids. Three paper coating color formulations were used, all based on 100 dry parts of clay, 10 of latex, 0.04 of dispersant and with different CMC and solids contents as shown in Table 7.1. The Cross model rheological parameters are showed in Table 7.2, and the details about the rheological characterization can be found in a related paper (Alonso et al. 2000c).

Table 7.1 CMC and solids content in the coating colors.

Coating color	CMC	% Solids
1	0.5	61.0
2	1.0	61.0
3	0.5	63.3

Table 7.2 Parameters of Cross model $\mu_{Cross} = \eta_\infty + [\eta_0 - \eta_\infty]/[1 + (t\dot{\gamma})^p]$.

Coating color Label	t (s)	p	η_0 (Pa.s)	η_∞ (Pa.s)	$\lvert(\mu_{exp}-\mu_{Cross})/\mu_{Cross}\rvert$
1	87	0.84	500	0.063	0.083
2	62.5	0.83	500	0.082	0.095
3	83	0.82	500	0.080	0.094

The computational approach described in Fourcade et al. (1999) was used for the flow simulations. The computational domain, the nomenclature and the finite element elastohydrodynamic model are recalled in the Appendix (the simulation parameters are given in Table 7.3). The rigid-roll fluid problem is first solved. Next, the stress at the fluid-solid interface is used to calculate the force exerted by the fluid on the transfer roll. This force is then used to predict the cover deformation. Once the cover is deformed, the new fluid-solid interface generates new fluid and solid domains that are remeshed for the next iteration. The fluid problem is thus solved again, and this process is iterated upon until the normal force exerted by the fluid becomes equal to the elastic stresses. In practice, the fixed point iteration procedure was applied until the fluid-solid normal stress residual value at the interface was equal or less than 3% of the fluid normal stress value $[(F_N-S_N)/F_N \leq 0.03]$.

Table 7.3 Operating and geometrical parameters.

Variable	Nomenclature	Range
Transfer speed	V_t	500 – 1900 m/min
Metering rod speed	V_m	30 m/min
Experimental metering load	–	0.25-2.0 kN/m
Numerical nip gap	–	$\sim 40 - 80 \bullet$ m
Transfer roll radius	r_t	0.40 m
Metering rod radius	r_m	0.02 m
Elastomer thickness	t_e	0.015 m
Metering nip length	l	0.02 m
Metered coated strip	–	0.2 m
Relaxation parameter	ω	0.3

In the present study, the two-dimensional elastohydrodynamic problem was discretized with the Galerkin finite element method by means of the CFD code POLY2D™ (Rheotek Inc.) The meshing procedure was achieved using IDEAS™ (SDRC Inc.) Both fluid and solid meshes contained around 3400 and 4800 quadratic-interpolated triangular elements, respectively. Mesh refinement tests were performed to ensure that the results were independent of the mesh size. The remeshing procedure was such that the variation of the number of elements did not change appreciably so as to affect the accuracy of the results from one iteration to the next one. Additionally, a relaxation parameter ω was used to avoid too large displacements and to ensure convergence.

The tangential force exerted by the fluid on the metering rod was used to calculate the torque T_n, namely

$$T_n = r_m \int_{\Gamma_{Fm}} (\sigma_F \cdot t_F) d\Gamma_{Fm} \tag{7.1}$$

where r_m is the metering rod radius and Γ_{Fm} the wetted surface of the rod to be integrated.

In order to assess the accuracy of the numerical procedure with respect to the torque, the flow between two concentric cylinders (Couette flow) was first solved. Figure 7.2 shows the excellent agreement obtained between the analytical solution and the calculated values for this problem. The plot gives results for different speeds of rotation of the inner cylinder and a range of Newtonian viscosities. As expected in the laminar regime, the torque is directly proportional to both the viscosity and the rotational speed.

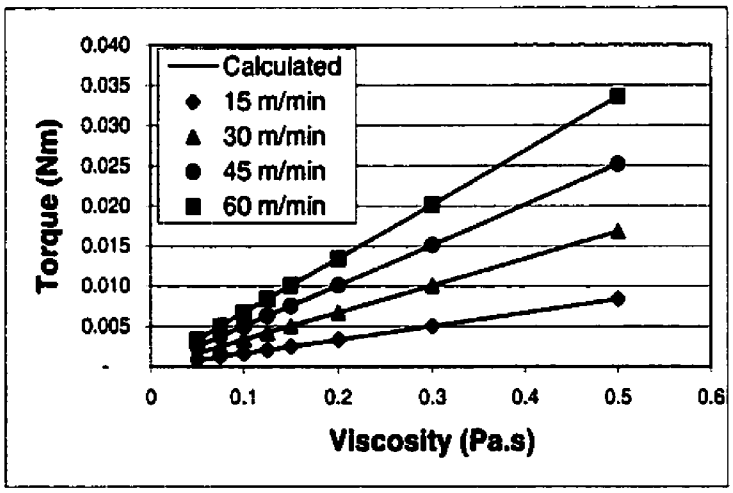

Figure 7.2 Validation of the torque values obtained with the numerical method (symbols represent the analytical solution).

7.4 Results and Discussion

In this investigation, it is important to consider that, as explained in Réglat and Tanguy (1997), the experimental error in the calibration of the metering rod relative position can be up to 20 μm, a value which may be kept in mind when analyzing the results. The size of the pressure transducer may be another source of systematic error. It is relatively large (2.5 mm in diameter) with respect to the total length of the nip (~ 13 mm) so that the experimental pressure is an average value on the surface of the

transducer. This effect was somehow considered in the numerical results by averaging the pressure profile in a distance of 2.5 mm, yet the error associated with this approximation may be added to the discrepancy between the numerical results and the experimental data (Réglat and Tanguy, 1997). Finally, the fluids used in this investigation contained a significant solids content, but the numerical model considers only one single phase and consequently neglects particle interactions. Assuming minimal sources of error, the numerical simulations were used to assess the methods of evaluation of the process viscosity models of Alonso et al. (2000a,c).

7.4.1 Process viscosity model based on the maximum pressure

The process viscosity μ_{proc}^{P} is defined as the shear viscosity of a Newtonian fluid that would yield the maximum pressure of a non-Newtonian fluid at the same flow conditions (Réglat and Tanguy, 1998). The method requires the use of Newtonian reference fluids and is based on the sensitivity of the maximum pressure with respect to the operating conditions (Réglat and Tanguy, 1998). With this procedure (Alonso et al. 2000a), the calculated process viscosity of the coating colors was found to be significantly higher than the steady state shear viscosity μ_{sh} obtained in a rheometer (Table 7.4).

Table 7.4 Process, transient, steady state and plateau viscosities for the coating colors.

Viscosity (Pa.s)	μ_{proc}^{P}	μ_{proc}^{T}	μ_{proc}	η^{+}	μ_{sh} at 1000 s^{-1}	η_{∞} (Cross)
Color	Alonso et al. (2000b)		Alonso et al. (2000a)			
1	0.478	0.063	0.019	0.082	0.095	0.063
2	0.645	0.069	0.022	0.140	0.129	0.082
3	0.641	0.062	0.070	0.103	0.108	0.080

Fig. 7.3 displays the variation of the maximum pressure values with respect to the metering rod position for two coating colors. From the fact that the experimental

curve is below the numerical results, one can infer that the parameters of the Cross model overestimate the viscosity of the coating colors. One can also infer that using the process viscosity μ_{proc}^{P} in the numerical model would result in an even higher maximum pressure. This is of course surprising since one would expect that using the process viscosity in the numerical model yields more accurate results.

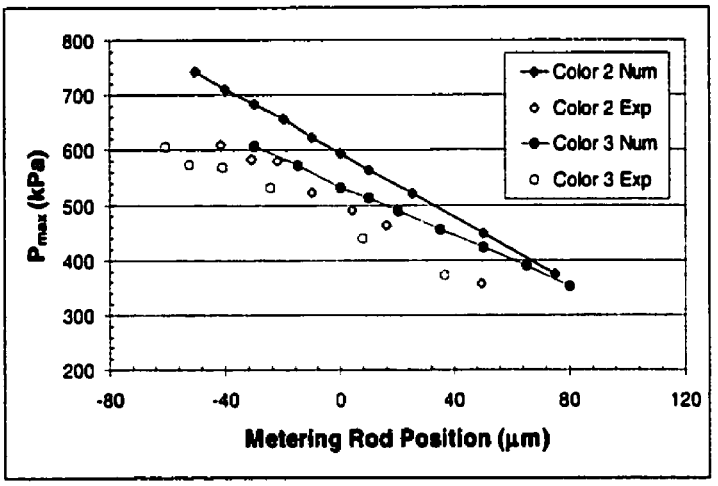

Figure 7.3 Variation of the maximum pressure with the metering rod position for two different coating colors (V_t = 1750 m/min, V_m = 30 m/min).

The discrepancies may be linked to the location of the maximum pressure and the rheological behavior of the coating colors under extensional flow. Between rolls, the maximum pressure is located upstream from the nip center (Gaskell et al. 1998), i.e., in the converging region of the nip, where shear and extensional flows coexist. The fact that a converging-diverging channel can be used to investigate the extensional behavior of the coating colors through pressure measurements (Isaksson et al. 1998; Lavoie et al. 1997) suggests that the extensional behavior of the coating colors greatly influences the values of the process viscosity μ_{proc}^{P}. This effect can be explained by the occurrence that, *for a set of operating conditions of transfer speed and rod position,* the maximum pressure depends on the extensional α_e and shear α_s flow contributions (Réglat and Tanguy, 1998) as

$$\frac{\Delta P_{max}}{\Delta \mu_{sh}} = \alpha_s + k\alpha_e \qquad (7.2)$$

where $\alpha_s = \partial P_{max}/\partial \mu_{sh}$ and $\alpha_e = \partial P_{max}/\partial \mu_{ex}$, and k is the Trouton ratio, i.e., the ratio of extensional to shear viscosity. For Newtonian fluids, there is no stretching, $\alpha_e = 0$, and the term $\partial P_{max}/\partial \mu_{sh}$ (or $\Delta P_{max}/\Delta \mu_{sh}$) can be evaluated directly from experiments (Alonso et al. 2000a; Réglat and Tanguy, 1998). For non-Newtonian fluids, α_s is still valid but k and α_e may be a function of the extension rate. k can be known from experiments in an extensional rheometer, but α_e can only be evaluated explicitly from tests in the film coater with fluids with different extensional viscosities and constant shear viscosity. As a result, the coating color process viscosity μ_{proc}^{P} evaluated from maximum pressure measurements may change –depending on the values of α_e and k– when the extensional behavior of the fluids is taken into account.

7.4.2 Process viscosity model based on the torque

The process viscosity μ_{proc}^{T} represents a value of the fluid viscosity based upon the global shear and extensional conditions that prevail within the metering nip. This procedure uses reference Newtonian fluids and an extension of the concept of Metzner and Otto (Metzner and Otto, 1957) for the evaluation of the process viscosity (Alonso et al. 2000a). Here (Table 7.4) the process viscosity μ_{proc}^{T} is lower than the viscosity μ_{sh} obtained in the rheometer (Alonso et al. 2000a).

Fig. 7.4 shows the variation of the experimental and numerical torque values with respect to the metering rod relative position. One may readily observe that the discrepancies are more significant than in the case of the maximum pressure measurements. One can also infer from these results that the rheological parameters of the Cross model overestimate the viscosity in all cases since the experimental results are below the numerical curve. From a rheological standpoint, two comments are in order. The Metzner and Otto concept (Metzner and Otto, 1957) was developed for

laminar flow. Since Alonso et al. (2000a) does not mention the regime underlying their process viscosity evaluations, their results are revisited in this work. In order to better account for the physics of the problem, a new dimensional analysis is carried out. The power number is redefined as $Np = \frac{T}{SV_t^2 R_m \rho}$, the Reynolds number is $Re = \frac{\rho V_t H}{\mu_{sh}}$ and Kp = Np·Re for Newtonian fluids, and $Re_n = \frac{\rho V_t^{2-n} H^n}{m(V_t/H)_s^{n-1}}$ and Kp_n = Np·Re_n for the coating colors; finally, both Kp and Kp_n are constants in the laminar regime. We give in Fig. 7.4 the Np and Kp curves obtained for Newtonian fluids and coating colors. It comes from experiments and dimensional analysis that the slope of an Np *vs* Re curve should be equal to -1 (logarithmic scale) in the laminar regime and decrease to near zero in the fully turbulent regime (Sterbacek and Tausk, 1965). The slope of -1 is independent of the index n of the power law rheological model so that the Metzner and Otto concept works for both shear-thinning and shear-thickening fluids (Tanguy et al. 1996), common rheological behaviors observed in coating colors (Laun and Hirsch, 1989; Roper and Attal, 1993).

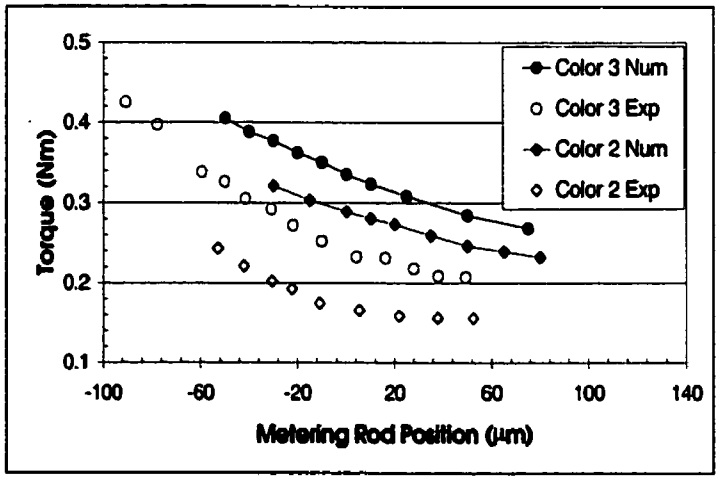

Figure 7.4 Variation of the torque with the metering rod position for two different coating colors (V_t = 1750 m/min, V_m = 30 m/min).

Fig. 7.5(a) shows the variation of Kp with respect to the Reynolds number. Each data series (represented by the dotted line) corresponds to a constant load but different transfer speeds and nip gaps. The geometric constant Kp (Fig. 7.5b) appears to be a function of the Reynolds number for Newtonian fluids. These variations are mostly owing to the fact that the different gaps correspond to different geometries and hence, in the spirit of dimensional analysis, to different processes. Fig. 7.5(c) shows the Np-Re_n curves for the coating colors, results which depict a behavior similar to that of the Newtonian fluids. Kp curves (Fig. 7.5b and 7.5d) reveal that the Kp values range from 0.2 to 2.15 in the Newtonian case and from 45 to 125 for the coating colors. Such Kp and Kp_n variations make it difficult to use the concept of Metzner and Otto. As a result, the concept of process viscosity should be applied at low speed, in order to ensure the laminar regime and minimize the influence of the nip gap on the geometric constant Kp.

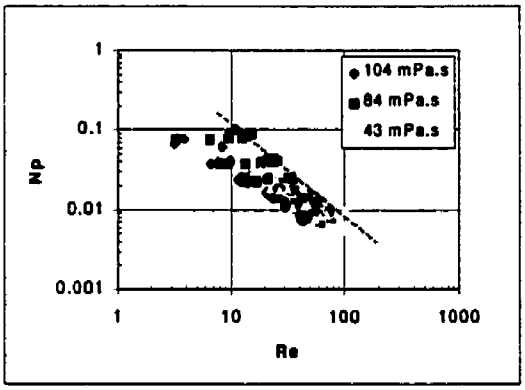

Figure 7.5(a) Power number as function of the Reynolds number for Newtonian fluids.

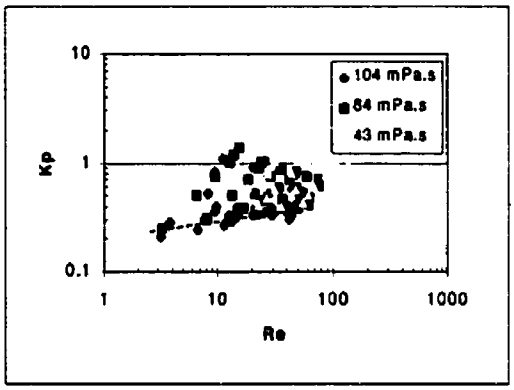

Figure 7.5(b) Kp as function of the Reynolds number for Newtonian fluids.

The torque-based methodology presented above considers that the coating colors are power law fluids. Consequently, the very high Reynolds numbers calculated for the coating colors (Figs. 7.5c and 7.5d) are a consequence of the very small viscosity predicted by the power law model. In the metering nip, however, the rheological model is likely to perform poorly because the shear rates are such that the viscosity may be on the Newtonian plateau (Alonso et al. 2000c). In order for the

coating colors to behave as power law fluids, the shear rates and speeds should be low, which were not the conditions in the work of Alonso et al. (2000a). As a result of both remarks, the torque-based procedure for evaluating the process viscosity is suitable only when the shear rates and process speeds are small.

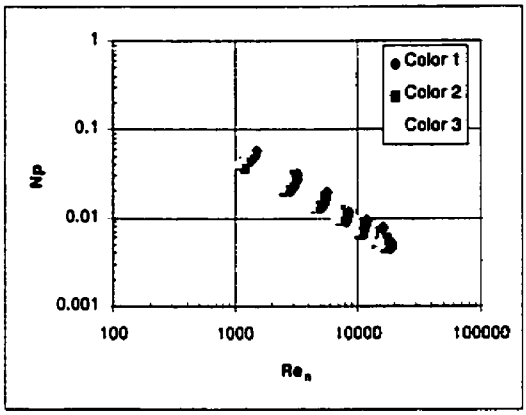

Figure 7.5(c) Power number as function of the Reynolds number for coating colors.

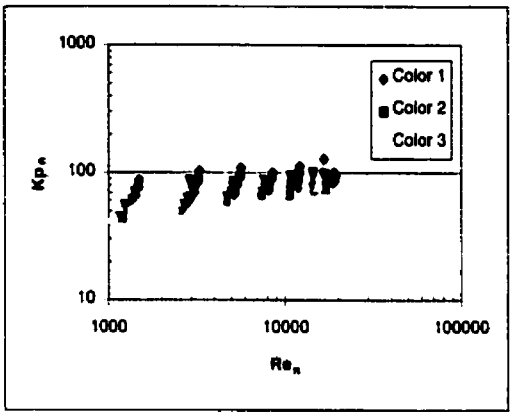

Figure 7.5(d) Kp as function of the Reynolds number for coating colors.

7.4.3 Process viscosity model based on the pressure gradient and torque

The two methods proposed above suffer from drawbacks that come from the speed and the converging-diverging geometry of the metering nip. Thus, by considering a region within the nip where the flow is shear-dominated –the nip center, for example–, the uncertainty with respect to the extensional effects on the flow can be considerably reduced. Additionally, the transient nature of the metering nip flow (Cohu and Magnin, 1995; Laun and Hirsch, 1989) brings the idea that the process viscosity should be compared with transient rheological tests in the rheometer. Both of these issues were considered in the methodology proposed in a previous paper (Alonso et al. 2000c). This methodology combines the pressure gradient and the torque by means of the lubrication theory applied in the center of the nip and requires no Newtonian reference fluids. With this method (Alonso et al. 2000c), the values of the process viscosity μ_{proc}

were found to be lower than the transient viscosity η^+ obtained with step growth tests (Table 7.4).

A few comments must be made about the coating color rheology. In Table 7.4, the values of the transient viscosity η^+ (obtained 0.1 s after a step growth test from 80 s^{-1} to 1000 s^{-1} in a rheometer; Alonso et al. 2000c) are very close to the steady state values μ_{sh} but higher than the viscosity plateau η_∞ predicted by the Cross model. Thus, one would expect that using the values of η^+ in the numerical simulations give a larger difference than the Cross model. The only suitable viscosity that allows to decrease the numerical results is then the process viscosity μ_{proc} (the process viscosity μ_{proc}^T could also shift down the numerical curve but the methodology does not perform properly).

The time and shear dependence of the coating colors does not allow us to use directly in the simulations the process viscosity μ_{proc}. We illustrate this in Fig. 7.6, which shows the steady state shear viscosity μ_{sh} for two coating colors. The other η^+ curves were constructed from the rheological results obtained after an initial preshearing of the sample at 80 s^{-1} for 30 s and then applying step growth tests up to 1000 s^{-1} (the readings were taken 0.1 s after the increase in shear rate). The values of this transient viscosity η^+ decrease with the step growth rate level and follow also the trend of the steady state viscosity. The transient values are slightly below, but the differences can be better seen by zooming the high shear region as shown in Fig. 7.4 (these differences in viscosity are enough to change the hydrodynamics of the metering nip flow, i.e., the pressure profile; Alonso et al. 2000b; Réglat and Tanguy, 1997, 1998). This transient viscosity η^+ behavior for coating color 3 could be fitted with the Cross model with the following parameters: $p = 0.79$ and $t = 150$ s.

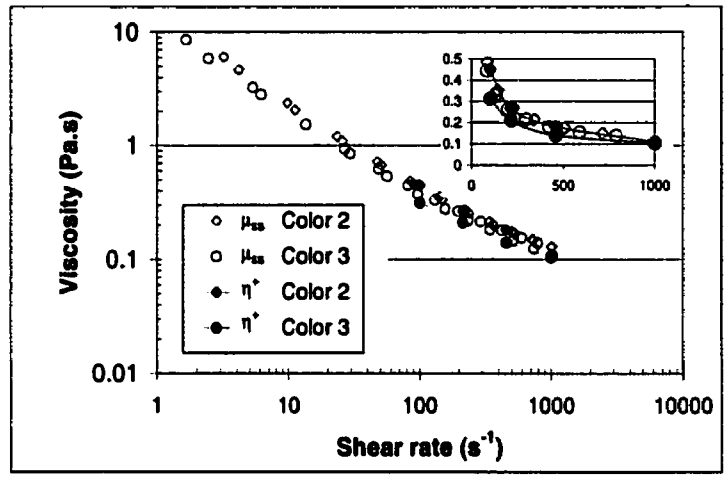

Figure 7.6 Steady state and transient viscosities for two coating colors (zoom of the high shear region un the upper-right side).

New numerical experiments were performed with these transient Cross model parameters in order to consider somehow the shear and time dependence of the fluid upstream the metering nip. In the center, we believe that the viscosity is that calculated from the combination of the pressure gradient and torque, μ_{proc}. Thus, the process viscosity μ_{proc} of color 3 was used as viscosity plateau in what we called a semi-analytical rheological model. The results are shown in Fig. 7.7, in which one can observe that the use of this rheological model shifts down the numerical curve and brings it closer to the experimental results. The remaining smaller difference then suggests that this model needs further improvements.

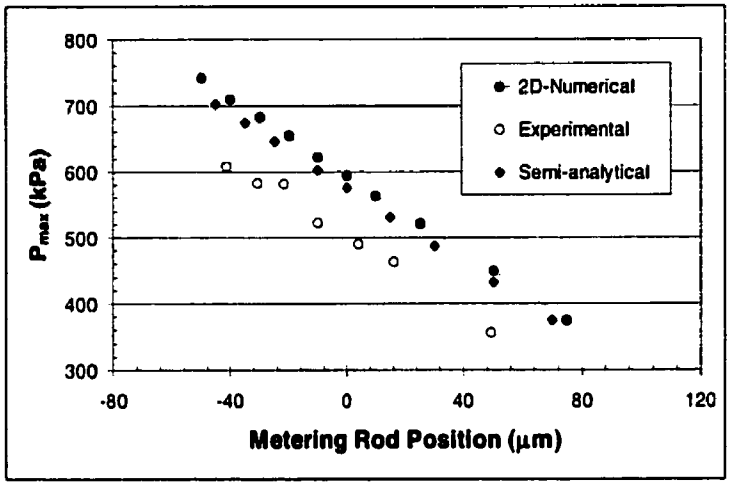

Figure 7.7 Maximum pressure vs metering rod relative position for color 3 (V_t = 1750 m/min, V_m = 30 m/min).

From the discussion of above, a very important question arises: what rheological model should be used in the simulations of the metering nip flow? Since the color has no time to restructure before arriving to the application nip (Alonso et al. 2000c), a suitable assumption may be to consider that the coating color behaves as Newtonian downstream the nip, with a viscosity equal to the process viscosity μ_{proc}. Upstream the nip, the fact that the mixing procedure used in the coating color makedown may affect the coating color rheological behavior and runnability (Alonso et al. 2000b; Persson, 1997) suggests that the shear preconditioning may affect the measurements in the film coater, plus the possible effect of the extensional behavior of the coating colors. Thus, more rheological tests are needed in order to clarify the relative influence of time, preconditioning and the extensional behavior of the coating colors. For the time being, the combination of transient rheological tests with the process viscosity in a semi-analytical model is a clear improvement of the metering nip flow although it certainly admits further enhancements. For example, improvements in the transient rheological tests may be made by using a more powerful rheometer (in this investigation the lowest reliable time to perform the step growth tests was 2 seconds with a data acquisition response time estimated in 0.1 s, far long compared to the residence time of milliseconds in the metering nip). We must also keep in mind that each coating

formulation has its own rheological behavior so that what was observed in this work may be different with other formulations. A further analysis with more complex coating industrial coating colors is needed. Finally, the process viscosity may also be related to the occurrence of instabilities in the metering and application nips, which will be the topic of future work.

7.5 Conclusion

In a laboratory film coater, the hydrodynamic pressure and the torque signal on the metering rod were used to investigate the coating color rheological behavior in the metering nip. Numerical simulations were used to assess the process viscosity of the coating colors from former publications. It was found that the maximum pressure may be preferably used to evaluate the process viscosity when the extensional behavior of the coating colors is known. The torque may be used to determine the process viscosity when the coating colors are subjected to low shear rates and follow the power law rheological model. The process viscosity evaluated in a region of shear-dominated flow can better describe the hydrodynamics of the metering nip flow than the former methods. The combination of the process viscosity with an adapted transient Cross model is proposed as a first attempt at exploring the numerical description of the coating colors rheological behavior in the nip since it better approximates the flow hydrodynamics than the steady state rheological model alone.

7.6 Appendix

The computational domain for the simulations is shown in Figs. A7.1 and A7.2. V_m and V_t are the speeds of the metering rod and the transfer roll, respectively, l is the length of the domain, H_n defines the minimum clearance between rod and roll before deformation, and t_e is the thickness of the elastic cover.

Ω_F is the computational domain for the fluid and Ω_S that for the solid, Γ_F is the fluid boundary, Γ_S the solid boundary, and Γ the solid-fluid interface along the transfer roll. Γ_{Ft} is the fluid boundary along the transfer roll surface, Γ_{Fm} the fluid boundary along

the metering rod surface, Γ_{St} the solid boundary along the transfer roll, $\mathbf{n}_F$ the unit vector normal to Γ_{Ft}, $\mathbf{n}_S$ the unit vector normal to Γ_{St}, and $\mathbf{t}_F$ the unit vector tangent to Γ_{Fm}.

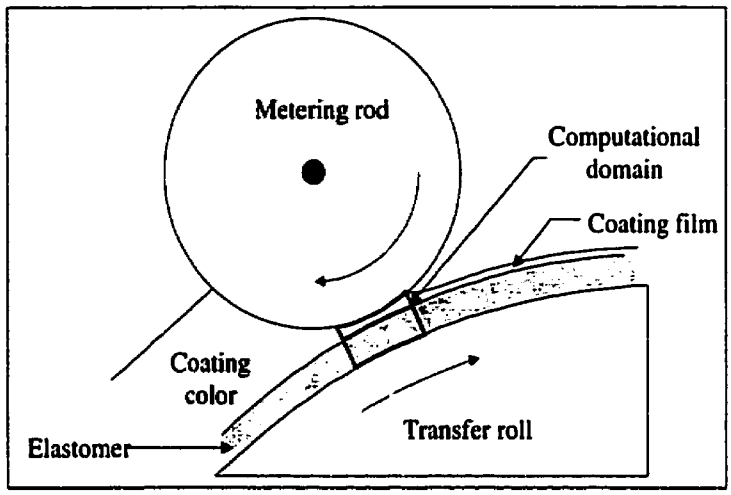

Figure A7.1 Computational domaine in the simulation of the metering nip.

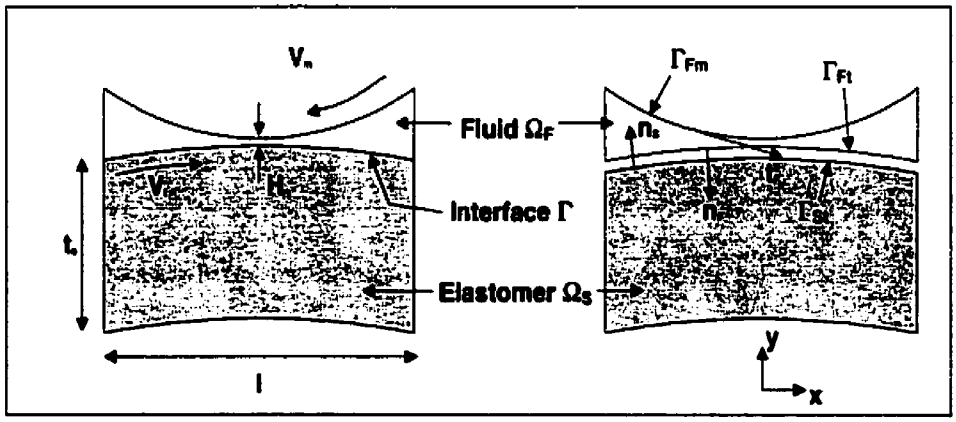

Figure A7.2 Nomenclature of the computational domain.

7.6.1 Fluid Problem

The flow of an incompressible fluid in the computational fluid domain Ω_F with boundary Γ_F is governed by the 2-D momentum and continuity equations

$$\operatorname{div}\sigma_F - \rho \mathbf{v}\cdot\operatorname{grad}\mathbf{v} = 0, \qquad \text{in } \Omega_F, \tag{A7.1}$$

$$\operatorname{div}\mathbf{v} = 0, \qquad \text{in } \Omega_F, \tag{A7.2}$$

where the total stress and the rate-of-strain tensors are defined as

$$\sigma_F = -p\delta + 2\mu\dot{\gamma}, \tag{A7.3}$$

$$\dot{\gamma} = \frac{1}{2}[\operatorname{grad}\mathbf{v} + (\operatorname{grad}\mathbf{v})^T]. \tag{A7.4}$$

In this paper, rheological behavior of the coating colors was approximated with the Cross model due to its improved numerical stability (Roper and Attal, 1993)

$$\mu_{Cr} = \eta_\infty + \frac{\eta_o - \eta_\infty}{1 + (t\dot{\gamma})^p} \tag{A7.5}$$

The following essential boundary conditions are imposed

$$\mathbf{v} = V_t, \qquad \text{on } \Gamma_{F_t}, \tag{A7.6}$$

$$\mathbf{v} = V_n, \qquad \text{on } \Gamma_{F_n}, \tag{A7.7}$$

together with the natural boundary conditions

$$(\sigma_F)_{nn} = 0, \quad \text{on } \Gamma_F \setminus (\Gamma_{F_t} \cup \Gamma_{F_n}), \tag{A7.8}$$

$$(\sigma_F)_{nt} = 0, \quad \text{on } \Gamma_F \setminus (\Gamma_{F_t} \cup \Gamma_{F_n}), \tag{A7.9}$$

where **n** stands for the outward unit vector normal to $\Gamma_F \setminus (\Gamma_{Ft} \cup \Gamma_{Fm})$, the extremities of the nip.

On the metering rod, the total torque exerted on the rod is calculated as

$$T = R_m \int_{\Gamma} (\sigma_F \cdot t_F) d\Gamma \quad \text{on } \Gamma, \tag{A7.10}$$

7.6.2 Solid Problem

The evaluation of the displacement **u** of the elastomer cover under the influence of hydrodynamic forces is carried out under the following assumptions

+ the displacements **u** are small.
+ the elastomer is isotropic and homogeneous.
+ the elastomer elasticity obeys Hook's law.
+ the elastomer is incompressible.

The linearized strain tensor is

$$\varepsilon = \frac{1}{2}[\text{grad}\,\mathbf{u} + (\text{grad}\,\mathbf{u})^T]. \tag{A7.11}$$

and the displacements **u** of the elastomer cover Ω_S are governed by the two-dimensional Stokes-like equations

$$\text{div}\,\sigma_S = 0, \qquad \text{in } \Omega_S, \tag{A7.12}$$

$$\text{div}\,\mathbf{u} = 0, \qquad \text{in } \Omega_S, \tag{A7.13}$$

with

$$\sigma_S = 2G\varepsilon + q\delta, \tag{A7.14}$$

where G is the shear modulus and can be related to the Young's modulus E as G=E/3, and where q is a Lagrange multiplier introduced to enforce the incompressibility constraint.

The cover of the transfer roll deforms only when it is in contact with the fluid. As a consequence, the following Dirichlet boundary condition is set

$$\mathbf{u} = 0, \qquad \text{on } \Gamma_S \setminus \Gamma_{S_t}. \tag{A7.15}$$

At equilibrium, the stress balance between the hydrodynamic and elastic stresses satisfies

$$\sigma_F \cdot \mathbf{n}_F + \sigma_S \cdot \mathbf{n}_S = (\sigma_S - \sigma_F) \cdot \mathbf{n}_S = 0, \qquad \text{on } \Gamma, \tag{A7.16}$$

which is in fact a Newmann boundary condition that provides the load for the elasticity problem (A12)-(A13).

The stresses that build up in the elastomer are stored so that they can be used in the following iteration. A continuation method can also be used when one-go simulations are difficult to carry out. A given set of parameters for which the solution is known can be used to generate a new solution for a different set of parameters where one or several variables can be modified. For example, this method has helped achieve convergence when negative gaps have been required (Fourcade et al. 1999).

CHAPTER 8

CONCLUSIONS AND RECOMMENDATIONS

Our objectives were to investigate the hydrodynamics of the metering nip flow with respect to the instabilities generated, and the rheological behavior of paper coating colors in the metering nip and in the rheometer. The objectives required both experimental and numerical work. The experiments were performed in a laboratory coater under industrial operating conditions. The main features of the lab coater allowed to acquire pressure profiles in the metering nip, torque in the metering rod, and temperatures; additionally, video recordings of the metered film were made. The numerical work was carried out with the commercial code POLY2D^{TM}, which is based on the Galerkin finite element method. The numerical model considered the deformation of the transfer roll, the rheology of the coating colors with the Cross model, and the operating conditions used in the experiments.

The analysis of the results concerning the objective of investigating the metering nip flow hydrodynamics with respect to the instabilities generated have led us to the following findings:

- Three hydrodynamic configurations can be observed, depending on the dominant hydrodynamic regime: inertia at narrow gaps, capillary at wide gaps, and air entrapment.
- The ribbing behavior follows the general trends of Newtonian and $CaCO_3$ suspensions, except that the rib width is smaller, i.e., the metering nip flow is more stable with coating colors.
- At very high speeds, the instabilities generated depend mainly on the formulation of the coating colors, i.e., on the rheological properties of the fluids.
- Two spitting regimes can be observed, depending on the formulation (usually with the more viscous) and the load applied on the metering rod.

- The overall pressure profile can be used to assess the stability of the metering nip flow in terms of the standard deviation of the data and the sub-ambient pressure.
- Creep flow tests and the peak in the transient stress do not always correlate with film coating runnability.
- The mixing makedown process affects directly the runnability of the coating colors; high shear rate coating color makedown improves runnability.
- Viscous dissipation in the metering nip is negligible.

Regarding the objectives of investigating the rheological behavior of the coating colors in the metering nip, we have found that:

- The process viscosity from maximum pressure measurements is about six times higher than that measured under steady state conditions in the rheometer.
- The process viscosity from torque measurements is lower than that measured under steady state conditions in the rheometer.
- The structure breakdown of the coating colors in the metering nip may be such that steady state may not be reached in the metering nip so that the process viscosity becomes relevant.
- In the center of the nip, the Poiseuille contribution to the flow is independent of inertia, constant for Newtonian fluids, and dependent of the shear-thinning index for coating colors.
- The process viscosity from the combination of the pressure gradient and the torque is lower than that measured in step growth experiments in a rheometer.
- The process viscosity model based on maximum pressure measurements should preferably be used when the extensional behavior of the coating colors is known.
- The process viscosity model based on torque measurements should be applied at low speeds, range in which the coating colors behave as power law fluids and the concept of Metzner and Otto better applies.

- A combination of an adapted transient Cross model with the process viscosity from the combination of the pressure gradient and the torque better represents the hydrodynamics of the metering nip flow than the other models.

This thesis has contributed significantly to the understanding of the metering nip flow about the high-speed instabilities that are generated, its behavior with respect to the coating color formulation and the operating conditions. Moreover, new knowledge has emerged about the rheological behavior of the coating fluids, the usage of the process viscosity models proposed, and the numerical modeling of the coating colors rheological behavior in the metering nip. Additional work is however worthwhile since new questions have arisen. For example, numerical simulations of the metering nip flow in two and three dimensions including the free surface and the elastomer deformation would permit to assess the stability of the reverse roll coating flow with respect to the ribbing instability in terms of the operating conditions, machine design, and coating color rheology.

A systematic study of the spitting phenomenon would bring new insights about its origin. This could be done by analyzing the sub-ambient pressure at the exit of the nip in order to clarify if its origin comes from cavitation. A droplet weight and size analysis would help to better understand the effects of the metering rod speed in the elimination of spitting.

Transient rheological tests can be used to investigate the importance of the destructuration time and the effects of the preconditioning of the coating colors. Rheological tests under extensional flow are still necessary to clarify the influence of the extensional viscosity on the metering nip flow hydrodynamics. Finally, new rheological tests with more complex coating color formulations would also help to generalize the methods proposed here to evaluate the process viscosity.

There are topics relative to the metering nip flow that are important but could not be studied in this thesis. Thus, these are suggestions that may be considered in further

research concerning the understanding of the metering nip flow to lead to an increased productivity of the process and a better controlled metered film quality.

The effects of the slippage on the metering rod are unknown. Its probably effects on the stability of the flow and on the torque measurements may be important. Although quantifying the slippage phenomena in the metering nip seems to be a very difficult task, similar techniques as those used in the analysis of slippage in a Couette geometry may be implemented.

The effects of the coating color elasticity on the measurements performed in the laboratory coater may be important. Elastic effects may also influence the stability of the flow. An assessment of the elastic effects may be carried out by using highly elastic fluids with similar viscous behavior. Rheological measurements would also be a powerful tool in assessing those effects.

The deformation of the transfer roll is calculated but it has never been validated with experiments. Visualization techniques may be used in order to better understand the transfer roll cover deformation and also carry out comparisons with the calculated roll cover profiles. This topic could also bring a new perception about the effects of the hardness of the cover on the runnability of the coating colors. The behavior of the elastic cover under dynamic conditions may also be investigated.

The knowledge acquired at the end of the development of the suggestions of above will define if further research is necessary in order to fully understand the metering nip flow, the coating color rheological behavior in the metering nip, and the influence of the elastic cover.

REFERENCES

1. ADACHI, K., TAMURA, T., NAKAMURA, R. (1988). Coating flows in a nip region and various critical phenomena. AIChE J., 34, 456-464.
2. ALONSO, S., RÉGLAT, O., BERTRAND, F., TANGUY, P.A. (2000a). Process viscosity in a film coater. Paperi ja Puu (Paper and Timber), 82, p1-7.
3. ALONSO, S., TANGUY, P.A. (2000b). Hydrodynamic instabilities in the metering nip of a film coater. Tappi J. (submitted in May 2000).
4. ALONSO, S., BERTRAND, F., RÉGLAT, O., CHOPLIN, L., TANGUY, P.A. (2000c). Process viscosity in reverse roll coating. Chem. Eng. Res. and Des. (submitted in May 2000).
5. AHLROOS, J., ALEXANDERSSON, M., GRÖN, J. (1999). Influence of base-paper filler content and precalendering on a metered film press coating-paper and print quality. Tappi J., 82, 94-100.
6. BAUMAN, T., SULLIVAN, T., MIDDLEMAN, S. (1981). Ribbing instability in coating flows: effect of polymer additives. Chem. Eng. Comm., 14, 35-46.
7. BENJAMIN, D.F., CARVALHO, M.S., ANDERSON, T.J., SCRIVEN, L.E. (1994). Forward roll film-splitting: theory and experiments. (1994) Tappi Coating Conference. Proceedings, 109-123.
8. BENKREIRA, H., EDWARDS, M.F., WILKINSON, W.L. (1981). Roll coating of purely viscous liquids. Chemical Engineering Science, 36, 429-434.
9. BIRD, R. B., STEWARD, W. E., LIGHTFOOT, W. N. (1960). Transport phenomena. Eds. John Wiley & Sons.
10. BOUSFIELD, D.W., ISAKKSSON, P., RIGHDAL, M. (1996). Particle motion analysis in a blade coater: stagnation zone results. XIIth International Congress on Rheology Proceedings, Quebec 1996 Canadian Rheology Group, 669-670.
11. BRITO-DE LA FUENTE, E., NAVA, J. A., LOPEZ, L.M., MEDINA, L., ASCANIO, G., TANGUY, P.A. (1998). Process viscosimetry of complex fluids and suspensions with helical ribbon agitators. The Canadian Journal of Chemical Engineering, 76, 689-695.
12. CARREAU, P.J., LAVOIE, P.A. (1993) Rheology of coating colors: a rheologist point of view. Tappi Coating Conference Proceedings, 1-12.

13. CARREAU, P.J., DE KEE, P., CHHABRA, R.P. (1997). Polymer rheology: principles and applications. Hanser Editors 1997.
14. CARVALHO, M.S., SCRIVEN, L.E. (1993). Effect of deformable roll cover on roll coating. Tappi Polymer, Laminations and Coating Conference Proceedings, 451-459.
15. CARVALHO, M.S., ANDERSON, T.J. SCRIVEN, L.E. (1994). Ribbing instability in forward deformable roll coating. Tappi Coating Conference Proceedings, 99-107.
16. CARVALHO, M.S., DONTULA, P., SCRIVEN, L.E. (1995) Non-newtonian effects on ribbing instability. Tappi Coating Conference Proceedings, 223-229.
17. CARVALHO, M.S., SCRIVEN, L.E. (1997). Deformable roll coating flows: steady state and linear perturbation analysis. J. Fluid Mechanics, 339, 143-172.
18. CARVALHO, M.S., SCRIVEN, L.E. (1999). Three-dimensional stability analysis of the free surface flows: application to forward deformable roll coating. Journal of Computational Physics, 151, 534-562.
19. COHU, O., MAGNIN, A. (1995). Rheometry of paints with regard to roll coating process. Journal of Rheology, 39, 767-785.
20. COHU, O., MAGNIN, A. (1997). Forward roll coating of Newtonian fluids with deformable rolls: an experimental investigation. Chemical Engineering Science, 52, 1339-1347.
21. COYLE, D., MACOSKO, C.W., SCRIVEN, L.E. (1986) Film-splitting flows in forward roll coating". J. Fluid Mechanics, 171, 183-207.
22. COYLE, D. (1988). Forward roll coating with deformable rolls: a simple one-dimensional elastohydrodynamic model. Chemical Engineering Science, 43, 2673-2684.
23. COYLE, D., MACOSKO, C.W., SCRIVEN, L.E. (1990a). A symple model of reverse roll coating. Ind. Ing. Chem. Res., 29, 1416-1419.
24. COYLE, D., MACOSKO, C.W., SCRIVEN, L.E. (1990b). The fluids dynamics of reverse roll coating. AIChE J., 36, 161-174.
25. COYLE, D., MACOSKO, C.W., SCRIVEN, L.E. (1990c). Reverse roll coating of non-Newtonian liquids, J. Rheology, 34, 615-636.

26. COYLE, D., MACOSKO, C.W., SCRIVEN, L.E. (1990d). Stability of symmetric film-splitting between counter-rotating cylinders. J. Fluids Mechanics, 216, 437-458.

27. COYLE, D., Roll Coating. (1992). In modern coating and drying technology. Ed. Cohen and Gutoff. VCH Publisers.

28. DECRÉ, M., GAILLY, E., BUCHLIN, J.-M. (1996) Meniscus control by string in roll coating experiment. AIChE J., 42, 1583-1589.

29. DELPLACE, F., LEULIET, J.C. (1995). Generalized Reynolds number for the flow of power law fluids in cylindrical ducts of arbitrary cross section. Chemical Engineering Journal, 56, 33-37.

30. DESBIENS, M. (1999). New millenium, new fat books? International Paperworld, 21-22.

31. DOOBELS, F., MEWIS, J. (1978). Analysis of nip flow operations involving a viscoelastic roller. Chemical Engineering Science, 33, 493-500.

32. ENGSTRÖM, G., RIGDAHL, M. (1990). The effects of some polymers dispersions on the rheological properties of coating colors. Nordic Pulp and Paper Research J, 4, 161-167.

33. ERIKSSON, J., ENGSTRÖM, G., RIGDAHL, M. (1990). Viscosity of some clay-based coating colors at high shear rates. Rheol. Acta, 29, 352-359.

34. FADAT, G., ENGSTRÖM, G., RIGDAHL, M. (1988). The effect of dissolved polymers on the rheological properties of coating colors. Rheol. Acta, 27, 289-297.

35. FERNANDO, R.H., GLASS, J.E. (1988). Dynamic uniaxial extensional viscosity (DUEV) effects in roll coating application II. Polymer blend studies. Journal of Rheology, 32, 199-213.

36. FOURCADE, E., BERTRAND, F., TANGUY, P.A. (1998). Numerical modeling of the hydrodynamics in the metering nip of a film coater. Sixth Annual Conference of the Fluid Dynamics Society of Quebec, Canada, V-17/V-22.

37. FOURCADE, E., BERTRAND, F., RÉGLAT, O., TANGUY, P.A. (1999). Finite element analysis of fluid-solid interaction in the metering nip of a metering size press. Comp. Meth. In Appl. Mech. and Eng, 174, 235-245.

38. GANE, P.A.C., HOOPER, J.J., GRONWALD, A. (1997). Coating pigment orientation: a comparative analysis of the application mechanisms and properties of blade and roll coaters. Tappi J., 80, p.109-115.

39. GASKELL, P.H., INNES, G.E., SAVAGE, M.D. (1998). An experimental investigation of meniscus roll coating. J. Fluid Mechanics, 355, 17-44.

40. GERSTENBERGER, M.R.C. (1999). What future for coating (International Symposium in Helsinki). International Paperworld, 28-29.

41. GHANNAM, M.T., AND ESMAIL, N. B. (1997). Effect of substrate geometry on dynamic contact angles in surface wetting. Chem. Eng. Comm., 159, 43-57.

42. GHOSH, T., LAVOIE, P.A., CARREAU, P.J. (1997). Rheology of coating colors and their runnability on a cylindrical laboratory coater. Tappi J., 11, 186-192.

43. GHOSH, T. (1998a). Rheology of kaolin-based pigment slurries and the coating colors they form, Part I. Tappi J., 81, 89-92.

44. GHOSH, T. (1998b). Rheology of kaolin-based pigment slurries and the coating colors they form, Part II. Tappi J., 81, 123-126.

45. GREENER, Y., MIDDLEMAN, S. (1975) A theory of roll coating of viscous and viscoelastic fluids. Polymer Engineering Science, 15, 1-10.

46. GREENER, J., SULLIVAN, T., TURNER, B., MIDDLEMAN, S. (1980) Ribbing instability of a two-roll coater: Newtonian fluids. Chem. Eng. Commun., 5, 73-83.

47. GREENER, Y., MIDDLEMAN, S. (1981) Reverse roll coating of viscous and viscoelastic liquids. Ind. Eng. Chem. Fund., 20, 63-66.

48. GREIFFENBERG, I., LOHMANDER, S., RIGDAHL, M. (1999). Effects of the air content on the rheological properties of coating colors. Tappi Advances Coating Fundamentals Symposium Proceedings, Tappi Press, 149-156.

49. GRÖN, J., SUNDE, H., NIKULA, E. (1996). Runnability aspects in high speed film-transfer coating. Tappi Metered Size Press Forum Proceedings, 21-50.

50. GRÖN, J., ANÄS, P., MOLARIUS-MÄYRÄNEN, S., (1997). Improving the process runnability and FCO quality by optimizing the coating color formulation. Tappi Coating Conference Proceedings, 23-41.

51. GRÖN, J., DAHLVIK, P. (1997). Effect of coating color chemistry and temperature on runnability and coated paper properties. Journal of Pulp and Paper Science, 23, 422-427.

52. GRÖN, J., SUNDE, H., NIKULA, E. (1998). Runnability aspects in high speed film transfer coating. Tappi J., 81, 157-165.

53. GURFINKEL, M.E., PATERA, A.T. (1997) Three-dimensional ribbing instability in symmetric forward-roll film-coating processes. J. Fluid Mechanics, 335, 332-359.

54. HAGEMEYER, R.W. (1997). A project of the coating pigments committee of Tappi coating and graphics art division. Tappi Press. Chapter 1.

55. HAO, Y., HABER, S. (1999) Reverse roll coating flow. International Journal of Numerical Methods in Fluids. 30, 635-652.

56. HASE, K.R., BOUSFIELD, D.W. (1994). Kaolin pigment-latex interactions during coatings. Tappi Coating Conference Proceedings, 49-62.

57. HASEGAWA, T., SORIMACHI, K. (1993). Wavelength and depth of ribbing in roll coating and its elimination. AIChE J., 39, 935-945.

58. HILDEN, K.K., MUSTONEN, I. (1998). Complete shear rate analysis provides a new means of optimizing coating performance on high speed coaters. Pulp and Paper Canada, 99, 57-60.

59. ISAKSSON, P., RIGDAHL, M., FLINK, P., FORSBERG, S. (1998). Aspects of the elongational flow behavior of coating colors. Journal of Pulp and Paper Science, 24, 204-209.

60. KANG, Y.T., LIU, T.J. (1991). Minimum film thickness for reverse roll coating". Chemical Engineering Science, 46, 2958-2960.

61. KANG, Y. T., LEE, K.Y., LIU, T.J. (1991). The effect of polymer additives on the performance of a two-roll coater. J. of Applied Polymer Science, 43, 1187-1195.

62. KISTLER, S.F., SCRIVEN, L.E. (1984). Coating flow theory by finite element and asymptotic analysis of the Navier-Stokes system. Int. J. Num. Meth. In Fluid Mech., 4, 207-229.

63. KLOSTERMANN, R., MEWES, D. (1998). Numerical calculation of the velocity and temperature field in reverse roll coating. International Polymer Processing XIII, 4, p379-388.

64. KOKKO, A., KUNI, S., GRANKVIST, T. (1999) The influence of elongational viscosity on coatweight in paperboard coating with a smooth rod. Tappi Advanced Coating Fundamental Symposium Proceedings, Tappi Press, 79-97.

65. KURATH, S.F., LARSON, W.S. (1990). Capillary viscosimetry of a rheologically complex coating color. Tappi J., 73, 235-241.

66. LAVOIE, P.A., GHOSH, T., CARREAU, P.J. (1996). The rheology of coating colors: a comprehensive approach. CPPA International Paper and Coating Chemistry Symposium Proceedings, 253-257.

67. LAVOIE, P.A., CARREAU, P.J., GHOSH, T. (1997) Rheology of suspensions: the flow behavior of coating colors. Journal of Pulp and Paper Science, 23, 543-547.

68. LAUN, H.M., HIRSCH, G. (1989). New Laboratory Test to Measure Rheological Properties of Coating in Transient and Steady State Flows. Rheol. Acta, 28, 267-280.

69. MACOSKO, C.W.: Rheology, principles, measurements, and applications. VCH Publishers, USA 1994, p. 78.

70. METZNER, A.B., OTTO, R.E. (1957). Agitation of non-Newtonian fluids. AIChE J., 3, 3-10.

71. MCGENITY, P.M., GANE, P.A.C., HUSBAND, J.C., ENGLEY, M.S. (1992). Effect on interactions between coating color components on rheology, water retention and runnability. Tappi Coating Conference Proceedings, 133-149.

72. MILL, C.C., SOUTH, G.R. (1967) Formation of ribs on rotating rollers. J. Fluid Mechanics, 28, 523-529.

73. PAUKSTA, P.M. (1998). Speed: its effects on coating equipment and formulations. Tappi J., 81, 58-60.

74. PEARSON, J.R.A. (1960). The instability of uniform viscous flow under rollers and spreaders. J. Fluid Mechanics, 31, 481-500.

75. PERSSON, T., JÄRNSTRÖM, L., AND RIGDHAL, M., (1997). Effect of method of preparation of coating colors on the rheological behavior and properties of coating layers and coater papers. Tappi J. 80, 117-124.

76. PHILLIPS, R.J., AMSTRONG, R.C., BROWN, R.A., GRAHAM, A.L., ABBOTT, J.R. (1994). A constitutive equation for concentrated suspensions that accounts for shear-induced particle migration. Phys. Fluids. 4, 30-40.

77. PITTS, E., GREILLER, J. (1961) The flow of thin liquids films between rollers. J. Fluid Mechanics, 11, 33-50.

78. PORANEN, J., NIEMISTÖ, A. (1999) Experimental and theoretical study for metering size press. Tappi Advanced Coating Fundamental Symposium Proceedings, 159-161.

79. PORANEN, J., NIEMISTÖ, A., KATAJA M., GRÖN, J. (2000) A novel technique for measuring pressure in the metering nip of a MSP process. Tappi Conference and Trade Fair Proceedings, Washington, 367-380.

80. POULIN, N., TANGUY, P.A. (1997). Numerical and physical modeling of the permeability of paper to CMC and coating liquids. Can. Journal in Chem. Eng., 24, 234-256.

81. PURKAYASTHA, S., OJA, R. (1993) Dynamic rheological behavior of paper coatings. Tappi Advanced Coating Fundamentals Symposium, 31-39.

82. RANTANEN, R. (1996). Smooth coating with sym-sizer. Paper Age, 112, 26-27.

83. RÉGLAT, O. (1997). Procédé de couchage par rouleau de transfert et barre de dosage. PhD Thesis, École Polytechnique de Montréal, Canada.

84. RÉGLAT, O., TANGUY, P.A. (1997). A experimental study of the flow in the metering nip of a metering size press. AIChE J., 80, 2911-2920.

85. RÉGLAT O., TANGUY, P.A. (1998). Rheological investigations of $CaCO_3$ slurries in the metering nip of a metering size press. Tappi J., 81, 195-205.

86. RITZ, J. B., BERTRAND, F., THIBAULT, F., TANGUY, P.A. (1998). Numerical modeling of shear-induced particle migration in a film coater. Sixth Annual Conference of the Fluid Dynamics Society of Quebec, Canada, V-23/V-28.

87. ROPER, D.A., ATTAL, J.F. (1993). Evaluations of coating high-speed runnability using pilot plant coater data, rheological measurements, and computer modeling. Tappi J., 76, 55-62.

88. ROPER, R.A., SALMINEN, P., URSHELER, R., MOORE, E. (1998). Optimization of formulation parameters to reduce misting and orange peel formation on metered size presses. Metered Size Press Forum II Proceedings. Tappi Press, 37-55.

89. RUSCHAK, K.J. (1982). Boundary conditions at a liquid/air interface in lubrication flows. J. Fluid Mechanics, 119, 107-120.

90. RUSCHAK, K.J. (1985). Coating flows. Ann. Rev. Fluid Mech., 17, 65-89.

91. SALMINEN, P., SRESHELER, R., ROPER, J., CHASE, D. (1996). Optimizing the coating formulation to reduce misting in high-speed film coating. Tappi Metered Size Press Forum Proceedings, 51-55.

92. SAVAGE, M.D. (1984) Mathematical model for the onset of ribbing. AIChE J., 30, 999-1002.

93. SMOOK, G.A. (1997). Handbook for Pulp and Paper Technologists. Angus Wilde Publications, Chapter 1.

94. STERBACEK, Z., TAUSK, P. (1965). Mixing in the chemical industry. Pergamon press, 78-81.

95. STRANGER, K.M. (1999). The film press -a versatile coating system-. Paper Age, 31, 12-16.

96. TANGUY, P. A., F. THIBAULT, E. BRITO DE LA FUENTE. (1996). A new investigation of the Metzner-Otto concept for anchor mixing impellers", Canadian Journal of Chemical Engineering. 74, 222-228.

97. TETLOW, N., GRAHAM, A.L., INGBER, M.S., SUBIA, S.R., MONDY, L.A., ALTOBELLI, S.A. (1998). Particle migration in a Couette apparatus: experiment and modeling. J. Rheol., 42(2)3, 307-327.

98. THIBAULT, F. (1999). Analyse du procédé de mélange solide-liquide: application à la préparation des sauces du couchage. PhD thesis. École Polytechnique de Montréal.

99. TRIANTAFILLOPOULOS, N.G., AIDUN, C.K. (1990). Relationship between flow instability in short-dwell ponds and cross directional coat weight nonuniformities. Tappi Coating Conference Proceedings, 309-323.

100. TRIANTAFILLOPOULOS, N.G., LEE, P.M. (1996). Troubleshooting rheology problems in metered size press. Tappi Metered Size Press Forum Proceedings, 171-186.

101. TRIANTAFILLOPOULOS, N.G., SMITH, M.K. (1998). Troubleshooting rheology problems in metered size press. Tappi Metered Size Press Forum II Proceedings, 13-36.

102. TSUJI, A., NITTA, J., SASAGAWA, Y., NIJIMA, N. (1990). A new rheometer for paper coating. Tappi, 73, 163-168.

103. VIDAL, F., EGURREGUY, D., POUYET, J. (1991). Rheology in situ des sauces de couchage. Les cahiers de rheology, 9, 171-179.

104. WANG, L., TIU, C., LUI, T. (1994). Post-metering reverse roll coating: Newtonian and Polymer liquids. Development in non-Newtonian flows. FED-VOL206/AMD-VOL191, ASME.

105. WIKSTRÖM, M., GRÖN, J. (2000) Formation of patterns on paper coated with metering size press. Tappi Coating Conference and Trade Fair Proceedings. Washington, 355-366.

106. YZIQUEL, F., MOAN, M., CARREAU, P.J., TANGUY, P.A. (1999). Nonlinear viscoelastic behavior of paper coating colors. Nordic Pulp and Paper Research J., 14, 37-47.